Delft University of Technology

Applied Earth Sciences
Master's in Environmental Engineering
CIE5060-09

Catalytic hydrothermal liquefaction of invasive species: A case study of Namibia's Encroacher Bush

Author:
Nikos Bias
Student number: 5263026

June 7, 2023

MSc Thesis Committee

Ralph Lindeboom (chair)	Assistant Professor, SE Group
Wiebren de Jong (supervisor)	Full Professor, LSE Group
Merle de Kreuk	Full Professor, WM Group
Luis Cutz (daily supervisor)	Assistant Professor, LSE Group

TU Delft Delft University of Technology

Preface

The global concern around anthropogenic CO_2 emissions is well known by now, but still not enough action has been taken to mitigate it. Reducing or eliminating fossil fuels by substituting them with biofuels is and will be crucial for the overall energy transition in the foreseeable future. One of the issues with biofuels, is finding a supply chain of biomass that can sustain the large energy demand. That challenge can be overcome by utilizing Namibia's encroacher bush (EB), an invasive species woody biomass that is harmful to the ecosystem. However, a suitable process is needed for that and Hydrothermal Liquefaction (HTL), a thermochemical process whose main product is a high energy bio-oil, can possibly valorize EB's vast amounts. Therefore, introducing HTL with EB can provide a solution both to the energy transition and Namibia's environmental crisis with bush encroachment.

During my previous bachelor's studies in Chemical Engineering, I came across a project involving HTL, but only with process simulation. I was since then intrigued by that process and always wanted to have the chance to study it more. Life got HTL in front of me once again, while attending an elective course on thermochemical biomass conversion processes (SET3070). A techno-economical analysis of HTL with EB was the final assignment of the course, which me and my group did quite well. Dr Luis Cutz caught my enthusiasm about the topic and later introduced me in the Process & Energy department's facilities where his team was already performing HTL experiments. And this is how my MSc Thesis on Environmental Engineering journey started. This MSc thesis project aims to assess the potential of the bio-oil produced from HTL of EB as a quality drop-in intermediate biofuel. This can be achieved by altering the operating conditions (temperature and residence time), adding a catalyst and optimizing for maximum bio-oil energy output.

I want to specially thank my daily supervisor Dr Luis Cutz for his continuous support and presence for the whole duration of the project. His passion for thermochemical conversion processes and biofuels was surely passed on to me. Furthermore, I would like to thank my Thesis committee - Prof. dr. ir. Wiebren de Jong, Prof. dr. ir. Merle de Kreuk and Dr. ir. Ralph Lindeboom - for their very insightful and constructive comments throughout our meetings, which helped me shape the goal of the current thesis. Finally, I would not be here without the support and love from family and friends, which stayed with me during this period and were always there for me.

Nikos Bias
Delft, June 2023

Abstract

Regulations and investments in new technologies for biofuel production as an alternative to fossil fuels have boosted in the last years due to concerns about climate change and anthropogenic CO_2 emissions. A valuable supply chain of biomass for biofuel production is one the most significant factors, in order to support the market's demand. A promising feedstock that is widely available and considered a residue can be Namibia's encroacher bush (EB). Namibia is facing an environmental crisis with bush encroachment, where EB takes over grasslands, reducing biodiversity and groundwater availability. A thermochemical process that can take advantage of EB can be Hydrothermal Liquefaction (HTL). With HTL, biomass feedstocks are liquefied under hot compressed water, producing bio-oil (BO), biochar (BC), an aqueous phase (AP) and gases. Catalytic HTL is a more attractive pathway, due to the increased BO yield and quality. To this day, there has not been a study investigating the potential of catalytic HTL with EB, thus the present MSc Thesis will attempt to close that knowledge gap and provide state-of-the-art insight.

To achieve that, *Acacia Mellifera* from Namibia was tested in sub-critical HTL conditions. In particular two campaigns were formulated with two different goals. The first one, focused on the selection of a suitable catalyst among 4 different categories of catalysts (zeolites, alkaline earth metals, lanthanides and transition metals). The catalysts performance was evaluated by comparing the Energy Recovery (ER) under same operational conditions. The catalysts used were ZSM-5, La_2O_3, Hydrotalcite and Ni/SiO_2-Al_2O_3, respectively. Then, the catalyst with the highest ER was used in the second experimental campaign using a Desing of Experiments approach. This approach had the goal to optimize HTL reaction conditions -temperature, residence time and catalyst loading- for maximizing BO yield and energy content. Central Composite Design (CCD) of experiments was used, with the parameters ranges being 250-340^{o}C, 5-60mins and 0-10wt%, respectively. Selected BO and BC samples from both campaigns were then characterized using various methods.

The HTL experiments with EB revealed that BO from EB could be produced. As for the catalysts, Ni/SiO_2-Al_2O_3 had the highest BO yield of 30.4wt%. However, hydrotalcite had the highest Energy Recovery (ER) with 41.1% and was deemed the most suitable. Main organic compounds found in all the BOs were phenolic derivatives, alicyclic ketones and fatty carboxylic acids. The CCD model indicated that the optimum conditions for maximizing BO yield were 340^{o}C, 60 minutes and 5wt%, which yielded 27.0wt% BO. However, the 330^{o}C - 60 minutes - 7.5wt% point gave both the highest yield and highest ER, 28.5wt% and 46.2% respectively. The CCD also reduced the O content in the BO samples by 54%. Finally, BC samples showed fuel characteristics similar to lignite and low concentration of heavy metals, making them legitimate alternatives for solid fuels or soil amendment.

Acronyms

BO	Bio-oil
BC	biochar
AP	Aqueous phase
CCD	Central Composite Design
DCM	Dichloromethane
DOE	Design of Experiments
EB	Encroacher Bush
ER	Energy Recovery
FC	Fixed Carbon
FCC	Fluid Catalytic Cracking
GC-MS	Gas Chromatography - Mass Spectrometry
HDO	Hydrodeoxygenation
HHV	High Heating Value
HTL	Hydrothermal Liquefaction
ICP-OES	Inductively Coupled Plasma-Optical Emission Spectroscopy
KF	Karl-Fischer
MAWL	Maximum Allowable Water Loading
MC	Moisture Content
NREL	National Renewable Energy Laboratory
RSM	Response Surface Methodology
TAN	Total Acidic Number
TGA	Thermogravometric Analysis
VM	Volatile Matter
XRD	X-Ray Diffraction

List of Figures

List of Tables

Contents

1| Introduction

Regulations and investments in new technologies that can provide an alternative to fossil fuels have sparked in the last years due to concerns about climate change and anthropogenic CO_2 emissions. Fossil fuels are deeply embedded in all sectors (e.g. industrial, transport, commercial and residential) and it is estimated that only technologies embedded in robust supply chains and in the global energy infrastructure will be capable of reorienting to greener routes in a reasonable timeframe [1]. Cost-effective mitigation options today are solar energy, wind energy, improved forest- and crop/grassland management, reduced food waste and loss, among others [2]. Among these, agriculture, forestry and other land use (AFOLU) is a driver of environmental impact (22% of total net anthropogenic GHG emissions in 2019 [2]) and a mitigator if sustainable practices and processes are developed for efficient mitigation options. The largest share of the projected economic mitigation potential of (AFOLU) options [4.2–7.4 $GtCO_2$-eq/yr] between 2020 and 2050 is expected to come from the conservation, improved management, and restoration of forest and other ecosystems [2]. Meeting this target will require to find options that do not compete with land and land-based resources such as low-risk feedstocks for bioenergy. A very promising low-risk feedstock lies within the heart of Namibia. An abundant and readily available second-generation biomass feedstock commonly known as "Encroacher Bush" (EB).

Namibia is currently facing an environmental crisis with the phenomenon of bush encroachment. It is defined as *"the densification and rapid spread of native shrub and tree species, resulting in an imbalance of biodiversity"* [3]. It is estimated that more than 45 million hectares of Namibia's land are affected by it, leading to reduction of biodiversity and groundwater depletion [4]. While this phenomenon causes various adverse effects, it also provides vast amounts of harvestable biomass. Based on reports [5],[6], the available biomass for harvesting is estimated around 260-300 million tonnes per year. As of now, only a small fraction of this biomass is used for charcoal and firewood production, while the leftovers from processing are burnt on the field [6]. Currently, charcoal produced via carbonization of EB is the only product produced economically at large scale [6]. Even though charcoal production improves the ecosystem by debushing, compared to the extent of bush encroachment, the overall effect is not environmentally significant. Consequently, Namibia needs cost-effective initiatives that ensure large-scale deployment of EB, which can be achieved by more efficient use of biomass feedstock and advanced technology for the production of high value-added products.

The use of biomass for liquid biofuels has been on the rise due to their numerous benefits, including their remarkable capacity to exploit the aromatic resources in biomass for the creation valuable by-products (e.g., chemicals), and potential to integrate with the existing energy infrastructure (e.g., the petroleum infrastructure) [7]. Thermochemical conversion processes transform biomass into biofuels, chemicals, heat and power [8]. Some of the main processes are combustion, gasification, pyrolysis and hydrothermal liquefaction [9]. Among them, Hydrothermal Liquefaction (HTL) offers an opportunity to directly produce "drop-in" intermediates oils, that later on can be converted into transport fuels, chemicals or bio-products [10]. For example, in Fig. 1.1, a suggested pathway for marine biofuel production is shown, by taking advantage of HTL with lignocellulosic biomass. HTL is performed by mixing biomass with water to create a slurry

(5-30% w/t dry biomass) and heating the mixture to 250-370^{o}C in high pressures (5-22 MPa) for a short residence time (15-60min) [9, 11]. The products are Bio-oil (BO), biochar (BC), an Aqueous phase (AP) and gases (mainly CO_2). The main advantages of HTL bio-crude oil are the low oxygen content (10-20%), higher calorific value (30-40 MJ/kg) and low water content (<1%) compared to typical pyrolysis oils [12] .

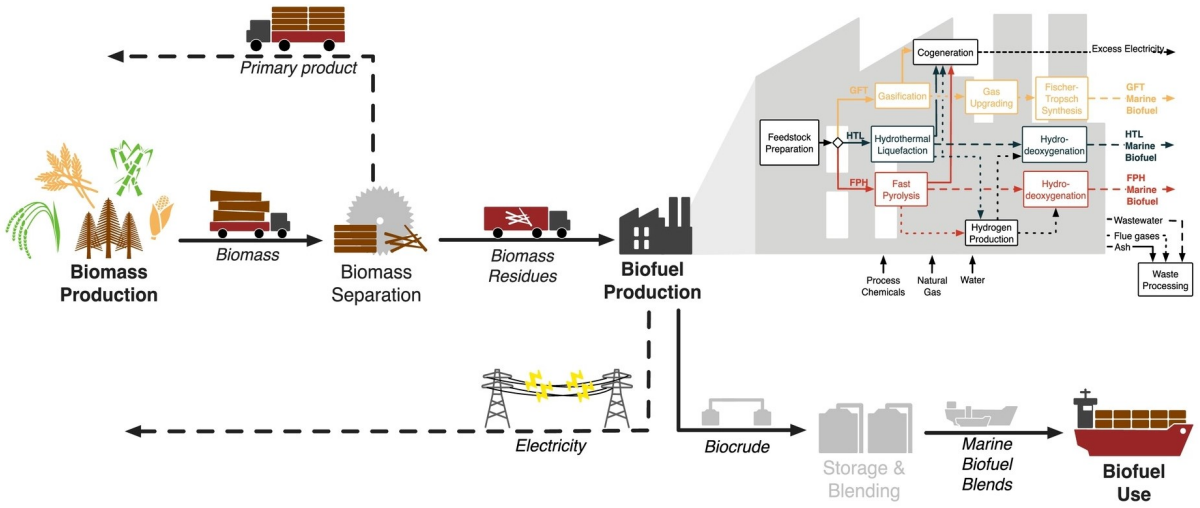

Figure 1.1: Suggested flowscheme for lignocellulosic biomass derived biofuel for the marine sector [13].

Despite HTL's advantages, there are still some challenges that hinder its commercialization. Scaling up the process has proved to be very challenging, due the size of the heat exchangers and the manufacturing of a robust pump for the hot compressed biomass slurry [14]. Furthermore, one of the more critical challenges involves increasing the BO yield to a percentage that the process becomes cost-effective, while also reducing the high amount of oxygenated compounds and improving its HHV [7, 15, 16]. These obstacles can be overcome or minimized with the addition of catalysts. Typical catalyst used in HTL are either homogeneous (alkali-based hydroxides and carbonates, organic and inorganic acids) or heterogeneous (transition metals and their oxides, zeolites, alkaline earth metals) [17, 18]. It has been found that both types can increase the quality and yield of BO [9, 16, 17]. Heterogeneous catalysts are overall preferred due to their higher selectivity, activity and recyclability [16]. However, the use of catalysts in such a process, makes its overall sustainability questionable, as rare metals (Nickel, Manganese, Cobalt among others) are the most commonly used in HTL studies [18]. Their accumulation in the biochar greatly reduces its quality, while environmental hazards increase. Consequently, while catalytic HTL might have the biggest potential for production of biofuels, some significant challenges still need to be overcome.

As far as the author is concerned, there is a knowledge gap regarding the use of EB as feedstock for HTL. Furthermore, the use of a more sustainable and environmentally friendly catalyst has not been the focus on HTL reports. In this report we will attempt to experimentally confirm the feasibility of producing a high-quality bio-crude oil from EB via HTL, while taking into account the sustainability of the catalyst.

1.1 Research question

Bsed on the information above, the following research question was formulated:

"What is the potential of Namibia's encroacher bush for the production of a quality drop-in intermediate bio-oil, using catalytic hydrothermal liquefaction?"

Which can be split into 3 sub questions:

1. "Which type of heterogeneous catalyst performs better for HTL with encroacher bush?"

2. "Which combination of temperature, retention time and catalyst amount lead to the highest energy yield?"

3. "What is the quality and properties of the EB bio-oil and biochar, compared to other feedstocks and thermochemical processes?"

For the first question, transition metal catalysts have been reported to significantly improve BO yield [18]. However, they might also reduce the HHV and accumulate in the biochar, which increases environmental hazard [19]. Zeolites or alkaline earth metals can be a better solution as they do not contain heavy metals and are more abundant than transition metals [20].

For the second question, lignocellulosic feedstocks (sugarcane bagasse, crude olive pomace, olive palm shell, walnut shell) have shown that temperatures up to 340^{o}C mostly increase BO and reduce the BC yields, while above 350^{o}C gas yields are favoured more and that there is an optimum temperature for maximum BO yield [21–24]. Retention time does not appear to have the same intense effect as temperature, but it has been found that after 45-60 minutes only the gaseous phase is increasing [16, 25]. For eucalyptus biomass, 15 minutes of residence time were found to be the point for optimal BO production [26]. Finally, the catalyst amount varies depending on the type of it, but in general amounts do not exceed 10-15 wt% [18].

For the third question, typical HTL biocrude oil from lignocellulosic biomass contains plenty of oxygenated, aromatic and unsaturated compounds [15, 16]. However, with the use of catalysts and different process conditions de-oxygenation and saturation can occur to improve the final product's quality [17, 27]. The BC produced is expected to have high carbon content [21, 26] but there is a high possibility of heavy metals and minerals accumulation [28].

1.2 MSc Thesis Project Scope - Outline

The objective of the present study is to experimentally assess the feasibility of producing a high-quality bio-crude oil from EB, in order to provide useful insight on a residue that negatively impacts both the environment and the people of Namibia.

In order to achieve that, two campaigns of catalytic HTL experiments will be performed at the Process & Energy lab setup in TU Delft. The first campaign will be the catalyst screening, where different types of catalysts, such as transition metals, zeolites and alkaline earth metals, will be compared in terms of performance. The second one will involve optimizing different reaction parameters (temperature, retention time and catalyst loading) via a Central Composite Design (CCD) of experiments for achieving maximum energy yield (BO and HHV). Characterization methods such as Proximate and Ultimate analysis, Bomb Calorimetry, X-Ray Diffraction (XRD), Inductively Coupled Plasma-Optical Emission Spectroscopy (ICP-OES), Gas Chromatography - Mass Spectrometry (GC-MS), and Karl-Fischer (KF) titration will be performed for the BC and BO, in order to obtain a better understanding of the effect of the process and catalysts on EB.

2| Theoretical Background

2.1 Namibia's bush encroachment: An environmental crisis

Namibia is a country located in the South West of Africa with a population of 2.55 million people, while taking up approximately 858.000 km^2 of land, making it the second least densely populated country in the world [29]. It is a mostly arid and semi-arid land while the climate is seasonal and characterised by frequent droughts [5]. As a result of that, there is a lack of surface water and Namibia is heavily depended on groundwater [30]. Climate change intensifies the already dry climate, but there is another phenomenon that has come to impact the wildlife and inhabitants of Namibia even more, called bush encroachment.

2.1.1 Bush encroachment drivers and negative effects

Bush encroachment is defined as *"the invasion and/or thickening of aggressive undesired woody species, resulting in an imbalance of the grass:bush ratio, a decrease in biodiversity, a decrease in carrying capacity and concomitant economic losses"* [5]. As of 2018, various types of bush species take up around 45 million hectares (450.000 km^2) of the Namibian Savannah [31], which is almost half of the country's entire area. This phenomenon interferes with almost 50% of the area used for agricultural and communal purposes [32], as also shown in Fig. 2.1. In Fig. 2.2, Namibia-Biomass Industry Group [31] projected the evolution of bush encroachment until the year 2030, with 5 different scenarios, where it can be seen that even with the low annual growth scenario, in less than 10 years the amount of land covered will increase from 45 to 53 million hectares.

The main drivers for the rapid growth can be associated with the global temperature increase in the past few years [32], but also the higher CO_2 levels in the atmosphere which support growth of woody and bushy species, acting as a fertilizer [31]. Moreover, according to the Namibia-Biomass Industry Group (2020) report, grass development is hindered due to the erratic rainfall pattern, while the bushes adjust better.

One of the most significant impacts of bush encroachment is the degradation of rangelands, which are critical for the livelihoods of many Namibians who depend on livestock for food and income [4]. As bush encroachment reduces the amount of grass available for grazing, it can lead to overgrazing, soil erosion, and decreased soil fertility [4, 5]. In addition to harming the livelihoods of local communities, bush encroachment also has a negative impact on wildlife. As woody plants take over grasslands, they can displace or alter the habitat of many species. This can lead to a decline in biodiversity and ultimately lead to the extinction of some species [5]. Furthermore, the denser vegetation can create ideal habitats for rodents and other pests, which can pose health risks to both humans and wildlife.

Bush encroachment can also have negative impacts on water availability, as the increased vegetation can reduce water flow and retention in rivers and streams [33]. This can affect both wildlife and humans who rely on these water sources for drinking, irrigation, and other activities. Additionally, bush encroachment can increase the risk of wildfires, which can further degrade the environment and cause harm to both people and animals [5].

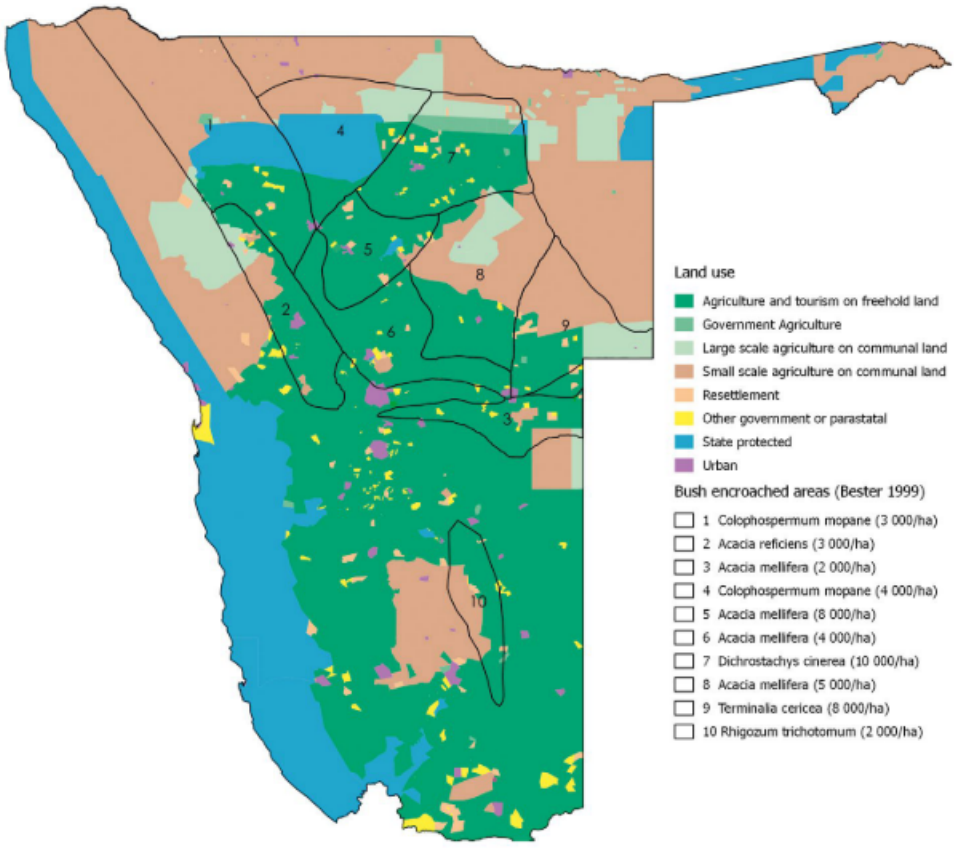

Figure 2.1: Land use in Namibia combined with EB affected areas [4]. The numbered areas also indicate which bush species is most dominant there.

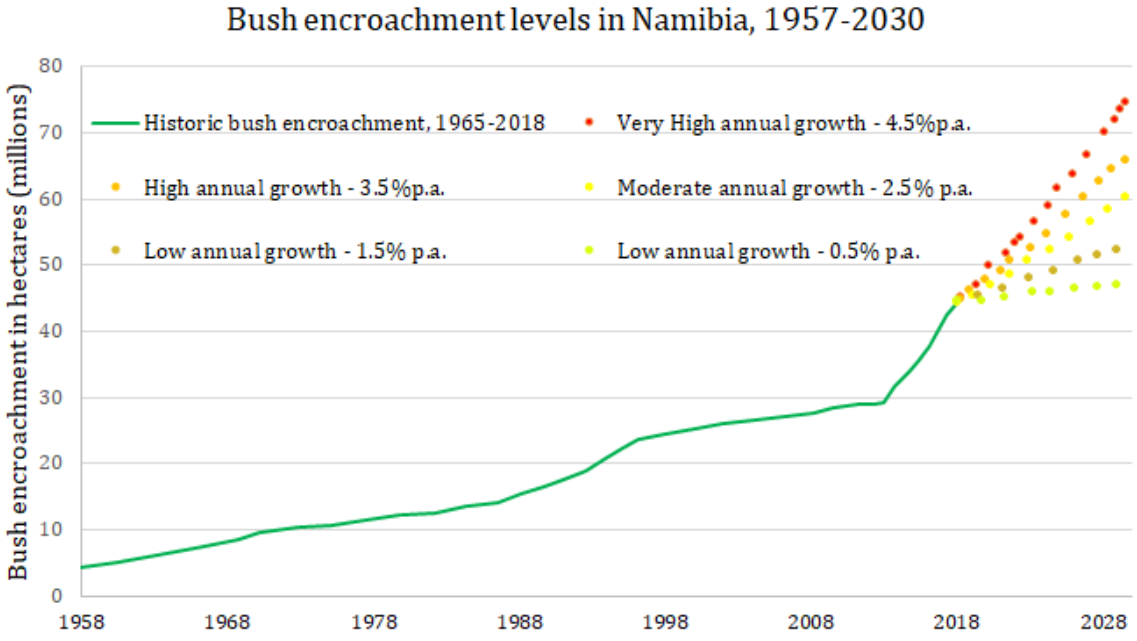

Figure 2.2: History and future projection on bush encroachment phenomenon for years 1957-2030 [31].

2.1.2 Current applications of EB

Although bush encroachment has numerous negative consequences, it also presents a significant opportunity for obtaining a large quantity of usable biomass. Based on reports [5], [6], it is estimated that approximately 260-300 million tonnes of biomass can be harvested annually. When considering the annual regrowth rate, the total amount of harvestable biomass exceeds 400 million tonnes per year [31]. This enormous number however, cannot be utilized due to two main reasons: the lack of harvesting industries in Namibia and the limited domestic demand [31]. Currently, the harvested woody biomass is primarily employed as either fuel or animal feed, with limited alternative applications.

As of 2020, 1 million tonnes of EB were used for approximately 0.2 milliton tonnes of charcoal production [31]. Namibia is one of the main exporters of charcoal to Europe [4]. Namibian charcoal is considered a sustainable bio-fuel, however its uses are limited and its production capacity not enough to mitigate the bush encroachment phenomenon [4]. Firewood is another fuel produced, but the utilized EB is much less than the amount for charcoal (approximately 600.000 tonnes per annum) [4, 31]. In addition, besides a fuel, EB is also used as animal fodder, especially during dry season, as some species contain higher amounts of fibre [32]. However, it can be concluded that the current uses of the harvested EB cannot meet its growth rate, making its utilization highly important.

(a) (b)

Figure 2.3: Difference between de-bushed (thinned) (a) and bushed land (b) in Namibia [6].

2.2 Thermochemical Conversion Processes

Identifying the appropriate low-grade, waste biomass streams is the first step towards the production of a sustainable biofuel. However, the conversion process to achieve that, is perhaps one of the most critical steps. One of the more common ways to transform biomass into a valuable biofuel is through thermochemical conversion processes. Through those, biomass waste feedstock is converted to biofuels, chemicals, heat and power [8]. There are 3 main processes that can achieve that: Gasification, Fast Pyrolysis and Hydrothermal Liquefaction.

2.2.1 Gasification

As the name suggests, gasification is a process that produces a gaseous product called syngas, which is mainly CO and H_2 [34]. It is produced at high temperatures, $\geqslant$800 ^oC, by breaking down all the complex molecules of the feedstock (municipal solid waste, wood biomass or agricultural residues), into simpler ones, ending up with mostly CO and H_2. Syngas can be further converted to conventional liquid fuels such as gasoline, diesel and kerosene through the Fischer-Tropsch method [35]. Currently, most of gasification plants use coal as the main fuel, which makes the process not sustainable [36]. By using biomass feedstocks instead of coal, gasification can become a more sustainable method of producing fuels, however the types of biomass used must

be dry and be able to flow, while overall maintenance and energy efficiency challenges come up [34].

2.2.2 Fast Pyrolysis

Pyrolysis is a thermochemical process that takes place in high temperatures (400-600 ^{o}C) in an inert or very low oxygen environment, that decomposes the feedstock to liquid, solid and gas products [37]. Fast or Flash pyrolysis is focused in the maximum output of a liquid product, called BO or pyrolysis oil, by operating at approximately 600 ^{o}C but with very short retention times (0.5-3s) [34, 37]. This method is generally preferred for biomass feedstocks, due to liquid bio-fuels being more attractive and easily utilized [34]. The pyrolysis BO yields are usually high (60-80%) but the quality of the BO is considered to be of a low degree, due to its high oxygen and water content (>50% and 5-20% respectively) [12]. Fast pyrolysis has also some requirements such as low feedstocks moisture (≤10%) and particle size (≤3mm) [34], which limits its use for different types of biomass or increases pre-treatment costs such as drying and grinding/milling.

2.2.3 Hydrothermal Liquefaction

HTL is a thermochemical process that converts various types of biomass mainly into a liquid fuel, by mixing them with water (5-30% w/t dry biomass composition) at high pressures (5-22 MPa) and moderate temperatures (250-370 ^{o}C) [15], [11]. The end product is called biocrude oil, due to its resemblance to crude oil, in composition and form [11]. Besides biocrude, the initial carbon content is divided into 3 other products. The solid phase consisting of char and ash, the gaseous phase (mainly CO_2) and the aqueous phase containing small concentrations of polar organic compounds [9]. Due to the biomass slurry that is created, HTL can handle highly heterogeneous materials such as lignocellulosic biomass, algal biomass, municipal and industrial wastewater sludge [14, 15, 25, 28]. This gives a significant advantage over other thermochemical processes such as gasification and pyrolysis which require pre-treatment steps such as drying.

2.3 Hydrothermal Liquefaction

2.3.1 HTL main reactions

Hydrothermal liquefaction takes advantage of the property of hot compressed water, in which it remains liquid but in a sub-critical state. In this state, its viscosity and dielectric constant decrease, with the ionic product increasing, leading to water having a weak polar behaviour, which favours the solubility of organics [14, 15]. Gai et al. [38] proposed three reaction pathways for HTL: depolymerization, hydrolysis and decarboxylation. According to their report, hydrolysis and depolymerization initially break down the large macromolecules (carbohydrates, proteins and lipids) to monomers forming monosaccharides, amino acids and fatty acids. Via these two reactions, the aqueous phase is created consisting of polar organics (phenols, alcohols, acids). Decarboxylation then decomposes some of these monomers to amines, non-polar organics (alkanes, alkenes) and gases. The bio-crude oil and biochar are formed by the repolymerization of some of the smaller molecules, generating high-energy organic compounds. The pathways can be seen more analytically in Fig. 2.4.

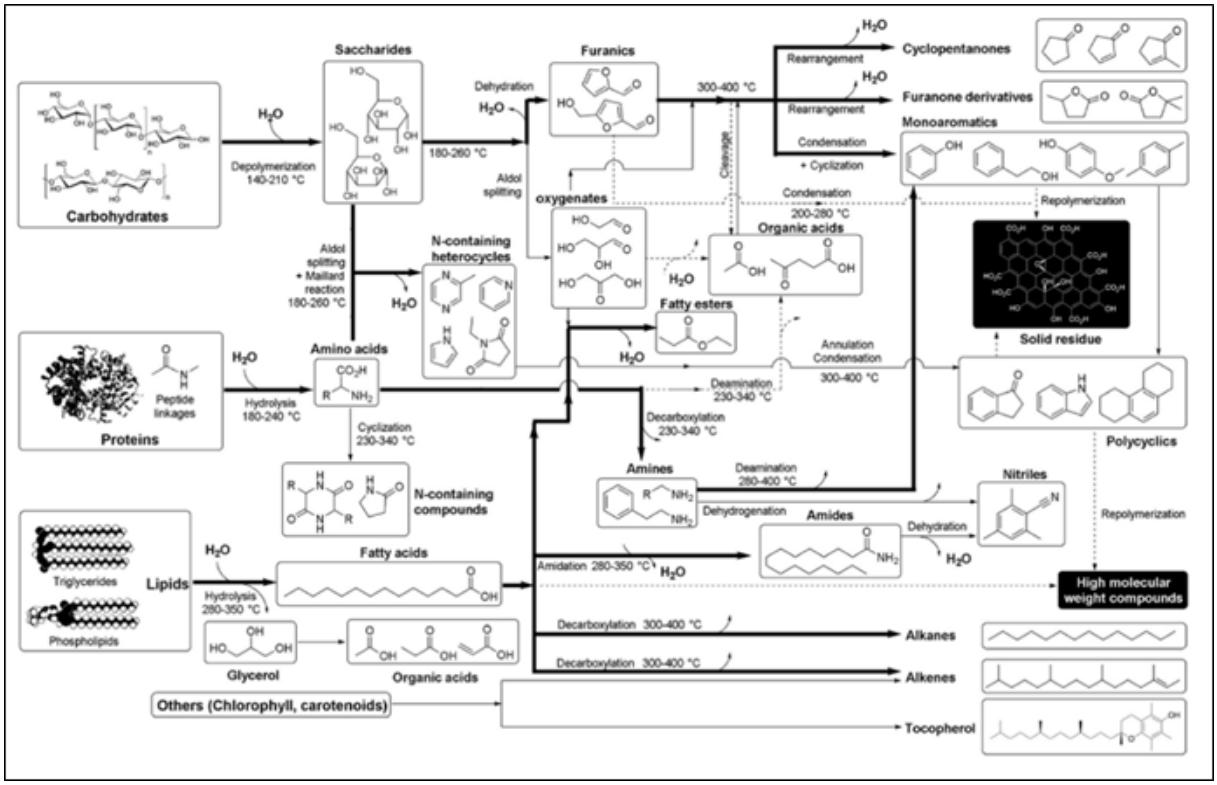

Figure 2.4: Reaction pathways of HTL for the 3 different macro-molecules [14, 39].

2.3.2 Lignocellulosic biomass HTL reactions

Lignocellulosic biomass is the most abundant feedstock worldwide [40], which makes it an attractive feedstock for HTL. With the term lignocellulosic biomass, we refer to the three major polymeric components this biomass consists of: cellulose, hemicellulose and lignin [41]. Their main compositions are usually 40–60%, 15– 30% and 10–25%, respectively [42]. Each one of these components, under HTL conditions, break down to form different compounds, which end up in the different process products [10]. In particular, cellulose is a polysaccharide which under HTL conditions, initially breaks down to glucose monomers and then further decomposes into mainly furfurals and hydromethyl furfural (HMF) [10]. Via ring opening, isomerization and dehydration reactions ketones and furanone derivatives are formed [39, 43]. Hemicellulose is composed from various sugar monomers such as xylose, glucose and arabinose [10], and under hydrothermal conditions performs similarly to cellulose, but decomposes easier [44]. Lignin is an amorphous aromatic polymer, which is not classified as a carbohydrate, protein or lipid [44]. The decomposition of lignin under hydrothermal conditions, produces various phenolic compounds, through hydrolysis and cleavage of the ether and C-C bonds. The degradation of cellulose, hemicellulose and lignin are shown schematically in Fig. 2.5.

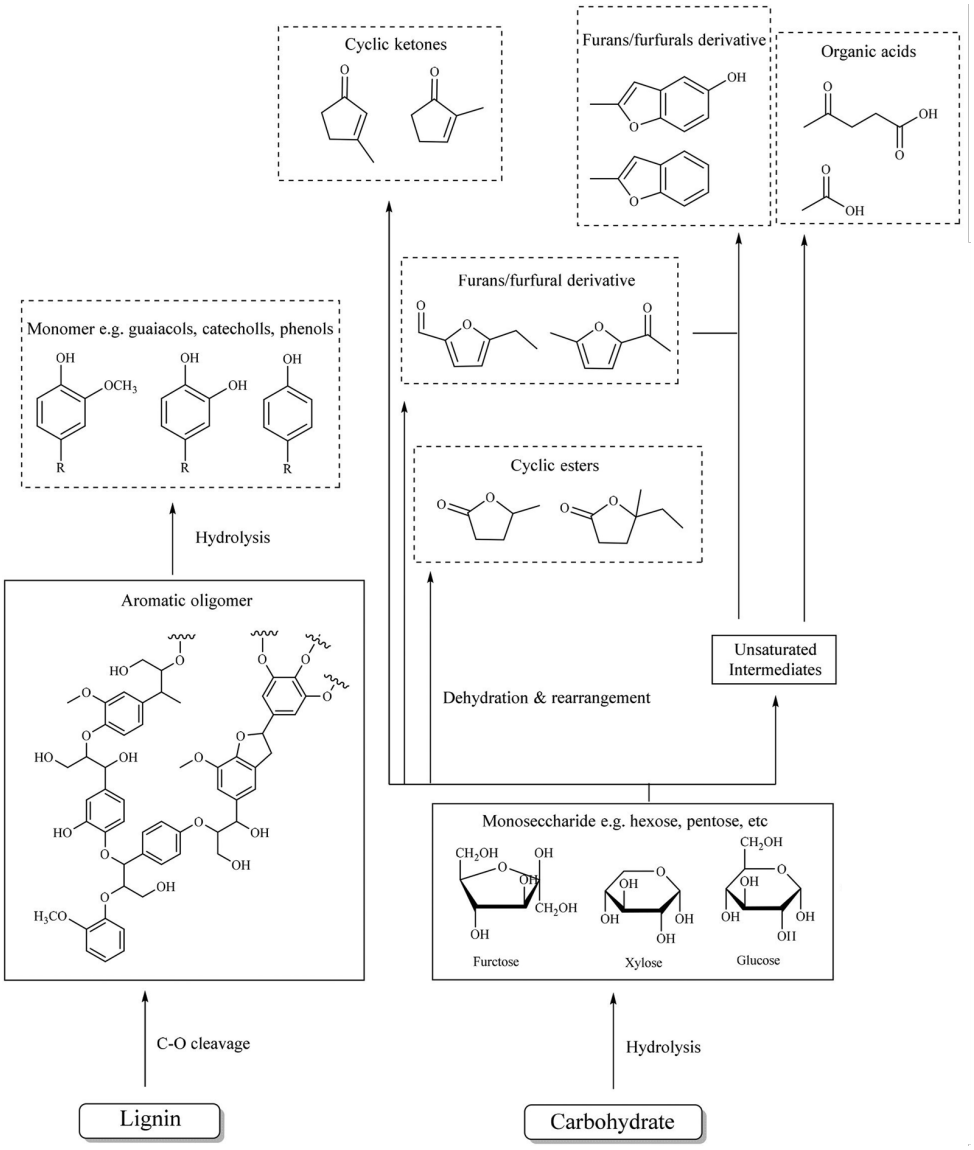

Figure 2.5: Simplified pathways for lignin and polysaccharides decomposition under HTL [45].

2.3.3 Lignocellulosic biomass as HTL feedstock

HTL is applicable for various types of biomass and it produces different quality BO for each one of them [15]. For lignocellulosic feedstocks in particular, due to their composition as mentioned above, they tend to have lower BO yields among other types, while algal biomass BOs have relatively higher High Heating Value (HHV). To assess that difference in a more accurate way, Energy Recovery (ER) ratio is used (see eq. 2.3.1), which quantifies the percentage of the feedstock's initial energy content that went into the bio-oil. Table 2.1 shows that algae feedstocks can provide high ERs, (up to 86.5%) due to their lipid and low oxygen content [46], which produces high BO yields, consisting of de-oxygenated compounds such as alkanes and alkenes (see Fig. 2.4) of higher calorific value. Lignocellulosic feedstocks ER is lower, around the 50% mark, which is caused by the nature of the feedstocks, resulting into BOs with high oxygen content (up to 30%) [25], which reduce the HHV. However, lignocellulosic biomass has little to no nitrogen content compared to algae and is already available and abundant [43], with no need for cultivation, which is a significant advantage for a scaled up process.

$$ER = \frac{HHV_{bio-oil}}{HHV_{feedstock}} * \text{BO}\% \tag{2.3.1}$$

Table 2.1: Non-catalytic HTL BO yields and calorific values for different types of feedstocks.

Type of biomass	BO yield (%)	HHV (MJ/kg)	ER (%)	Reference
Algal biomass				
Spirulina platensis	39.9	35.3	68.6	[47]
Arthrospira platensis	30.0	38.7	46.3	[48]
Nannochloropsis Sp	54.2	37.7	86.5	[39]
Macroalgal blooms	14.3	23.3	36.1	[49]
Lignocellulosic biomass				
Eucalyptus	33.0	31.7	57.6	[26]
Wheat straw	26.0	35.3	55.4	[26]
Birchwood sawdust	19.0	29.0	32.6	[50]
Miscanthus x giganteus	30.0	29.6	51.2	[28]
Manures				
Cow manure	41.0	31.0	66.5	[51]
Swine manure	30.2	34.7	53.2	[52]

2.3.4 HTL products and applications

Bio-oil

Bio-oil or bio-crude oil is the target product of the hydrothermal liquefaction process [17]. It contains a wide range of organic compounds, such as straight and branched aliphatic compounds, aromatics and phenolic derivatives, carboxylic acids, esters and nitrogenous organics [52]. These compounds are derivatives from the decomposition of proteins, lipids, carbohydrates and lignin [43, 53]. It is a viscous and dark liquid with a calorific value ranging from 25-38 MJ/kg [17, 18], depending on the process conditions and type of feedstock. In general, the high content of hetero-atoms (i.e. oxygen, nitrogen and sulfur) lowers its quality and make its use in a conventional combustion engine impossible [52]. Furthermore, the high oxygen content makes it prone to polymerization and unstable under storage conditions [54]. Even though the typical HTL process uses water as solvent, the final water content of the oil is quite low (<1%) compared to pyrolysis oils which can be 10-20% [12]. With the appropriate post treatment upgrading through hydrodeoxygenation (HDO), fluid catalytic cracking (FCC) and hydrotreating, the final product contains much higher HHV, lower oxygen and nitrogen content and is much less viscous [55, 56]. Another option for final use can be the production of bio-phenolic or epoxy resins, if the phenolic content of the biocrude oil is high [57, 58]

Biochar

Biochar is the solid by-product of the HTL process. It is a charcoal-like bio-fuel with much increased carbon content compared with raw biomass [59]. It is usually neglected from HTL studies, which solely focus on the optimization of BO production [59]. That is because BC is a difficult bio-fuel to handle, store and utilize for the transportation sector [34]. Nonetheless, recently there has been increased attention regarding other pathways of valorizing it. In particular, it is considered a mesoporous substance [59], which can be utilized as an adsorbent. Some studies used BC as heavy metals and dye adsorbent with success [60, 61] and performance similar to activated carbon [61]. Another interesting application is the use of BC as an additive for anaerobic digestion, which has showed it can increase methane production and improve COD removal [62]. An application with even more potential however, is the soil amendment one. By sequestrating BC in soil, there is a crop productivity and soil quality is enhanced [63]. Additionally, it reduces nitrogen losses, improves nutrient retention, and stimulates root growth [63, 64]. As a fertilizer, it enhances soil fertility, remediation of polluted soils, and improves various soil properties such as bulk density, pH, water holding capacity, and cation exchange capacity [63].

Aqueous phase

AP is considered a by-product of the HTL process, consisting of mainly water and light polar organics such as acids, alcohols and phenols, and inorganic compounds (K, Na, Mg, Al, Ca and Fe) [65]. Due to the organics concentration, the COD concentration is high (24-85 g/l) making it difficult to treat directly via anaerobic digestion, where usually the total COD loading is lower (up to 10 g/l) [65]. Besides recycling it in the HTL process, the AP solution can be valuable based on the post treatment it receives. Chemicals such as acetic acid, ethanol and phenol can be separated and used in other industries, while nutrients (N, P and K) can be used for fertilizer production [65]. In addition, biological conversion with the appropriate pre-treatment, can yield hydrogen and methane, with low operating costs and sludge production [65, 66].

Gas phase

The HTL process additionally produces a gaseous phase, which mainly consists of CO_2 gas [15]. That concentration can range from 75-95% depending on the feedstock, with other gases such H_2, CO and CH_2 following [67]. The source of carbon in the gas phase derives from the decomposition of oxygen-containing groups via decarboxylation and decarbonylation reactions [44]. Due to the high CO_2 amount, the gas phase is the least valuable to the process, but can still be a useful heat integration stream in a scaled up process or be used as a fertilizer in greenhouses [44].

Table 2.2: HTL products applications based on their characteristics.

Type of product	Characteristic	Upgrade required	Application
Bio-oil	High alkane and alkene concentration, low oxygen (<10wt%) and nitrogen content (<1%)	Hydrodeoxygenation (HDO)	Replacement of heavy oil in cargo ships, drop-in biofuel
	Intermediate oxygen content (10-25wt%), mostly aromatic compounds	HDO, fluid catalytic cracking, hydrocracking, hydrotreating	Sustainable gasoline, diesel and jet fuels
	High oxygen content (>25wt%), high amount of phenolic compounds (>50wt%) and OH groups, fatty long chain acids	Mix with petroleum based phenol/ epichlorohydrin (ECH)/ NaOH, fractionation	Bio-phenol and bio-epoxy resins, other chemicals
Biochar	High calorific value, high carbon content, low nitrogen and sulfur content, low moisture content	Catalyst recovery via leaching and separation	Replacement of coal or lignite for power generation and gasification
	High surface area, higher volatile matter (more polar functional groups)	-	Metal or dye adsorbent
	Low heavy metal concentration, nutrient content (N, K and P)	-	Carbon sequestration, soil amendment
Aqueous phase	High in macronutrients (N, P, K), heavy metals, phenols, organic acids	Nutrient and metal recovery, anaerobic digestion, recycling	Fertilizer, metals, biogas production, used as catalyst
Gas phase	High CO_2 concentration (90-95%)	Water scrubber	Fertilizer for greenhouse use, heat recovery stream

2.3.5 Catalytic HTL

Due to the fact that HTL's main product is the BO, the goal is to maximize its yield, quality and lower the intensity of operational conditions. Normally, the yields, especially for lignocellulosic biomass, do not exceed 35wt% (as seen on Table 2.1) but also the high amount of oxygenated and nitrogen compounds curb the overall quality of the product. To overcome this issue the addition of catalysts has been attempted and showed great results.

Two categories of catalysts have been tested, homogeneous and heterogeneous. Homogeneous catalysts are mostly carbonates and hydroxides of alkali metals (Na, K and Ca) which are easily dissolved in the water [16], while also acids such as formic, acetic and hydrochloric [17]. They have shown to increase BO yield significantly, reaching yields up to 61wt% [16, 23, 68]. The other category is heterogeneous catalysts which are split into transition metals (Ni, Mn, Co...) and their oxides (NiO, MnO, Co_3O_4...), alkaline earth metals (CaO, Colemanite, MgO...), lanthanide oxides (La_2O_3, Dy_2O_3 and CeO_2) and zeolites [18]. Most recent studies focus on the

use of heterogeneous catalysts due to their high activity, selectivity and recyclability compared to the homogeneous ones [16].

Table 2.3: General information regarding the different types of catalysts used in HTL.

Type of catalyst	**Main properties**	**Causes for deactivation**
Transition metals	Active in oxidation, hydrogenation and isomerization reactions [18, 69]	Coke formation, adsorption of phenolic derivatives on active sites [70]
Alkaline earth metals	Alkaline pH promotes decomposition of carbohydrates [71]	Neutralization of basic sites due to low pH [72]
Lanthanide oxides	Act as base, resistance to coke deposition, promote deoxygenation [73]	CO_2 production can poison the catalyst and deactivate it [18, 74]
Zeolites	Acidity and shape selectivity promotes deoxygenation, dehydrogenation, cyclization and aromatization [75]	Coking that blocks the pores [75]

Predicting the behaviour of a catalyst for its performance in HTL is complex, due to the complexity of the process itself. In Table 2.3, some general information about the functionality of the aforementioned types of catalysts are shown. While all of them seem to promote reactions that are necessary for breaking down complex compounds like lignin and cellulose, there are also plenty of causes for their deactivation. Transition metals in particular have been thoroughly tested in HTL experiments, but the nature of the BO itself (viscous and sticky) [70] is more likely to block their active sites and reduce activity. Moreover, the alkaline types of catalysts can be deactivated, due to the low pH and high Total Acidic Number (TAN) of the BO [12].

Table 2.4: Comparison of parameters and effect between different heterogeneous types of catalysts for HTL.

Type of catalyst	**Average change in BO yield (%)**	**Average HHV change (%)**	**Sustainability & Safety**
Transition metals	35	20	**Very Low**: Lack of abundance [76], unwanted accumulation on BC, can be toxic and carcinogenic [77]
Alkaline earth metals	40	-10	**High**: Abundant, do not contaminate BC, non-toxic
Lanthanide oxides	33	18	**Low**: Rarer than transition metals, unwanted accumulation on BC, non-toxic [78]
Zeolites	-20	15	**High**: Sustainable and available [20], non-toxic, do not contaminate BC

In Table 2.4 a comparison between the different categories of heterogeneous catalysts is being shown, including varying factors, from HTL performance to sustainability. There is not a clear option for the "best" or most appropriate type of catalyst. More sustainable ones such as zeolites, seem to not perform well on HTL (lower BO yields than without it), while transition metals, which are much rarer and more toxic [76], give out the best results according to literature. Alkaline earth metals can potentially be a better option, due to their positive effect on BO yield and their overall higher sustainability, but their negative effect on the HHV is not desirable.

3| Materials and Methods

3.1 Design of Experiments

3.1.1 Catalyst screening campaign

For the screening experimental campaign, four different catalysts were used, one of each type: nickel on silica alumina (Ni/SiO_2-Al_2O_3), lanthanum oxide (La_2O_3), Hydrotalcite and ZSM-5 (zeolite type). The Ni/SiO_2-Al_2O_3 catalyst was chosen as it has already been used in HTL experiments with the same experimental setup but with different type of biomass providing high bio-crude oil yields [18]. This is due to Ni/SiO_2-Al_2O_3 promotion of hydrogenation reactions, which produces high concentrations of hydrocarbons and ketones in the bio-crude oil [68] and foster H_2 production in the gas phase by means of redox reactions [18]. The La_2O_3 and hydrotalcite were selected based on the findings from [18, 73], who report high bio-crude oil yields compared to other lanthanide oxide catalysts (e.g., CeO_2 and Dy_2O_3) or heterogeneous alkaline earth metals based catalysts (e.g., MgO and $MgMnO_2$). La_2O_3 has basic sites that can break cellulose hydrogen bonds, increases hydrolysis and cracking processes, and suppresses dehydration reactions [73]. Meanwhile, hydrotalcite catalyst is reported to increase the bio-crude oil yield by 82% compared to experiments without catalyst [50]. Finally, ZSM-5 increases the bio-crude oil yield due its acidity and shape selectivity [18], hence its selection. Overall, five experiments were performed in duplicates with the same experimental conditions, a non-catalytic one and 4 for each type of catalyst. The HTL operational conditions were 300°C, 15 mins residence time, 15 wt% dry biomass load and 5 wt% catalyst loading. This based on results from previous studies [79, 80] who report maximum bio-oil production at this operational condition. The final selection of the catalyst was a combination of BO yield, HHV and its potential impact on the environment. To quantify the effect on the yield and HHV, ER was used, as shown in eq. 2.3.1.

3.1.2 Optimization campaign: Central Composite Design

As already mentioned, HTL performance is a multi-variable problem. Therefore, in order to be optimized, an appropriate procedure should be followed. A Design of Experiments (DOE) is *"a branch of applied statistics concerned with the planning, execution, analysis, and interpretation of controlled tests to determine the factors that influence the value of a parameter or group of parameters"* [81]. Essentially, a DOE can manipulate different factors and parameters to determine a desired output (response) [81]. There are different types of designs that can be used, such as the two-level factorial, central composite design, optimal design and mixture designs [81]. However, a DOE is not enough by itself, as in a multi-variable problem the total number of combinations between the factors, is going to be too large. That is why a Response Surface Methodology (RSM) can be used to reduce the total experiments down to the only ones necessary, while indicating which parameters are more significant than others [80].

CCD is one of the more common RSMs that is used for optimizing a certain target response by taking into account the influence of other synergistic parameters [80]. The design incorporates a factorial or fractional factorial pattern with center points and includes an additional set of "*star points*" that enables the evaluation of curvature [82]. For the present report, a 3-factor design was chosen, with the 3 factors being temperature, residence time and catalyst loading,

in order to maximize BO yield. Software Design-Expert was used to create a CCD cube, as seen in Figure 3.1. This produced 20 experimental points with random executing order and combinations of the 3 factors, as shown in Table A.3.

With the collection of the results (BO yields), a quadratic equation was suggested as the best fit from Design-Expert, with the following structure:

$$Y = a_0 + \sum_{i=1}^{3} a_i X_i + \sum_{i=1}^{3} a_{ii} X_i^2 + \sum_{i=1}^{3} \sum_{i<j} a_{ij} X_i X_j \tag{3.1.1}$$

Where:
Y: predicted value of BO yield,
X_1, X_2, X_3: temperature, residence time and catalyst loading respectively,
α_0: intercept
α_i, α_j, $\alpha_i j$: coefficients of linear, quadratic and terms respectively

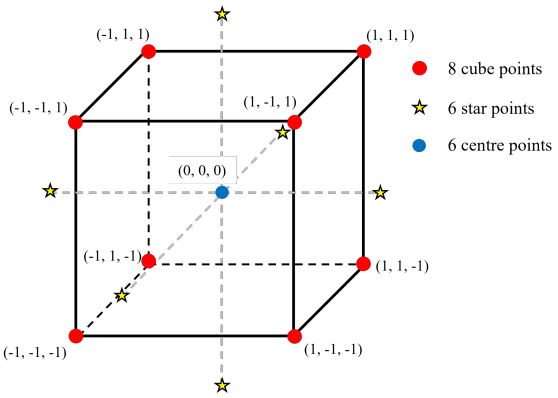

Factors	Levels				
	-1.633	**-1**	**0**	**1**	**1.633**
Temperature (^{o}C)	250	270	300	330	340
Residence time (min)	5	10	15	30	60
Catalyst loading (wt%)	0	2.5	5	7.5	10

Figure 3.1: Cube of CCD (left) and levels of each factor (right).

3.2 Hydrothermal Liquefaction experimental procedure

The type of Encroacher Bush (EB) used as feedstock for the HTL experiments was *Acacia Mellifera* obtained from Namibia. It was received in a shredded form with a maximum particle size of 4cm. EB was not grinded further more.

3.2.1 Slurry preparation

Before the start of the experimental run, the slurry containing biomass, water and potentially catalyst needed to be made. For that, the Maximum Allowable Water Loading (MAWL) of the autoclave vessel (reactor) was calculated based on the instructions manual from Parr, the reactor's manufacturer. Then for safety reasons, 80% of MAWL was taken as the total slurry mass. In order to accurately create the mixture, *Acacia Mellifera's* moisture content was determined every time before each run, based on the analytical procedures of National Renewable Energy Laboratory (NREL), namely TP-510-42621. The dry biomass concentration was 15wt% for every experiment, thus wet biomass was weighed accordingly. Milli-Q water was used as solvent for the slurry and added so the biomass to water ratio is approximately 15wt%. Finally, the catalyst was added when needed, with each concentration being on a dry biomass basis ranging from 0-10wt%.

3.2.2 HTL experimental run

The HTL experiments were performed in a pressurized 300-mL autoclave mini-reactor (Parr Instrument Company, IL., USA., Series 4560), with temperatures varying from 250-340^{o}C and retention times of 5-60 minutes. Initially, the reactor was purged and then filled with nitrogen

to obtain an inert environment. During its operation, the pressure rose according to the temperature increase, reaching 85-110 bar (depending on the catalyst loading and temperature). The reactor was then cooled first with a warm water bath and an ice bath afterwards. The gases produced were released in the fume hood and not collected. The slurry was placed into beakers for further analyzing.

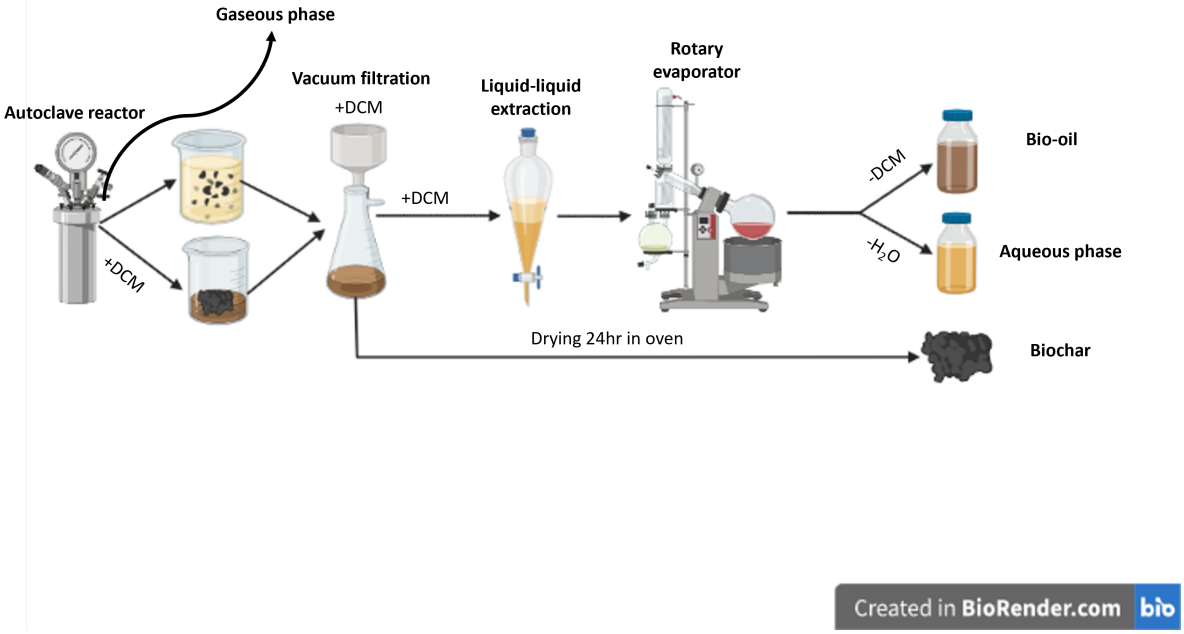

Figure 3.2: Experimental procedure flowscheme for the HTL experiment.

3.2.3 Collection of each phase

After the completion of the experimental run, there were 2 visible phases, a liquid and solid one. The solids in the reactor and the leftovers on stirrer were removed using Dichloromethane (DECM, Sigma-Aldrich 99.8% purity). The solids phase contained BC and BO. The separation of the BC from the liquid phase was performed via vacuum filtration with a buchner funnel with a 2.5μm pore size filter paper (Whatman Grade 5). The BC wet cake was rinsed with DCM to extract the oil and then dried in 105^{o}C for 24hr (Furnace Nabertherm 30 - 3000 °C). As seen from Figure 3.2, after the filtration two liquid phases were collected, one oily (containing BO and DCM) and an aqueous one. In order to recover the maximum amount of oil contained in the AP, a liquid-liquid extraction in a separatory funnel was performed with the addition of DCM to assist the separation. Finally, DCM and water were removed via a rotary evaporator from the oily and AP respectively, to finally obtain the BO and polar organics and close the total mass balance. For ease of understanding, the concentrated polar organics will still be referred to as AP. HTL product yields were calculated with he following equations:

$$BO\ yield(\%) = \frac{m_{BO}}{m_{dry}} * 100\% \tag{3.2.1}$$

$$BC\ yield(\%) = \frac{m_{BC}}{m_{dry}} * 100\% \tag{3.2.2}$$

$$AP\ yield(\%) = \frac{m_{AP}}{m_{dry}} * 100\% \tag{3.2.3}$$

$$Gas\ yield(\%) = 100\% - BO\ yield(\%) - BC\ yield(\%) - AP\ yield(\%) \quad (3.2.4)$$

Where: m_{dry}: mass of dry EB
m_{BO}, m_{BC}, m_{AP}: measured final mass of BO, BC and AP

3.3 Feedstock and product characterization

EB, BO and BC were characterized in order to gain more in-depth information about the performance of the HTL experiments. The methods that were performed are described in the following sections.

3.3.1 HHV - Bomb Calorimetry

Bomb calorimeter Model 1341 (Parr Instrument Company, IL., USA) was used for the measurements. For the solid fuels (EB and BC) approximately 1.0g was weighed and pelletized. The bomb was charged with 26 bar(g) of oxygen and after ignition the sample was combusted. The final value of HHV was displayed on the screen. For the liquid BO, the procedure was sightly different. A small amount of cotton of known calorific value was dipped into 0.5g of oil and then combusted with the same process. The final HHV was calculated by subtracting the cotton's HHV by the one calculated from the machine.

Due to the stoichiometric combustion reaction, water vapor is also produced together with CO_2. Therefore, when referring to the HHV, the water vapor condensation energy is also included, besides the combustion heat.

3.3.2 Proximate and CHNO Analysis

Proximate analysis gives the composition of Moisture Content (MC), Ash, Volatile Matter (VM) and Fixed Carbon (FC) in a solid sample, thus it was only performed on EB and BC. Methods TP-510-42621, TP-510-42622 and ASTM D3175-20 were used for MC (total solids), ash and VM respectively. Fixed carbon was calculated by difference.

The moisture content method includes drying the sample for 24hr at 105°C and then calculating the total mass loss, which can either give the water content or the total solids in the sample. Ash determination method was performed through dry oxidation of the sample at 575°C, where a Nabertherm 30-3000°C muffle furnace was used. Volatile matter was measured via Thermogravometric Analysis (TGA).

CHNO analysis gives information about the sample's main elements' composition: carbon, hydrogen, nitrogen and oxygen (CHNO). EB, BO and BC samples were sent to Intertek Belgium N.V. for analysis where the ASTM D5291 standard was followed.

3.3.3 Products composition determination

BO consists of various organic compounds, with unknown composition. Moreover, BC's heavy metal composition is very important to know, in order to assess its quality for future use, such as soil amendment. Thus, this section is going to describe the methods used for analysis.

Gas Chromatography - Mass Spectrometry (GC-MS)

The samples for GC-MS analysis were prepared by diluting the BO with 2-propanol (VWR Chemicals) on a 1:10 mass ratio. Then filtration followed, using a syringe 0.2 μm PTFE filter (Whatman Puradisc 13). The GC-MS was carried out using an Agilent 8890 gas chromatograph (Agilent Technologies, Wilmington, USA) equipped with an HP-5MS column from Agilent (model: USR577054H), a split-splittles liner (Agilent 5190-2295) and coupled with both mass spectrometer detector. The detailed routine for GC-MS can be seen in the report from Brandi et al., 2021 [83].

Water content of bio-oils

The water content of the bio-oils was determined via Karl-Fischer Titration using an 831 KF Coulometer (Metrohm, Herisau, Switzerland). For this, a sample of bio-oil of around 1 mL was injected into the titration vessel. Once the endpoint was reached, the value of the water content was recorded along with the mass of the sample being injected. The measurements were performed in duplicates.

X-Ray Diffraction (XRD)

BC and EB samples were measured via XRD. XRD patterns were obtained using Bruker D8 Advance diffractometer Bragg-Brentano geometry Lynxeye position sensitive detector and Cu Kα radiation with the following measurement method: Diffraction patterns were scanned with 2ϑ range of 5° to 80°, step size 0.020° 2ϑ, and counting time per step 1.25 s.

Inductively Coupled Plasma-Optical Emission Spectroscopy (ICP-OES)

EB and BC samples were prepared by digesting approximately 0.1g solid and diluting it in 1:3:1 volume ratio of water, hydrochloric acid and nitric acid respectively. Data for elemental composition were acquired using a Spectro-Arcos EOP combined with Spectro Smart Analyzer Vision software.

4| Results and Discussion

4.1 Feedstock Characterization

Table 4.1: Proximate and Ultimate analysis of *Acacia Mellifera*

.

MC (%)	Ash(%)	FC[a](%)	VM(%)	HHV (MJ/kg)[b]	C	H	O[a]	N
9.42 (0.21)[c]	1.26 (0.05)	23.22 (0.13)	75.52 (0.13)	19.34 (0.28)	44.78	6.44	45.76	1.87

[a] Calculated by difference
[b] Dry basis
[c] Values in parenthesis correspond to standard deviation

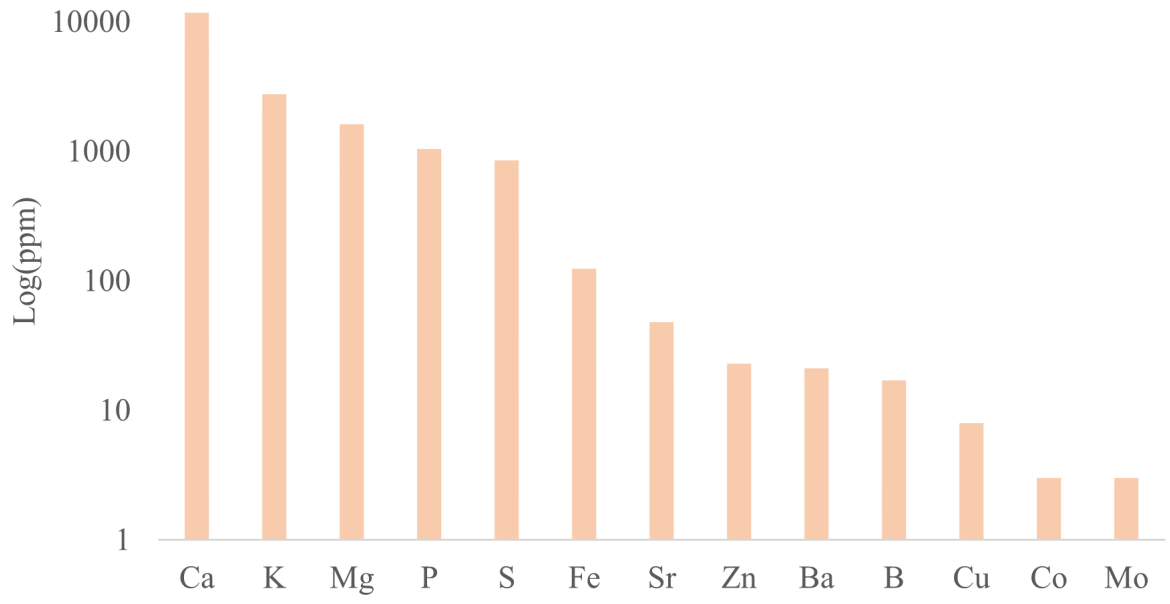

Figure 4.1: ICP-OES elemental composition for raw EB. The scale is logarithmic for better illustration.

The proximate analysis of the feedstock resembles a woody type of biomass [84], containing high amounts of VM and very low ash content. Moisture and ash content are similar to other bush and *Acacia* species (5-10% and 1-5% respectively) [85]. EB's ultimate analysis places it within the typical ranges for C, H, N and O for a lignocellulosic biomass, according to literature [11, 84]. Figure 4.1 shows the mineral and metal composition of EB in logarithmic scale in order to visualize the big differences between them. Sulphur is present in low concentrations (0.08 wt.% from table A.5). The most prominent elements are Calcium, Potassium and Magnesium

which belong to alkaline earth metals. Heavy metals such as Zinc, Cobalt and Molybdenum are at very low concentrations (<30ppm). The ICP-OES analysis results reveal that EB is a "virgin" type of feedstock, as it hasn't been polluted with metals coming from human activity such as Nickel, Chromium, Cadmium etc [86], reducing the complexity of potential downstream processing.

4.2 Catalyst screening campaign

In this chapter, the results of four different catalysts that were used in HTL will be presented. The BO and BC produced were characterized using various methods in order to assess the performance of each catalyst on the quality and yield of BO. Based on this comparison, a selection for the best overall performing catalyst was made.

4.2.1 Product distribution for each catalyst

The effect of the 4 catalysts on the product distribution of HTL is shown in 4.2. The presence of a catalyst can greatly affect which product and by-product is favoured [17]. Homogeneous catalysts tend to enhance depolymerization of the feedstock, thus increasing the yield, while heterogeneous catalyst are more prone to deoxygenation of BO, improving its quality [17]. Nevertheless, the 4 heterogeneous catalysts were chosen due to their advantages in terms of recovery, recyclability and corrosivity [16, 17].

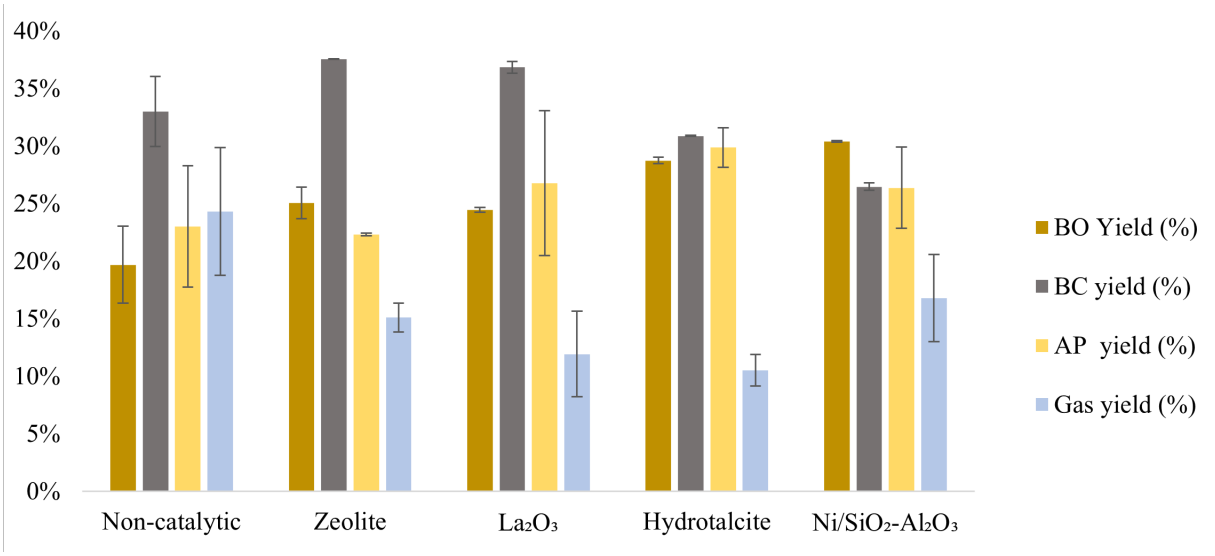

Figure 4.2: Product distribution for the 5 samples of the catalyst screening campaign. Operating conditions where 300^{o}C, 15min and 5wt% catalyst (except non-catalytic).

As it can be seen in Figure 4.2, all catalysts caused an increase in BO yield, in comparison with the non-catalytic sample. The highest effect was achieved by the Ni/SiO_2-Al_2O_3 catalyst, which yielded 30.4wt% biocrude oil, while the lowest yield was obtained when no catalyst was used, 19.7wt%. Overall, there is an increase between 24% (La_2O_3) to 54% (Ni/SiO_2-Al_2O_3) in the BO yield in comparison to not using a catalyst. Therefore, the addition of catalysts improved the C-C cleavage of structural compounds in biomass due to the acidity (zeolite and Ni/SiO_2-Al_2O_3) or alkalinity (La_2O_3 and hydrotalcite) and porosity of these materials [50, 71].

The highest BC yield was achieved using the zeolite catalyst, 37.6wt%, while the lowest using Ni/SiO_2-Al_2O_3, 26.5wt%. It is also observed that compared to the other HTL fractions, BC production is dominant, except for the Ni/SiO_2-Al_2O_3 sample. Nickel catalyst's low BC yield is attributed to the properties of the catalyst itself which prevents the repolymerization of biochar and enhances the bio-oil yield [87].

Hydrotalcite had the highest AP yield with an average value of 29.9 wt% and zeolite the lowest at 22.3wt%. These results are in agreement with findings from Nazari et al. [50], where hydrotalcite increased the AP yield compared to non-catalytic experiments mainly due to the alkalinity of the catalyst [17]. Regarding the zeolite, Yan et al. [21] also reported a reduction in the AP yield, which could be a result of its acidity [17].

Gas yields were on average the lowest among the other products. Hydrotalcite had the lowest yield, 10.5wt%, and non-catalytic the highest, 24.3 wt%. The overall lower values compared to other products, are attributed to the HTL reaction temperature (300^{o}C), which is sub-critical and favours more the BO production, instead of gas production [11, 46].

4.2.2 High Heating Value (HHV) of BOs

In Figure 4.3, a comparison between the 5 samples HHV is shown, which gives a more informative view regarding the trade-off of choosing an appropriate catalyst for HTL.

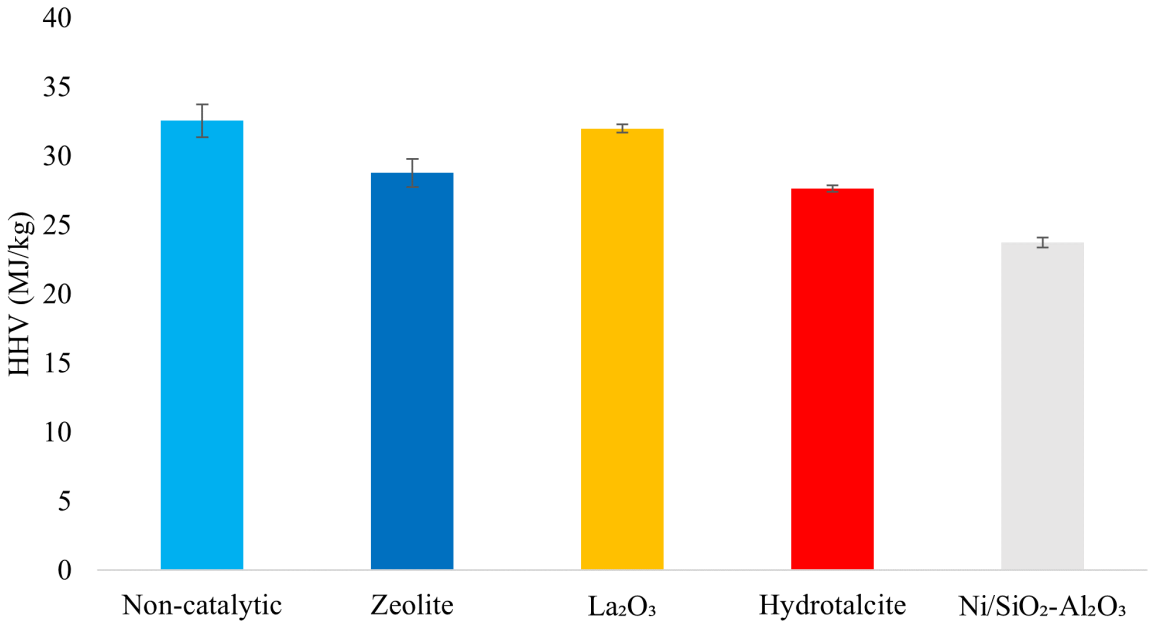

Figure 4.3: Effect of different catalysts on the BOs HHV.

The trend of the BO yield is already known from the previous section (see section 4.2) however HHV gave an opposite effect, where the highest HHV was obtained using no catalyst, 32.5 MJ/kg, while catalysts reduced it. The BO with the lowest calorific value, 23.7 MJ/kg, was the Ni/SiO_2-Al_2O_3 sample. The La_2O_3 catalyst provided a good HHV of 32.0 MJ/kg, very close to the non-catalytic sample. All the 4 catalysts reduced the HHV of the BO compared to the non-catalytic experiment, which contradicts literature findings for the zeolite and La_2O_3 [21, 88]. A reason for this difference could be that in those reports, HHV is calculated by an equation based on the CHNO composition and not through a bomb calorimeter. Hydrotalcite and Ni/SiO_2-Al_2O_3 on the other hand behaved similarly to Nazari's et al. [50] and Misar's [22] results respectively, which reported a 5 MJ/kg and 4 MJ/kg decrease in HHV for same operating conditions.

4.2.3 Catalyst effect on CHNO composition of the BOs

The CHNO analysis of bio-oil can provide a useful insight about its quality. Typically, BOs with with high amount of C and H but low O and N content are preferred [12]. The presence of oxygenated compounds in BO causes instability, low heating value and high corrosiveness [73],

while N-containing compounds can lead to unwanted NOx emissions and poison the catalyst [17, 84].

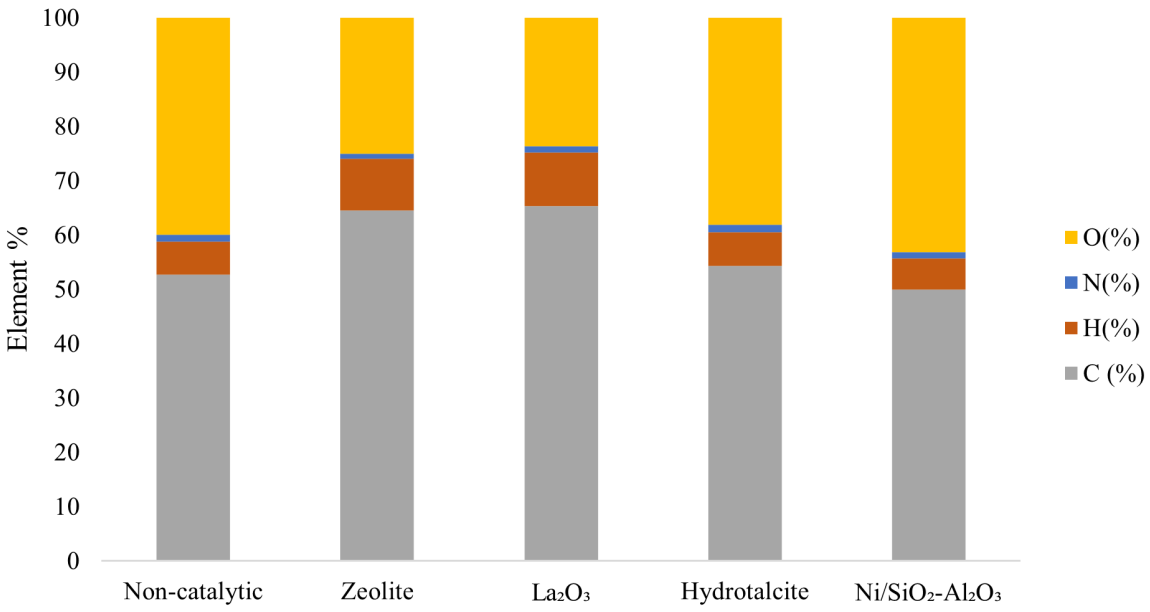

Figure 4.4: Effect of different catalysts on the BO's CHNO composition.

According to Figure 4.4, La_2O_3 BO provided the highest C content (65.3wt%) and lowest O content (23.6wt%) compared to the rest of the BOs. On the other hand, Ni/SiO_2-Al_2O_3 BO had the lowest amount of C and the highest O content, 50.0wt% and 43.2wt%, respectively. Additionally, the BO with La_2O_3 contained the highest amount of H, at 9.9wt%. Zeolite BO had similar CHNO composition with the La_2O_3 sample. The N content in all the biocrudes was similar to raw EB, with the zeolite one having the lowest at 0.9wt%.

In general, dehydration and decarboxylation reactions remove H_2O and CO_2 molecules respectively, leading to deoxygenation of the product [10]. La_2O_3 enhanced hydrolysis and cracking reactions improving the quality of the bio-crude oil and backing up the findings reported in [18, 73]. Hydrotalcite's small decrease of oxygen is also in accordance with literature, as it mostly favours dexarboxylation reactions but overall it has not shown good oxygen removal efficiency [18, 50]. The Ni/SiO_2-Al_2O_3 catalyst increased O content and reduced C content. This is attributed to hydrogenation reactions which could have cracked down the lignin polymer, thus fostering the production of oxygenated - phenolic compounds, which increase O content and reduce HHV [68], despite the total increase of the BO yield. The results of the CHNO analysis indicate that the La_2O_3 produces the best quality BO, but also confirm the theory that removal of oxygen from lignocellulosic feedstock BOs is less efficient than with algal ones [28].

4.2.4 Bio-oil GC-MS results for different catalysts

GC-MS was performed for the 5 samples of the catalytic campaign in order to get insight of their effect on the chemical composition of the biocrude oil. In Figure 4.5 the composition of main categories of organic compounds is presented.

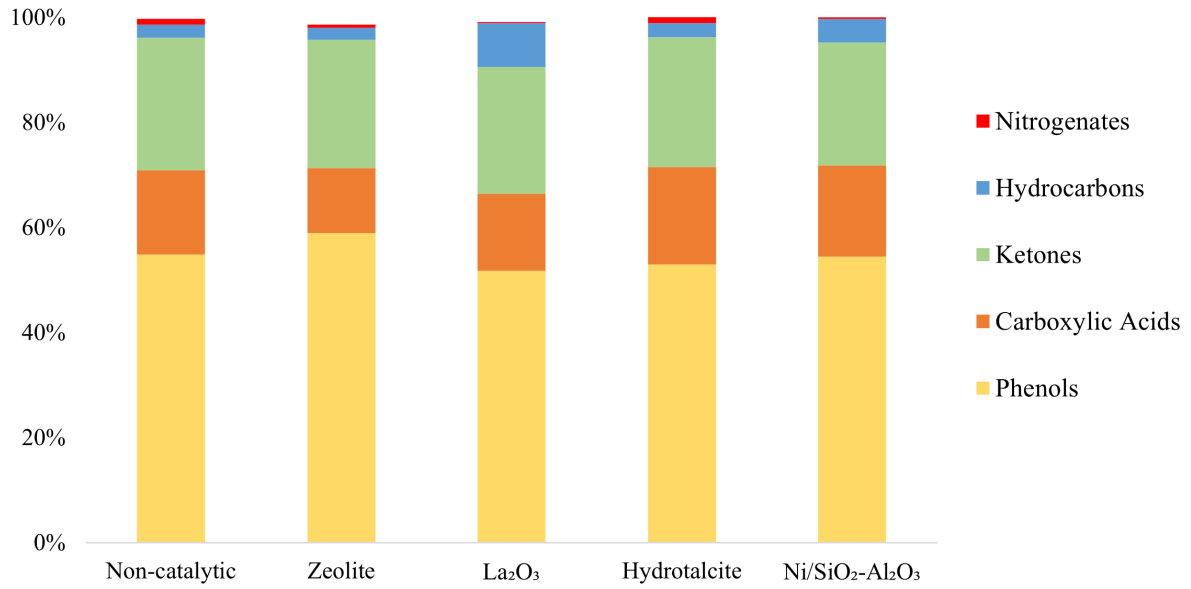

Figure 4.5: Main organic compounds composition based on GC-MS results

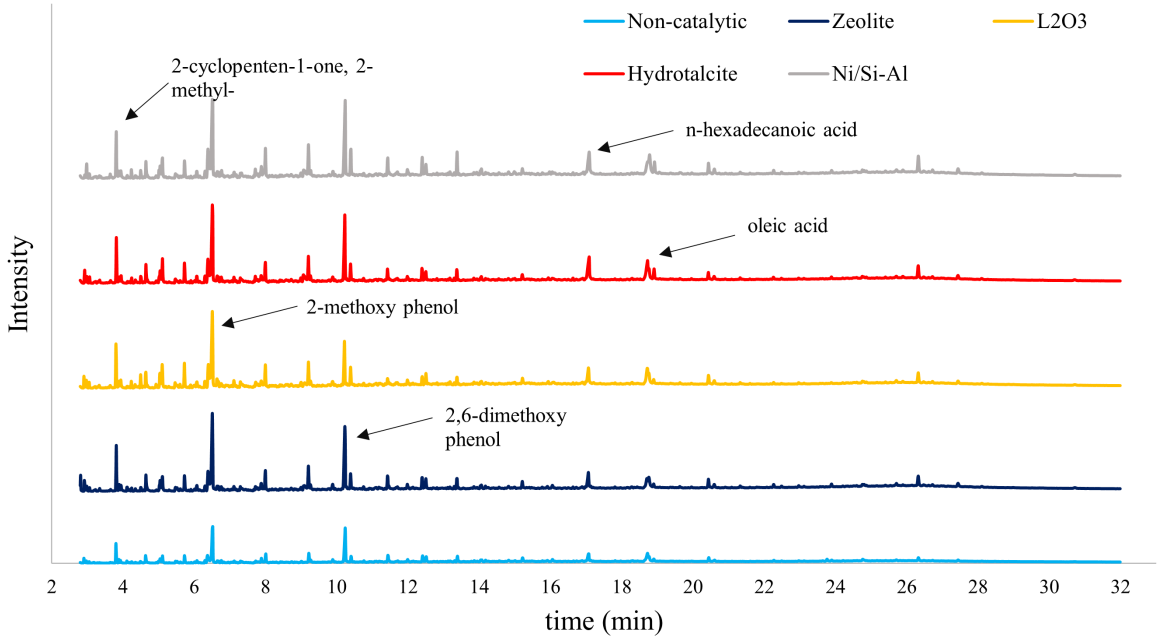

Figure 4.6: GC-MS peaks for each different catalyst. The 5 main components and their structure are shown below together with their residence time.

As it can be observed in Figure 4.5, the most prominent category found in all samples were phenols. This result is in accordance with literature using lignocellulosic feedstock via HTL, where catalysts promote decarboxylation reactions but are not able to hinder dehydration reactions which decompose lignin into phenolic derivatives such as 2-methoxy-phenol and 2,6-dimethoxy-phenol [18, 24, 50, 73, 89], which is in fact seen in Figure 4.6. The sample with the highest amount of phenolic compounds was the zeolite one with 59.0wt%, while La_2O_3 had the lowest amount of 51.7wt%. The high amount of phenolics, can make the BO an attractive raw material for bio-phenolic and epoxy resins [57, 58].

The second major type of organic compound was ketones, mostly alicyclic. They are a

product of the decomposition of cellulose and hemicellulose from dehydration, isomerization and ring-opening reactions [45, 80]. All the samples contained approximately the same amount of ketones, around 24wt%, the presence of the catalyst did not have an effect on ketone composition. In Figure 4.6, one of the highest peaks in every sample is the 2-cyclopenten-1-one, 2-methyl-compound, which has been reported to appear in HTL BO from lignocellulosic feedstocks [24, 50, 73].

Carboxylic acids were also present in the BO mix. Long chain fatty acids such as oleic and n-hexadecanoic (palmitic) acid were the most prominent. They are most likely formed by the extractives contained in EB [80, 85]. The hydrotalcite BO contained the highest amount with 18.5wt%, while the zeolite one had the lowest concentration of 12.4wt%. In general, high acid content makes BO a low quality fuel, as it can cause corrosion in engines and piping [55], while it worsens stability during storage and transportation [55]. However, it can possibly provide a source for bio-diesel production depending on the post-treatment [80].

The rest of the hydrocarbons that were found in the composition of the BOs, were aldehydes, esters, alcohols and nitrogen-containing compounds. Aldehydes and alcohols are also a product from the decomposition of cellulose and hemicellulose [80], while esters can derive from esterification of the fatty carboxylic acids [90]. Nitrogenates are a product of amino acids reacting with monosaccharides via the Maillard reaction to form heterocyclic compounds such as indoles, pyrroles, pyridines and pyrazines among others [43, 45].

4.2.5 Energy recovery and catalyst selection

As mentioned in chapter 3.1.1, in order to make the selection for the catalyst the energy recovery value is going to be prioritized. Therefore, BO yield and HHV were taken into consideration. In Figure 4.7, it is observed that Hydrotalcite achieved the best energy recovery with a value of 41.0%, while La_2O_3 followed with 40.4%. These findings are highly significant because even though literature highlights the inability of hydrotalcite to remove oxygen from phenolic compounds[18], the EB bio-crude yield and HHV were not significantly affected compared to the performance of the other studied catalysts. The lowest energy recovery was obtained for the non-catalytic BO, at 33.1%. Normally, the small difference between La_2O_3 and hydrotalcite BOs, combined with the former's much better CHNO composition, would lead to its selection. However, another factor should be taken into consideration, that is sustainability.

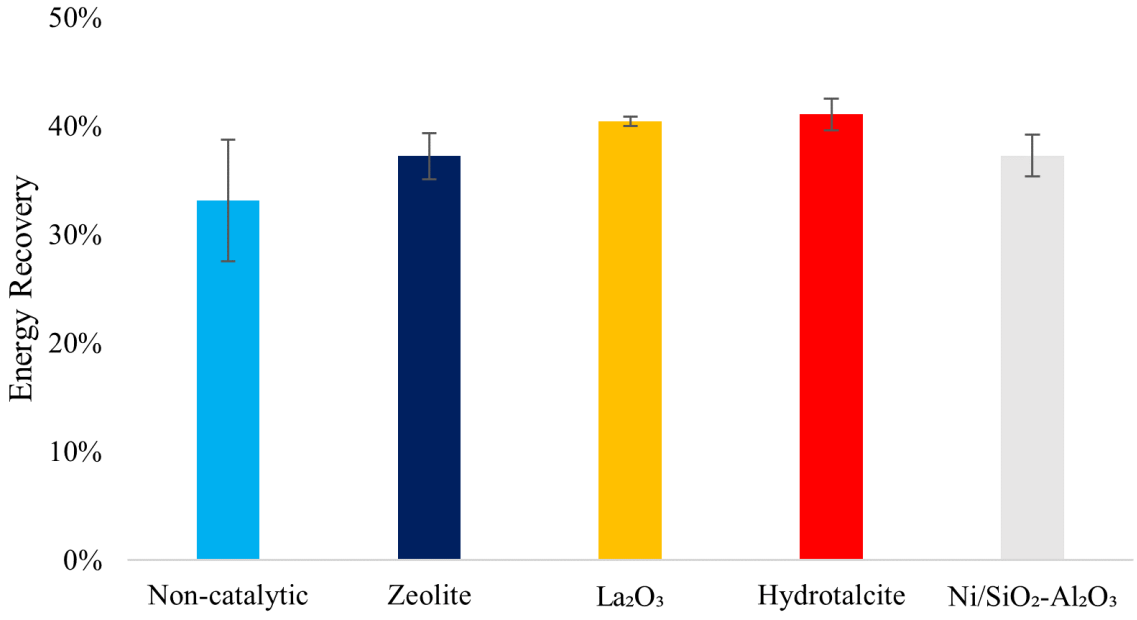

Figure 4.7: Energy recovery for each catalyst.

Lanthanum is a rare earth metal that is used mostly in the petroleum industry and battery production [91]. Its extraction is expensive and it occurs naturally in rare-earth minerals such as Monazite and Bastnäsite, that are found in the USA, Brazil, India, Sri Lanka and Australia [92]. If La_2O_3 were to be used in a scaled up hydrothermal liquefaction plant in Namibia, then possible logistic issues could come up, and the overall sustainability of the process would be decreased. Also, its accumulation on the BC could potentially harm its properties and quality, making it hazardous for applications such as soil amendment.

Hydrotalcite one the other hand, is a more abundant, naturally occurring layered double hydroxide with the formula $Mg_6Al_2(OH)_{16}CO_3{\cdot}4H_2O$ [93]. It is more easily accessible, as it can be synthesized from coal-fired power stations' fly ash [94]. In particular, this method was studied with fly ash from South African power stations [94], which makes logistics a much easier case, as South Africa is a neighbouring country to Namibia. In addition, hydrotalcite can also be produced via green synthesis (hydrothermal dissolution-precipitation) from untreated magnesium oxide and aluminum hydroxide, producing almost zero waste, making it more environmentally friendly [93]. Finally, its accumulation on the BC is not concerning, as metals such as magnesium and aluminum are not considered harmful for the soil [95], in case that BC is used as type of fertilizer/soil amendment.

By taking all of the above into account, the catalyst choice for the optimization campaign was decided to be hydrotalcite.

4.2.6 Effect of catalysts on biochar composition

The BC produced from each different catalyst was also characterized in order to study the potential energy, elemental and structure differences.

Proximate and Ultimate analysis

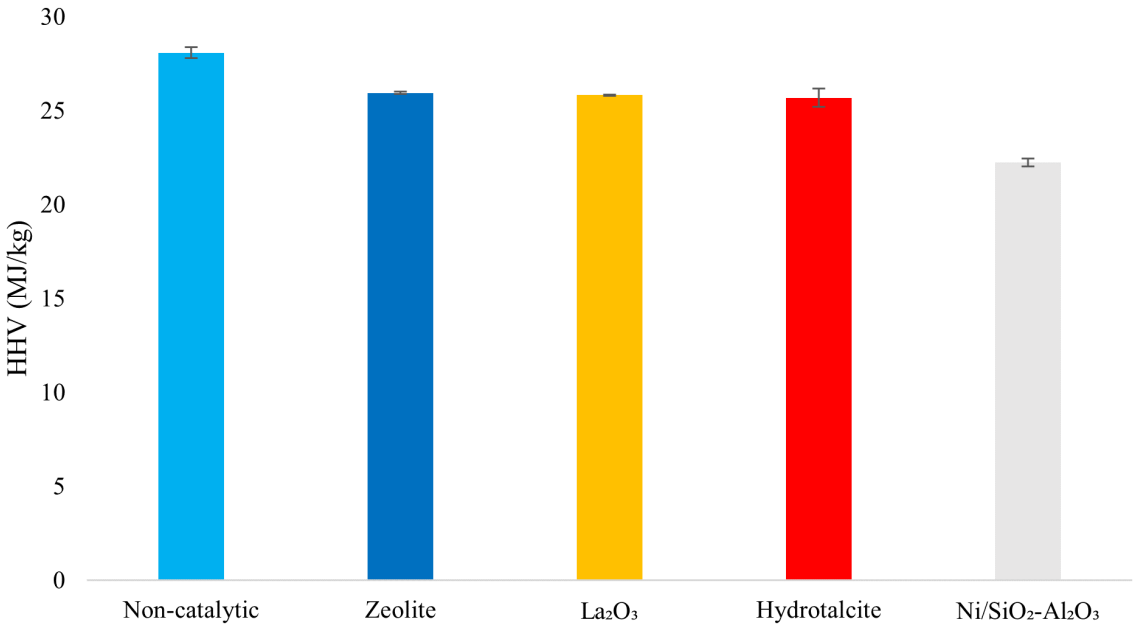

Figure 4.8: Effect of catalyst on biochars HHV.

Table 4.2: Proximate and ultimate analysis of BCs from different catalysts.

Sample	**VM (%)**	**FC (%)**	**Ash (%)**	**C (%)**	**H(%)**	**N(%)**	**O(%)**
Non-catalytic	40.32 (0.64)	56.11 (0.76)	3.56 (0.12)	64.9	5.7	3.1	26.3
Zeolite	35.38 (0.19)	52.77 (1.78)	11.85 (1.59)	59.3	5.5	2.2	33.0
La_2O_3	40.17 (0.61)	45.88 (1.87)	13.95 (1.27)	69.3	5.3	2.6	22.8
Hydrotalcite	40.03 (0.49)	52.02 (1.96)	7.94 (1.47)	58.7	5.0	2.2	34.1
Ni/SiO_2-Al_2O_3	30.30 (6.34)	44.00 (7.38)	25.70 (1.05)	63.2	4.9	2.2	29.7

The catalyst effect on the biochars' energy content can be seen in Figure 4.8. The highest calorific value was obtained from the non-catalytic sample (28.08 MJ/kg), while the lowest from the Ni/SiO_2-Al_2O_3 catalyst (22.23 MJ/kg). The other 3 catalysts resulted in almost the same HHV of approximately 25.8 MJ/kg. The difference of the non-catalytic sample's HHV with the rest can be explained by the difference in ash content, as seen on Table 4.2. Heterogeneous catalysts tend to accumulate on the biochar, ultimately increasing the ash content, as they are either metals or minerals. Thus, besides the nickel catalyst, it can be concluded that the other 3 did not have a significant effect on the HHV of the BC.

The proximate as seen in Table 4.2, shows that the non catalytic sample also had the highest FC content at 58.34wt% , while the Ni/SiO_2-Al_2O_3 catalyst produced the BC with the lowest at 44.45wt%. While all the catalytic samples had 5wt% of catalyst loading, it is observed that their ash content is different. For the zeolite and La_2O_3 samples, the ash content correlates to the amount of catalyst added. Hydrotalcite however had a much lower ash content, which could indicate that part of the catalyst was distributed in the aqueous phase. Finally, the Ni/SiO_2-Al_2O_3 sample contained a much higher ash content, which is a result of the smaller amount of BC produced compaired to the other samples.

A way to classify and compare the elemental composition of biofuels to conventional ones is the van Krevelen diagram, which combines the H/C and O/C ratios [96] and gives a rough prediction of a fuel's quality either solid or liquid. In general, high ratios of H/C and low O/C are always preferred, as both high content of hydrogen and low content of oxygen lead to higher calorific values [96].

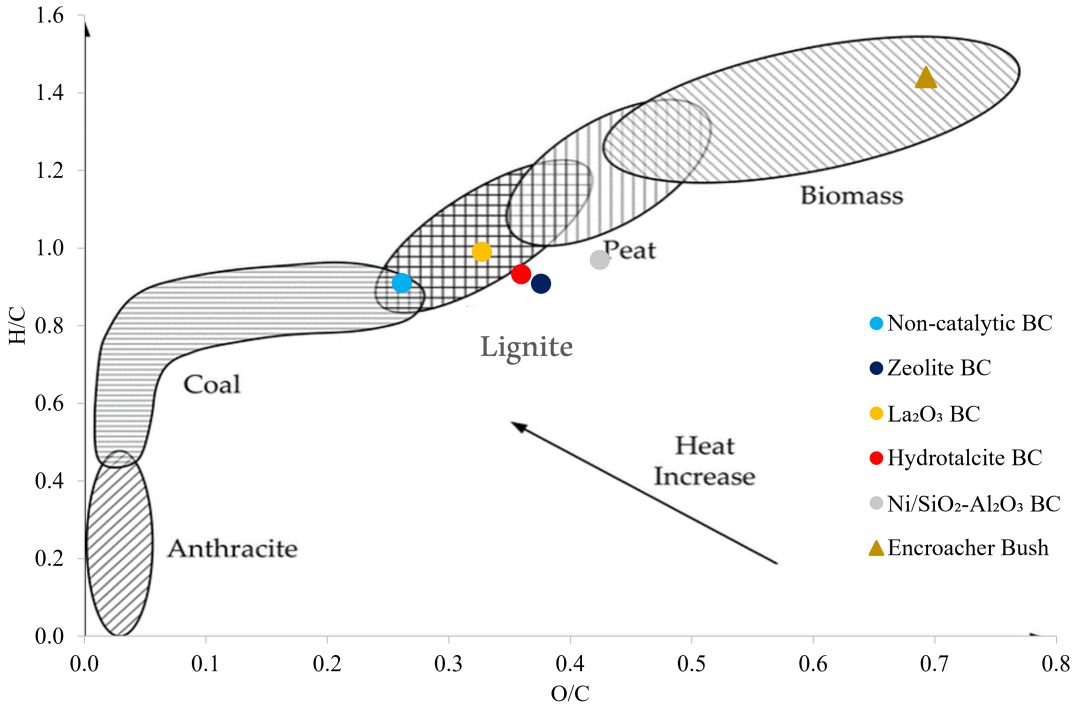

Figure 4.9: Van Krevelen diagram for the different BC samples and comparison with conventional solid fuels.

Figure 4.9 demonstrates the distribution of the BC samples on the Van Krevelen diagram. All the samples fall approximately in the same graph area, which is the lignite - peat one. That is a positive result, considering lignite is a fossil fuel that is still being used to for power generation [97], so an alternative such as biochar could be promising. In fact, the non catalytic sample is closer to coal rather than peat, which is also backed by its higher HHV. Compared to raw EB, BC samples are much improved (higher carbon and lower oxygen content) and can be potentially considered as a solid fuel that could replace coal or lignite.

XRD analysis

XRD measurements were performed on the biochar samples to evaluate the influence of HTL operational conditions on the crystallinity of the biochars compared with the parent biomass. Sharp peaks indicate higher crystallinity, while blunt peaks reveal an amorphous structure.

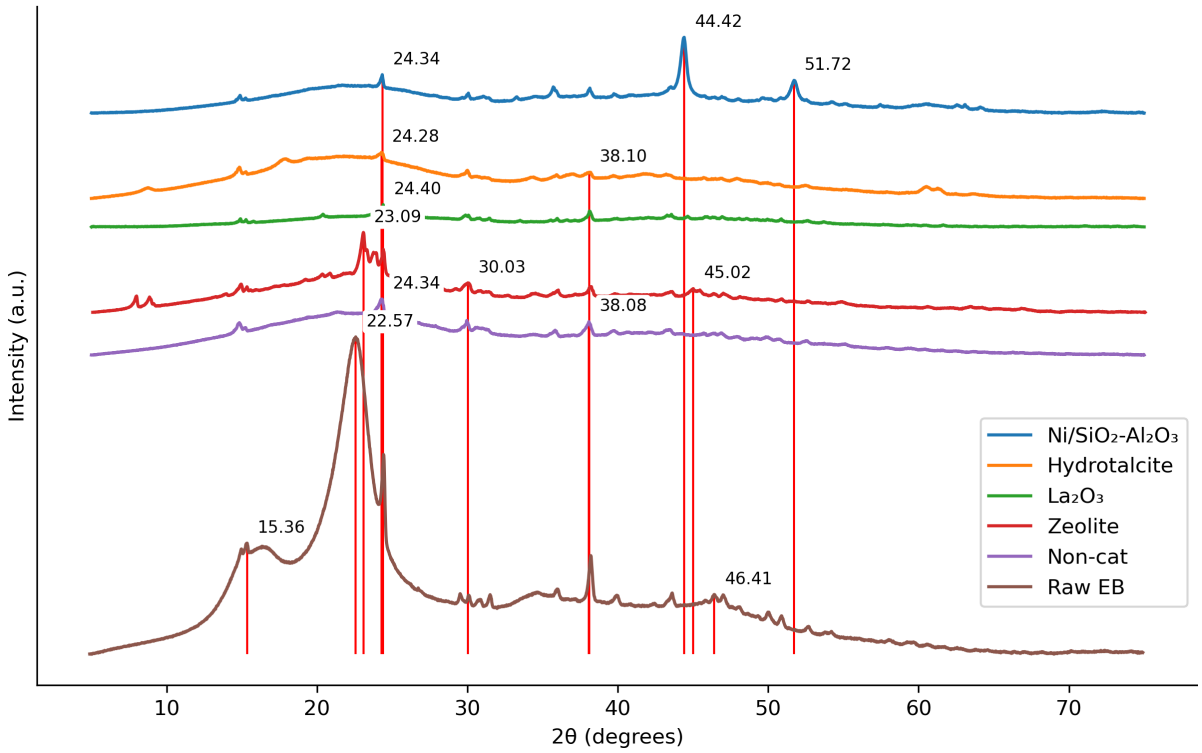

Figure 4.10: XRD patterns for raw EB and catalyst screening biochars.

The degradation of cellulose in the biochar samples is observed by the flattening of the sharp peak at 15°, 17° and 22.5° for the raw EB sample. Based on the intensity of the crystalline C peak in Figure 4.10, the biochars are ranked as follows: La_2O_3>Ni/SiO_2-Al_2O_3 >Hydrotalcite>Zeolite>Non-catalytic. XRD results indicate that whewellite ($CaC_2O_4 \cdot H_2O$), a stable calcium oxalate [98], was the main crystalline mineral in all biochars. Whewellite is considered a biomineral and has been detected in trees/woody species that grow on nutrient-poor soils [98], which fits the description of EB. Only the Ni/SiO_2-Al_2O_3 and zeolite samples included an additional crystalline phase. Sodium aluminum silicate hydrate ($(Na_2O)0.07(Al_2O_3)(SiO_2)70 \cdot 0.97H_2O$) was detected at 8-9° and 22°, which most likely indicates the deposition of zeolite on the BC. That is further supported by the type of zeolite that was used, ZSM-5, which has a chemical formula of $Na_nAl_nSi_{96-n}O_{192} \cdot 16H_2O$. As for the Ni/$SiO_2$-$Al_2O_3$ catalyst, the sharp peaks of Figure 4.10 at 44° and 55° indicate the accumulation of Nickel on the BC and a more crystallized form.

4.3 DOE - Optimization campaign

This chapter will present the results of the DOE campaign for the catalytic hydrothermal liquefaction with EB, using hydrotalcite as the catalyst. As discussed in chapter 3.1, 20 experiments were conducted with varying reaction parameters (temperature, residence time, catalyst loading) in order to model the HTL product yields. Additionally, another 2 experiments were performed for validation and testing of the predicted maximum BO yield.

4.3.1 Product distribution and response surfaces

The RSM was applied for each different phase and the resulted 3D surfaces are illustrated in Figure 4.11.

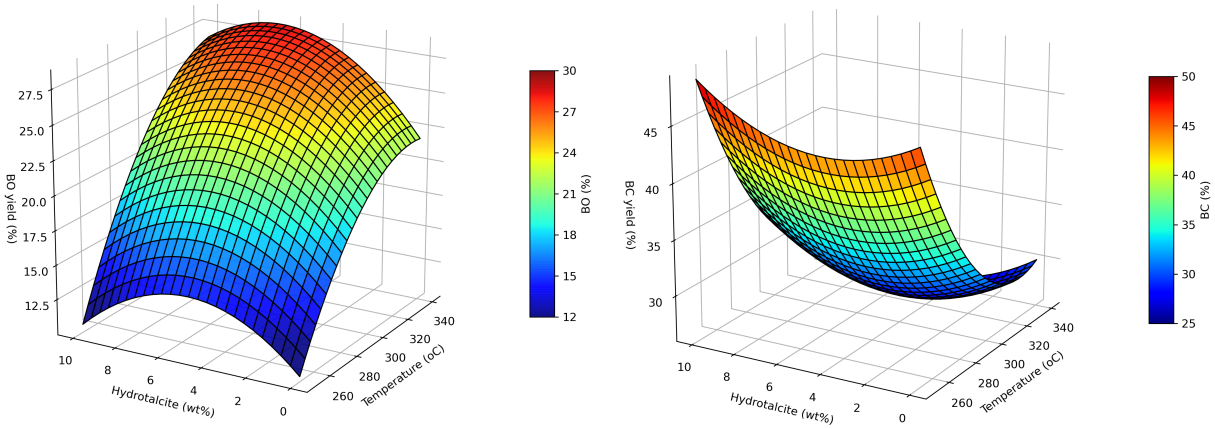

(a) Bio-oil

(b) Biochar

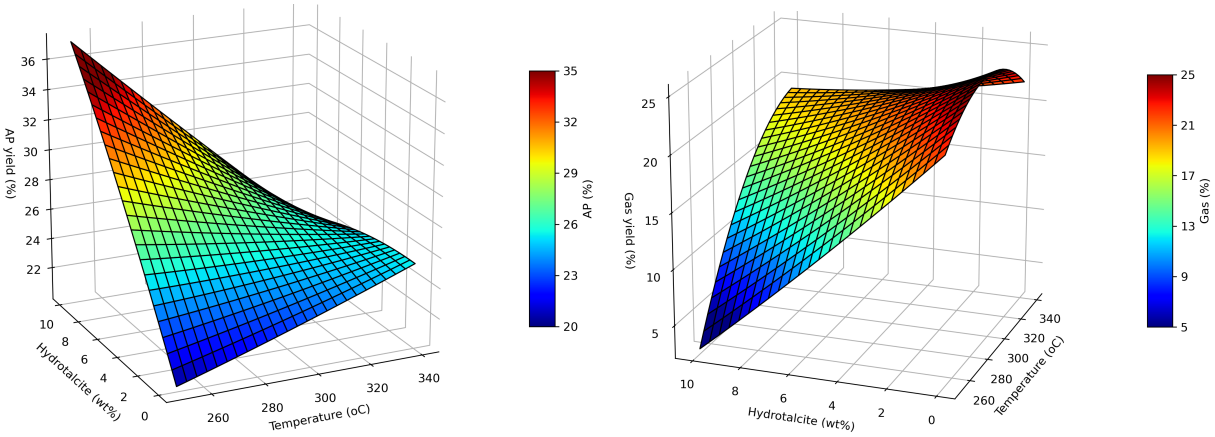

(c) Aqueous phase

(d) Gaseous phase

Figure 4.11: Response surfaces for each HTL product, showing effect of temperature and catalyst loading at 30 minutes residence time.

The response surfaces are a way to visualize the effect of multiple parameters within one graph. In Figure 4.11, temperature and catalyst were the chosen parameters, as they were the most statistically significant for each predictive model (see section A.4). Residence time was 30 minutes for better optical representation of the effect on the yields.

For BO yield, temperature seems to have the biggest influence, which is something supported by multiple studies [23, 24, 26, 99]. That is however, until around 340^{o}C, where the curve seems to reach its maximum point. The catalyst appears to have a different effect, with the optimum point being around 6-7%. Furthermore, the presence of the catalyst indicates a reduction in the HTL's energy requirement. For example, for a bio-crude yield without catalyst (14.6wt%) obtained at 300°C and 15min, using hydrotalcite will require lower operational conditions (260°C, 38min and 1.6wt% - calculated from the model) to meet the same yield.

The surface for BC yield shows an opposite trend with temperature compared to the BO one. The lower the temperature, the higher is the yield, which indicates limited devolatilization and carbonization[22, 59]. The addition of catalyst appears to have a slight increasing trend, which can be explained mostly by its accumulation on the BC, thus increasing the overall yield.

AP yield surface shows a significant dependence on the catalyst loading, but only in lower temperatures (<280^{o}C). Higher amount of catalyst leads to higher AP yield. However, at higher temperatures the quadratic model indicates that neither of the studied operational variables have much of an effect on the yield. This result could indicate the intensified effect of hydrotalcite on hydrolysis reactions which occur from 250^{o}C [24], increasing sugars, which are water soluble [24]. Furthermore, at higher temperatures there is an increased thermal degradation of the aqueous

phase which partitions the compounds into the gas phase and bio-crude oil.

Gas yield appears to be highly influenced by the catalyst loading. The presence of hydrotalcite in lower temperatures reduces the gas yield due to limited decarboxylation which is agreement with high biochar production (Figure 4.11b). With the increase of the temperature, all HTL products are thermally degraded reaching plateau conversion mainly due to further degradation of hydrocarbons [38].

4.3.2 Model equation and optimization parameters

The 20 HTL experiments that were conducted gave 20 responses (results) for the product yields. Based on those responses, via Design Expert, a model that fit best was chosen to create a quadratic equation (see equation 3.1.1). The focus of this thesis was to maximize the BO yield, thus only the model for BO will be shown in this section. More detailed information about the statistical analysis can be found in section A.4.

$$BO(\%) = -138.241 + 0.985\mathbf{A} - 0.610\mathbf{B} + 1.311\mathbf{C} + 0.004 * \mathbf{AB} + 0.005\mathbf{AC} - 0.035\mathbf{BC} - 0.002\mathbf{A^2} - 0.006\mathbf{B^2} - 0.153\mathbf{C^2} \quad (4.3.1)$$

Where:
A: Temperature (^{o}C)
B: Residence time (minutes)
C: Catalyst loading (wt%)

Equation 4.3.1 gives the prediction for BO yield as a function of temperature, residence time and catalyst loading. The equation coefficients shown have been reduced to 3 decimals for fitting to text reasons and the full ones can be found in Table A.19. Based on that model, a maximization point was found by giving the range of each parameter. That range was given according to the table in Figure 3.1.

Table 4.3: Predicted yields for CCD's maximum BO point. Relative and absolute errors are included.

Parameter	**Bio-oil**	**Biochar**	**Aqueous phase**	**Gas phase**
Maximum point	340^{o}C - 60 minutes - 5wt%			
Predicted yield(%)	29.35	28.21	22.97	19.36
Measured yield (%)	26.98 (1.35)	25.85 (0.27)	18.43 (3.04)	28.88 (1.23)
Relative error (%)	-8.79	-9.14	-24.56	32.95
Absolute error (%)	-2.37	-2.36	-4.53	9.52

The goal of the CCD campaign was to optimize the energy yield of the produced bio-oil. That is why some of the CCD points' HHVs were measured to produce a predictive model for HHV. That model was then added as a constraint for optimizing the BO yield model. Due to the few HHVs measured, the HHV model did not have a high accuracy, so the priority for HHV maximization was set lower than the BO yield one (and not equal). The optimized parameters given from the CCD model were also used as the validation point for the model's accuracy.

In Table 4.3 the results from the CCD model optimization and validation are shown. The predicted optimum point for maximum BO yield was at 340^{o}C - 60 minutes - 5wt%. The Analysis of variance (ANOVA) showed that the BO model was significant (p=0.0028 and F=7.67) and had a good fit (R^2=0.885). The predicted maximum BO yield was 29.35%, while the measured one 26.98%. This means that the model overestimated the yield, with a -8.78% relative error. The same type of model has been used again in other HTL reports [22, 80], and gave a relative error of 6-8%, which is very similar to the one on this case. BC yield model also was significant

($p<0.0012$ an $F=8.64$) and had a good fit ($R^2=0.886$). Similarly to the BO model, BC's yield relative error was -9.14%, thus overestimating BC production. AP yield model was not significant ($p=0.1523$ and $F=1.97$) with a much worse fit ($R^2=0.640$). The model's lack of fit is significant ($p=0.0387$) and there is a large relative error of -24.56%. Finally, even though gas phase's model had good statistical data ($p=0.0005$, $F=10.36$ and $R^2=0.903$), it also had the highest relative error of 32.95%, which could be due to the accumulation of experimental errors of the other phases.

The highest BO yield from the 20 CCD experiments was in fact 28.48wt% at the 330^{o}C-30 minutes-7.5wt% point, which means that the predicted optimum point of 340-60-5 that yielded 26.98wt% BO is not the correct one. A reason for that could be that two of the axial points of the CCD are outside of the DOE cube forcing extrapolation of data over the experimental range [82]. However, the difference between the experimental maximum (330^{o}C-30 minutes-7.5wt%) and the predicted maximum yield (340^{o}C-60 minutes-5wt%) is still small, around 1.5%.

4.3.3 DOE bio-oil characterization

For this section, 5 BO samples from the optimization campaign with hydrotalcite were characterized to obtain a better understanding of the effect that different HTL operating conditions have on them. The 2 highest and lowest points based on BO yield were chosen, additionally with the predicted maximum BO point from the model. It has to be noted that the 2 actual lowest points did not yield enough product to be able to characterize it, thus the next 2 lowest were chosen. Those points were 330-30-7.5, 330-30-2.5, 270-30-7.5, 270-30-2.5 and 340-60-5.

Energy recovery and CHNO composition

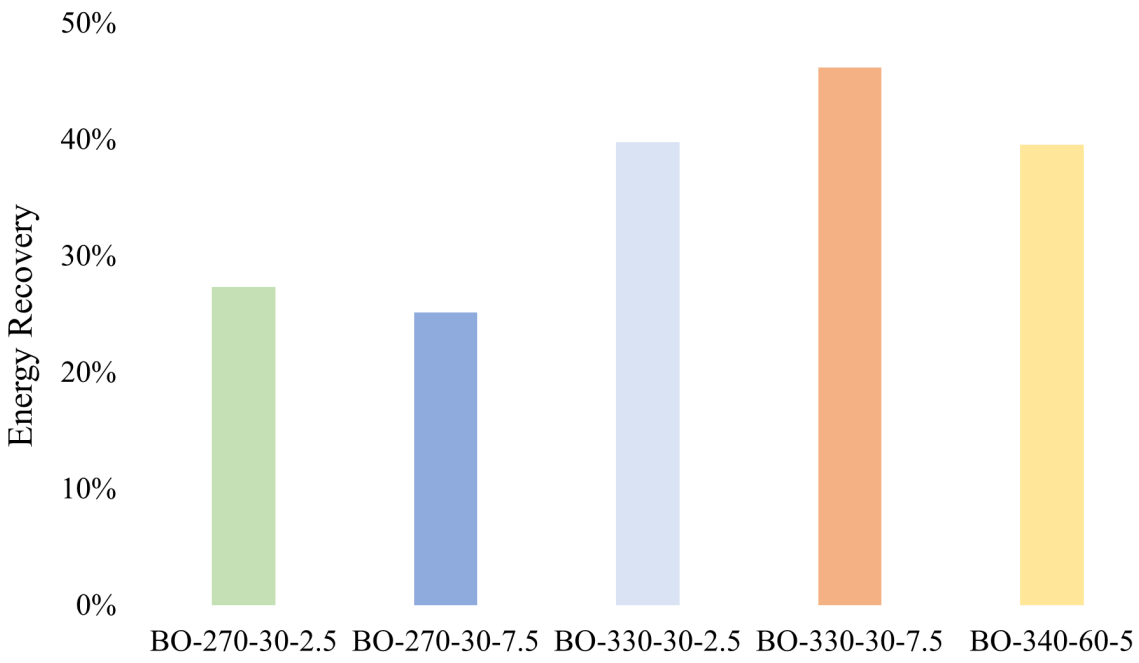

Figure 4.12: Energy recovery for the 5 selected samples from DOE.

The ER results demonstrate that the highest ER was obtained at high temperatures and high catalyst loading. The 330-30-7.5 point obtained the highest value, with 46.2%. The lowest value was at the 270-30-7.5 point with 25.1%. It is also observed that the predicted optimal condition showed a lower ER value (39.5%) than the two samples at 330^{o}C. The ER values are in accordance to literature, as studies with lignocellulosic biomass have shown that the ER ranges between 32.6-57.6% [50, 79]. In our case, the 340-60-5 sample, besides higher temperature

had also higher residence time, which could have caused cracking of the bio-oil to lower energy compounds (reducing HHV) or gas formation from intermediates (reducing BO yield) [44]. In total, there was a 12.4% increase in ER, between the 300-15-5 point (central point of CCD) and the maximum 330-30-7.5 point. This is an indication that the CCD, achieved its goal which was to maximize both the yield and energy output of the BO, within the operational parameters that were set.

CHNO composition of CCD BOs

In Figure 4.13, CHNO analysis of the 5 BO samples from the optimization of the CCD.

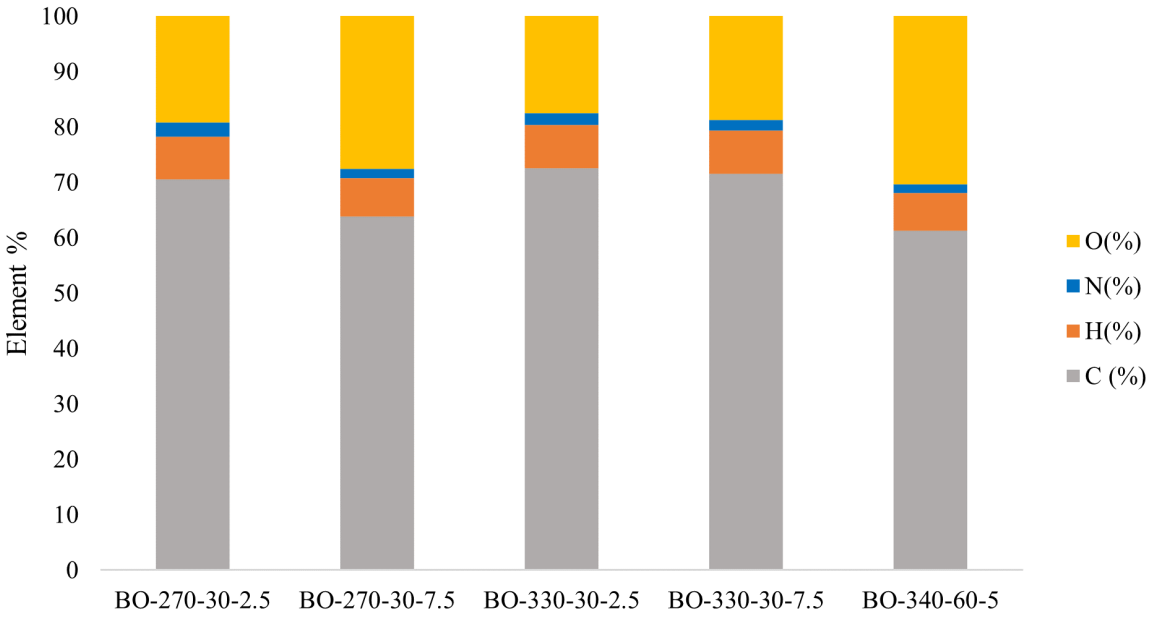

Figure 4.13: CHNO analysis of the 5 DOE bio-oil samples.

It is observed that the samples 270-30-2.5, 330-30-2.5 and 330-30-7.5 have a similar distribution for C, H and O. In particular, the 330-30-2.5 sample had the highest C and H content of 72.5wt% and 7.9wt% respectively, while also the lowest O content at 17.5wt%. In comparison with the hydrotalcite sample from the catalyst screening campaign (at 300-15-5), the C, H and O content have all improved significantly, even the low yield points at 270^{o}C. That effect can be attributed to the difference in residence time, as the 5 samples tested were held in their operational temperature for 30 or 60 minutes. Therefore, with the increase in residence time, further decarboxylation or dehydration reactions occurred, leading into O content reduction. The 340-60-5 point from the model, had the lowest C content (61.3wt%) and highest O content (30.3wt%), making it the BO with the lowest quality. Again, through CCD a large improvement in O content (up to 54% reduction) in the BOs was achieved.

Water content in BOs

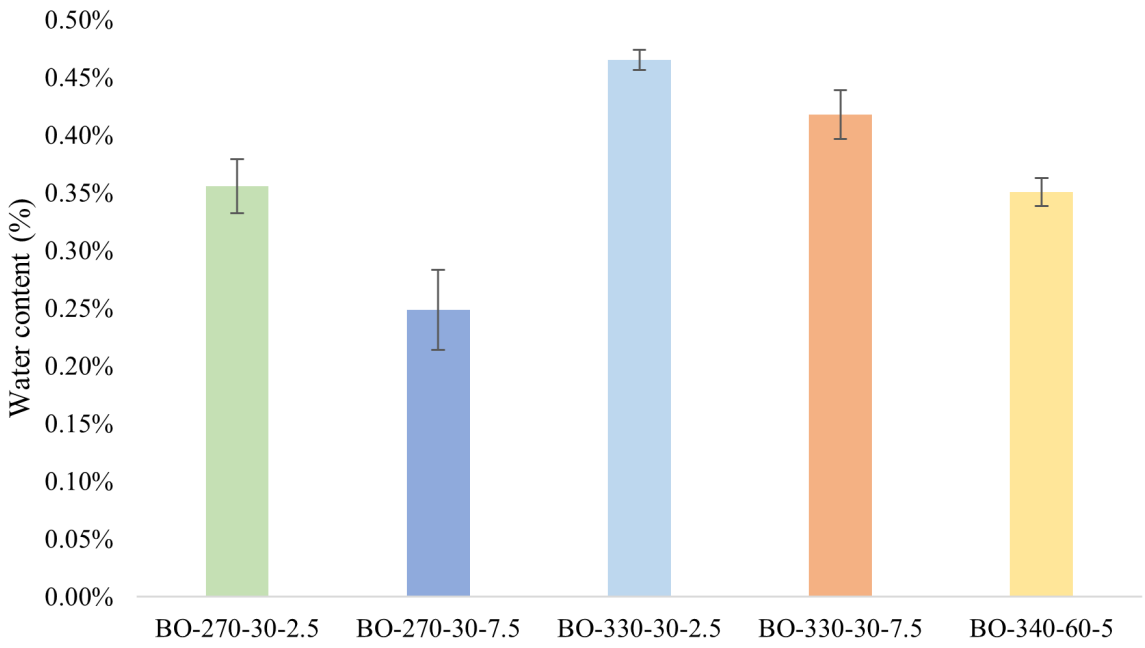

Figure 4.14: Water content in DOE bio-oil samples.

Water content of the 5 DOE samples was measured via Karl-Fischer Titration. It is observed that water content does not exceed 0.47wt% in any of the samples. That is a desirable effect of the HTL BO, that can reduce potential post-treatment costs for water removal. The 270-30-7.5 point had the lowest water content, 0.25wt%. There is not a particular trend detected between the samples, although the higher temperature samples appear to have slightly higher water content, compared to the low temperature ones.

GC-MS results

Only 3 of the 5 samples that were sent for GC-MS analysis could be analyzed up until this point, hence only 3 are shown in Figure 4.15.

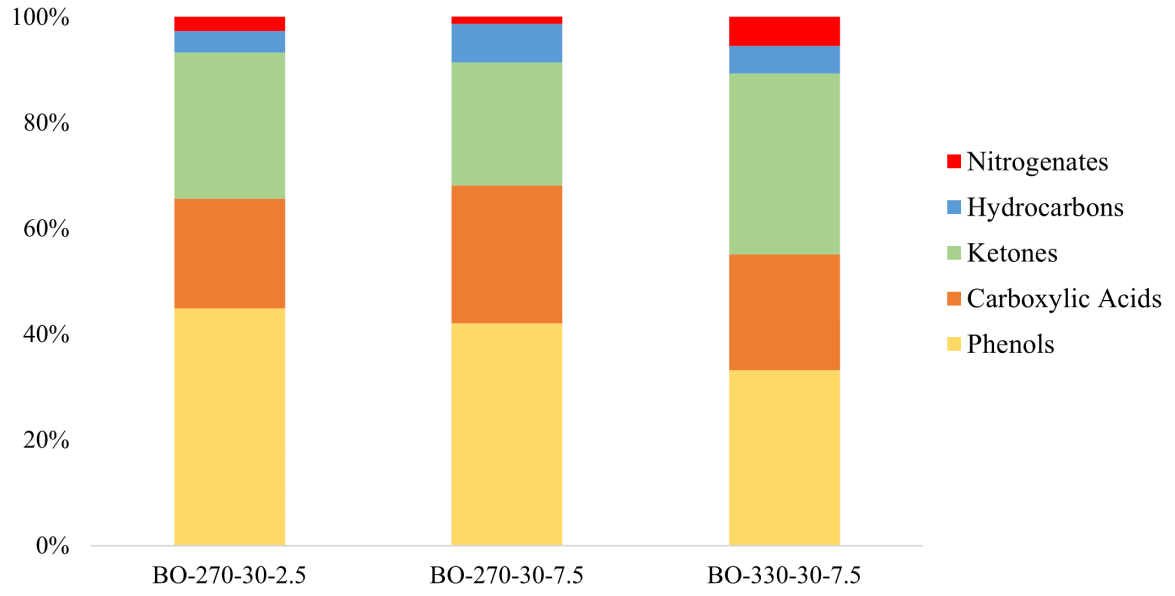

Figure 4.15: GC-MS composition for DOE bio-oils.

Chemical compound composition for the DOE samples showed a big change compared to Hydrotalcite's catalyst screening sample. In Figure 4.15, a significant reduction in phenolic content is observed, where the maximum concentration is 44.9% (at 270-30-2.5), compared to hydrotalcite's 300-15-5 sample which had 53.0%. The 330-30-7.5 had the lowest phenolics and highest ketones composition (33.2% and 34.2% respectively). In addition, the carboxylic acid content is also increased compared to the 300-15-5 point of the catalyst screening campaign, ranging from 20.7-26.1%. The main difference between the DOE samples and the 300-15-5 one, is the increased residence time. Higher residence time could have resulted in further decomposition of the phenolic compounds [10] or repolymerization to form char [44], further degradation of furans or furfurals to ketones [45] and further decomposition of the EB's extractives. The increased ketone content for the 330-30-7.5 sample in particular, could have likely been caused by the increased cracking reactions on the basic sites of hydrotalcite, which would yield more alicylcic ketones from cellulose and hemicellulose [50].

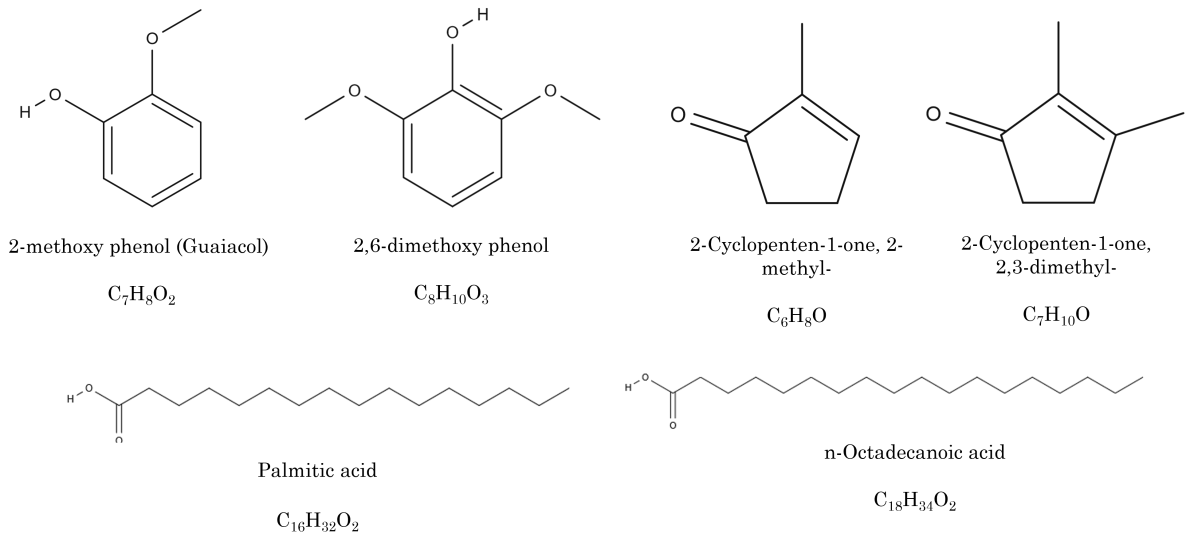

Figure 4.16: Structure and chemical formula of the main compounds found in DOE bio-oils.

In Figure 4.16, it is observed that the phenolic compounds contain more oxygen than the alicyclic ketone ones. With the further decomposition or repolymerization of lignin, those compounds reduced, thus reducing overall O content. The 2 fatty carboxylic acids (palmitic and octadecanoic) contain 2 molecules of oxygen too, but they have much more carbon, thus their increased presence in the bio-oil actually improves the carbon content more.

4.3.4 DOE biochar characterization

This section will present the characterization results for BC, for the same 5 points that were chosen in section 4.3.3.

Proximate and ultimate analysis

Table 4.4: Proximate and CHNO analysis of optimization campaign's BC samples.

Sample	**VM (%)**	**FC[a](%)**	**Ash (%)**	**C (%)**	**H(%)**	**N(%)**	**O[a](%)**
BC-270-30-2.5	46.03 (0.76)[b]	47.04 (0.89)	6.93 (0.13)	64.9	5.7	3.1	26.3
BC-270-30-7.5	47.72 (0.77)	43.12 (0.90)	9.16 (0.13)	59.3	5.5	2.2	33.0
BC-330-30-2.5	36.63 (0.79)	56.45 (1.70)	6.92 (0.25)	69.3	5.3	2.6	22.8
BC-330-30-7.5	35.40 (1.45)	49.82 (1.09)	14.78 (0.30)	58.7	5.0	2.2	34.1
BC-340-60-5	34.79 (0.79)	53.41 (1.10)	11.80 (0.31)	63.2	4.9	2.2	29.7

[a] Calculated by difference,
[b] Values in parenthesis correspond to the standard deviation

Similarly to the catalyst screening campaign, the range of HHV remained between approximately 25-28 MJ/kg. The highest calorific value came from the EB-330-30-2.5 sample, with 28.30 MJ/kg, which indicates a very good value for a solid fuel. The lowest value came from the EB-330-30-7.5 sample, 24.30 MJ/kg. That difference is explained firstly by their difference in catalyst loading, as the EB-330-30-7.5 has three times the amount of catalyst, resulting in a higher ash content, as supported by table 4.4. Additionally, the difference in the catalyst loading may have resulted in other reactions occuring, which could have lowered the energy content even more. This can also be supported by the difference in C and O content of the two 330 samples, where the 330-30-2.5 had 69.3wt% and 22.8wt% respectively, while the 330-30-7.5 sample 58.7wt% and 34.1wt%. Higher amount of catalyst could have caused more phenolic compounds to repolymerize into biochar, thus reducing the overall energy and C content [10].

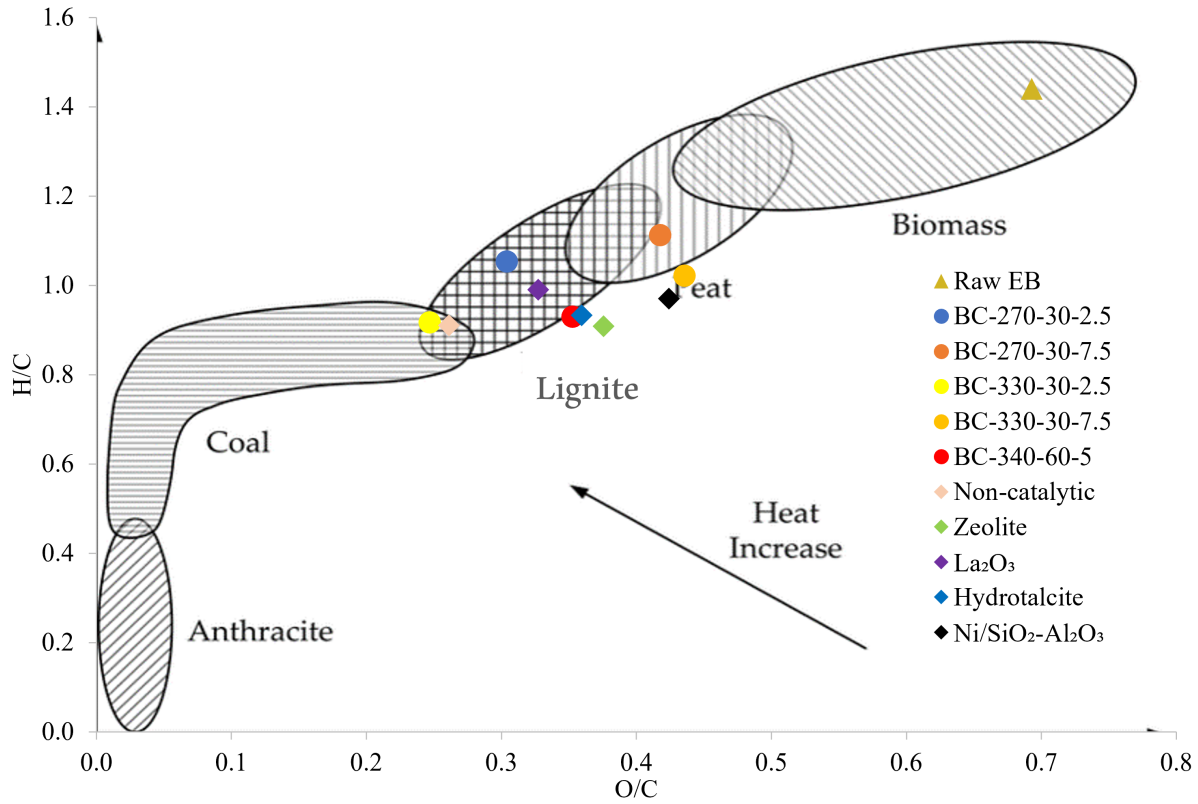

Figure 4.17: Van Krevelen diagram for 5 DOE BC samples.

The van Krevelen diagram with all the BC samples, indicate a clear trend for the biochar's C, H and O content. Samples which had higher catalyst loading are placed in the Peat area (more upper right), with higher oxygen content. As the catalyst loading decreases, the samples are moving towards the coal area (more lower left), where C content is higher and O content is lower. This is a more desirable outcome for biochar's application as a fuel, due to less smoke produced during combustion [59]. The 330-30-2.5 sample is placed in the coal area which makes it the best quality, even better than the non-catalytic sample. Moreover, there is a trend with temperature, as the lower temperature samples are placed higher than the high temperature ones. This is a result of a higher H content in the low temperature biochars, which could be due to the less hydrolysis reactions occurring at 270^{o}C [67].

ICP-OES

The 5 DOE biochars where measured for inorganic elemental composition via ICP-OES, in order to confirm the catalyst's presence and other heavy metals that could have poison the biochar. The results are shown in Figure 4.18. Supplementary material on AP and catalyst screening campaign IPC-OES measurements can be found in Tables A.2 and A.1.

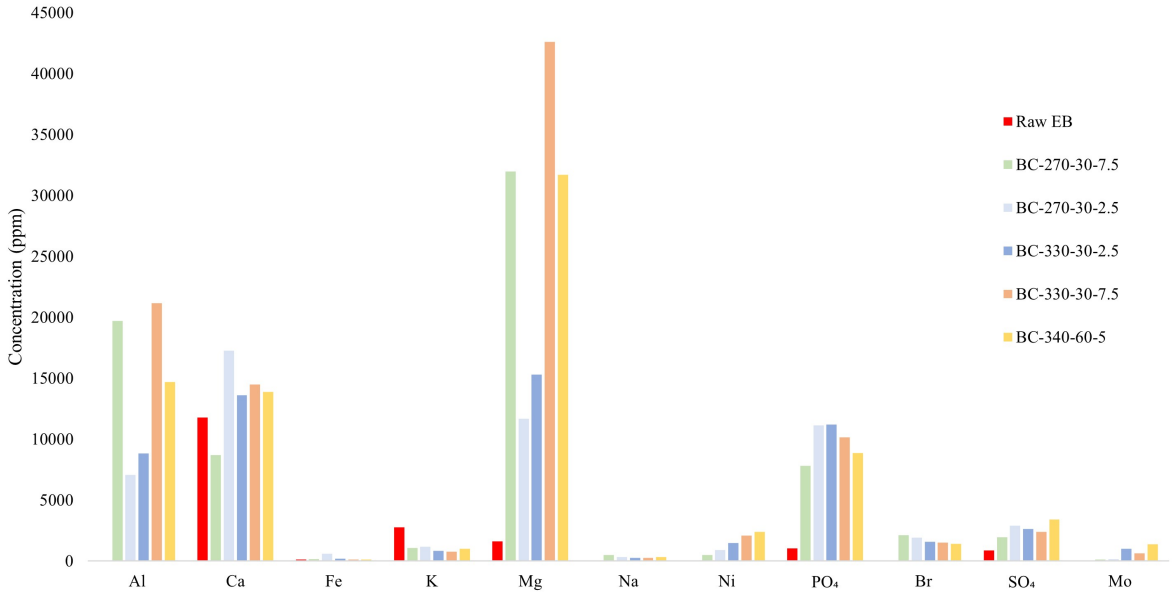

Figure 4.18: ICP-OES inorganic elemental composition for the 5 DOE biochars and raw EB.

Mg and Al, the two main metals from hydrotalcite, had the highest concentration among other elements in all the HTL samples. That result confirms the assumption that the catalyst deposits on the biochar. Higher temperature samples seem to have higher Mg and Al concentrations, which could mean that in lower temperatures some of the catalyst remains in the aqueous phase. Moreover, heavy metals such as Ni and Mo are present in all the BC samples, whereas raw biomass did not have any. The concentrations for Ni and Mo range from 500-2400 ppm and 100-1400ppm, respectively, and in fact are increased with process temperature. Their presence is a side-effect from scraping the inner autoclave's walls with a metal spoon, which could have transferred Ni and Mo (included in stainless steel) in the biochars. Moreover, under higher HTL temperatures, the effect could have been intensified. That result can have a much negative impact for applications into soil, as the allowed soil concentrations for Ni and Mo are 38 and 254 respectively. An interesting compound that was found in the biochars was actually a halogen, Br in particular. That is result related to the use of HCl solution for the digestion of the samples, which could contain traces of Br. No other part of the process could have included it. Finally, increased PO_4 was found in all of the BC samples, which is a positive aspect, due to P being a macronutrient for soil.

XRD

XRD analysis was performed on the 5 DOE samples is shown in Figure 4.19, with the raw EB sample included.

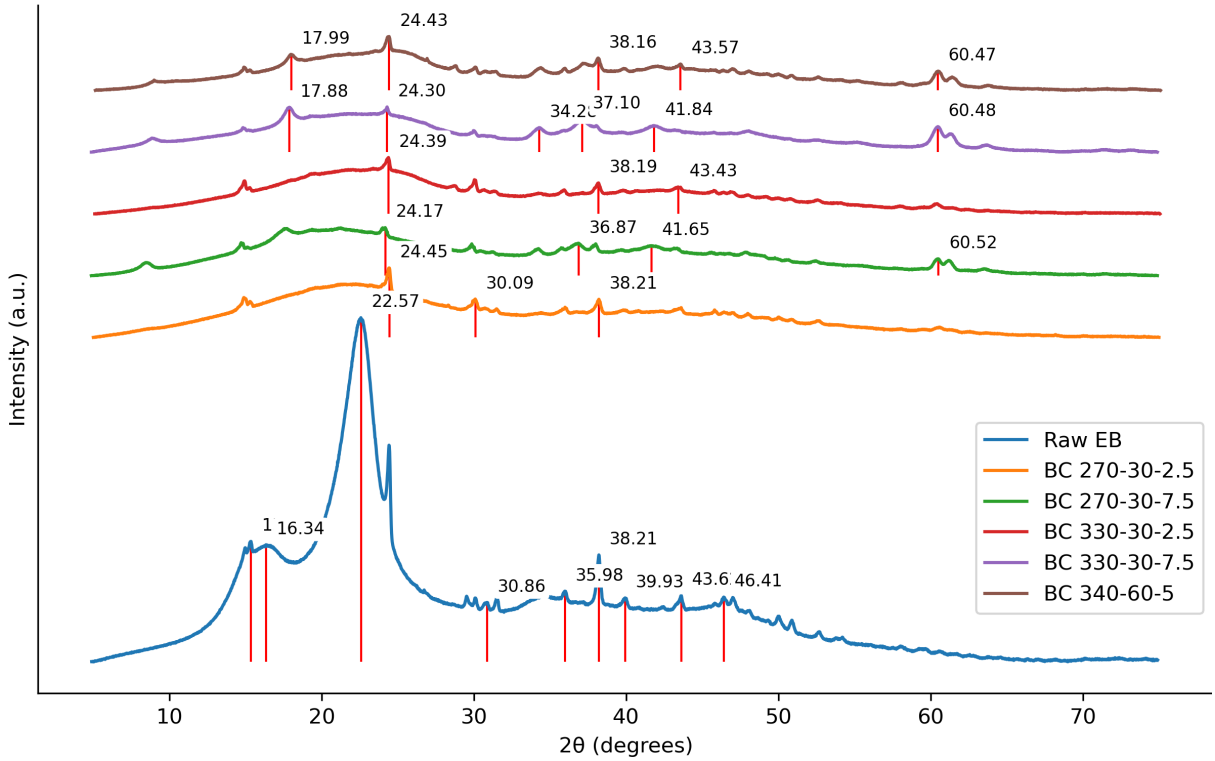

Figure 4.19: XRD pattern for the 5 BC DOE samples

Whewellite was detected in all BC samples. Cellulose degradation seems more intense in the high temperature samples, as expected due to further degradation. Additionally to whewellite, hydrobiotite was also detected in all but the 270-30-2.5 sample. Hydrobiotite's formula is $K(Mg,Fe)_6((Si,Al)_8O_{20})(OH)_4 \cdot 4H_2O$. While this mineral was not added in any of the samples, its detection most likely indicates the presence of hydrotalcite, which has a formula of $Mg_6Al_2(OH)_{16}CO_3{\cdot}4H_2O$. Potassium and silica might have been additionally detected, as they already exist in EB (see table A.5). However, iron's presence might come from the reactor's inner walls, during scraping it for BC recovery. Even so, EB-330-30-7.5 showed the most sharp peaks overall, indicating better crystallinity, but still all of the BC samples were mostly amorphous. In addition, high temperature and higher wt% of catalyst, seemed to make the deposition of the catalyst in the BC clearer, thus its recovery can be easier.

4.4 Product assessment

In this section, the overall product qualities, for BO and BC, will be presented and assessed based on existing literature. Furthermore, a comparison with other technologies and current market products will be made.

4.4.1 HTL bio-oil from EB as a drop-in intermediate

In order to properly assess the quality of the bio-oil, a comparison with other similar studies and technologies is needed. This current study used HTL in subcritical conditions (T<370^{o}C and P<250 bar) and a woody type lignocellulosic feedstock, that is *Acacia Mellifera*. Bio-oil from HTL cannot directly be used as a biofuel due to the oxygen, nitrogen and low HHV it contains compared to processed fossil fuels [7]. Therefore, one of the comparisons must be with crude oil, which is also one of the reasons that HTL BO is also called bio-crude oil. Moreover, a competing technology with HTL is fast pyrolysis, that produces pyrolysis oil. In addition, as mentioned in Table 2.2, HTL BO requires post-treatment, therefore a comparison with upgraded BOs is also needed.

Table 4.5: EB HTL biocrude fuel characteristics and comparison with other intermediates and final products.

Type of fuel	**HHV (MJ/kg)**	**N(%)**	**O(%)**	**S(%)**	Water (%)	**Reference**
Intermediates						
Acacia Mellifera HTL BO[a]	31.3	1.9	18.7	N.A.[b]	0.41	
Miscanthus HTL BO	32.2	1.7	19.6	<0.1	N.A.	[56]
Steeper Energy HTL BO	38.6	0.1	10	0.01	0.8	[100]
Licella HTL BO	34-36	0.1-0.2	10-14	0.01	N.A.	[101]
Pyrolysis oil	16-20	<0.4	28-40	<0.05	15-30	[55]
Crude oil	44	<1	<1	<4	0.1	[55]
Upgraded fuels						
Hydrotreated HTL BO	42-44	0-1.5	0-0.8	- [c]	-	[56, 102]
Marine fuel oil	40	0.3	1.0	0.033	0.1	[12, 103]
Diesel	45.6	-	-	-	-	[104]

[a] Composition from the BO obtained at 330^{o}C-30 mins-7.5wt%
[b] Not available
[c] Below detection limit

Table 4.5 contains the most important characteristics of EB's bio-oil, other similar intermediate fuels and fully processed products. First of all, compared to pyrolysis oils, a competitive technology's product, our HTL BO has a much lower O content (33-53% less) and little to no water (>97% less). Those two qualities place the HTL intermediate much above pyrolysis, and is something that was expected as discussed in section 2.2. An additional benefit from those 2 characteristics is the higher calorific value that the EB bio-oil has, approximately 10-15 MJ/kg more. The other three BOs shown, come from either pilot or commercial plants. Steeper Energy's and Licella's products derived from woody feedstock (pine or spruce) [100, 101], while Castello's et al. [56] used miscanthus, a more herbaceous type of lignocellulosic biomass. Steeper Energy and Licella both operate in supercritical conditions, which explains the much improved HHV and reduced O content in their BOs. However, miscanthus BO (which was produced in subcritical conditions) has very similar composition and energy content to the EB one. This is a first indication that the bio-oil we obtained from EB at 330^{o}C-30 mins-7.5wt% is of a high quality and it was indeed optimized for the given conditions of the CCD. Nevertheless, all of the bio-oils are still far from crude oil's characteristics, which can be considered as an drop-in intermediate for refineries. Sulphur content can be considered crude oil's only disadvantage compared with the the HTL bio-oils and pyrolysis oils, and that is one of the benefits of using lignocellulosic biomass feedstock.

To improve the intermediate products' qualities further upgrading is needed via HDO, FCC and hydrotreatment [7]. The upgraded HTL BOs presented in 4.5 have been hydrotreated and come from Steeper Energy and Castello et al. . The upgraded bio-oils show a very significant improvement in HHV (14-31%), while O content is almost zero. Additionally, for Steeper Energy's product, N content is completely removed. The final qualities of the upgraded BOs are almost similar or better than conventional fuels such as marine fuel oil or diesel, which makes the post-treatment crucial. The most promising result, however, is that Miscanthus BO oil which had very similar characteristics to the EB one, resulted in a high quality drop-in biofuel after upgrading. Essentially, EB BO's elemental composition is within the limit for sufficient deoxygenation and denitrification through hydrotreating. Therefore, an upgraded bio-oil derived from EB could be a very promising replacement of heavy oil for the marine sector.

4.4.2 HTL biochar from EB

The BC samples that were produced from HTL of EB were characterized mostly for their fuel properties. That is why the main part of their quality assessment is going to focus on their use as a solid biofuel.

Table 4.6: Proximate analysis composition of solid fuels.

Type of fuel	**HHV[a](MJ/kg)**	**Moisture (%)**	**VM[a](%)**	**FC[a](%)**	**Ash[a](%)**
BC-330-30-7.5	24.3	N.A.[b]	35.4	49.8	14.8
BC-330-30-2.5	28.3	N.A.	36.6	56.5	6.9
Coal (Lignite, Bituminous)[c]	20-24	13-22	27-42	31-44	6-25

[a] Dry basis
[b] Not available
[c] Based on [105]

Table 4.6 contains the 2 samples of BC: the 330-30-7.5 one (bio-oil's best point) and the 330-30-2.5 one (best BC according to figure 4.17). Moisture content is not available, as the biochar samples were always dried after filtration to record the actual weight. However, due to the reduced amount of oxygen (table 4.4) there is increased hydrophobicity [63], which is an appealing quality for long term storage. Moreover, it is observed that both BC samples characteristics are within or better than coal (lignite or bituminous coal). In fact, the BC-330-30-2.5 has a higher HHV than coal, which could make it a better and more sustainable alternative. In addition, both the HTL samples seem to have higher fixed carbon content than coals. Realistically, the HTL process is always optimized for BO production, due to its potential profitability, thus the sample which would be chosen here is the BC-330-30-7.5 one, but it would still be a good alternative.

Regardless of fuel application, EB is a virgin type of biomass, which resulted in very low amounts heavy were accumulated on the biochar, mostly due to the interaction with the stainless steel walls of the reactor. The catalyst that was chosen for HTL was hydrotalcite, an alkaline earth metal mineral, which did not contaminate the BC, even though it increased Mg and Al concentrations a lot. Soil amendment application could be a great alternative, especially for a dry country like Namibia. In fact, biochar can increase the soil's pH, organic carbon and water holding capacity [63]. Those improvements can be vital for the agricultural economy of Namibia, however further characterization the HTL BC is needed to better assess this application.

5| Conclusions

5.1 Catalyst screening campaign

Catalytic Hydrothermal Liquefaction of encroacher bush (*Acacia Mellifera*) from Namibia was performed to assess its potential as a feedstock for the production of high-quality drop-in intermediates. Initally, 4 different catalysts (Zeolite, La_2O_3, Hydrotalcite, Ni/SiO_2-Al_2O_3) were used and tested at the same operational condition (300^oC,15 minutes residence time and 5wt% catalyst loading). In general, the use of catalysts improved the BO yield compared to the non-catalytic sample, while La_2O_3 had the best performance in deoxygenation (41% reduction). GC-MS analysis revealed the significant presence of phenolic compounds in all the BO samples, followed by alicyclic ketones, fatty carboxylic acids, various hydrocarbons and N-containing compounds. Hydrotalcite achieved the highest ER of 41.1% and was also deemed the most sustainable and appropriate for the HTL process.

Biochars were also analysed to gain insight of the effect of each catalyst on them. Proximate analysis showed that the non-catalytic sample had the highest calorific value, 28.1 MJ/kg, and the lowest ash content (1.34wt%). In general, all BC samples except from the Ni/SiO_2-Al_2O_3 one, had a CHNO composition very close or better than lignite. XRD analysis showed that most of the catalyst samples were amorphous, with only the bio-mineral whewellite being detected. Zeolite and Ni/SiO_2-Al_2O_3 BCs had additional compounds detected, Sodium Aluminum Silicate Hydrate and Nickel respectively.

5.2 Optimization campaign

Hydrotalcite was used as catalyt in order to maximize the energy yield of the produced bio-oil. A Design of Experiments approach was used in order to optimize 3 HTL parameters, temperature, residence time and catalyst loading. A Central Composite Design was selected , which included 20 experimental points with operational conditions ranging between 250-340^{o}C, 5-60 minutes and 0-10wt%. The central point of the CCD was set to 300^oC - 15minutes - 5wt%. Bio-oil, biochar, aqueous phase and gas yields were measured gravimetrically and used to create 3D response surfaces. Results from the CCD indicate that temperature was the most significant factor for bio-oil yield, followed by the catalyst loading. The quadratic models from the CCD were optimized for maximum bio-oil yield while keeping the HHV at high level. The suggested optimal operational condition from the bio-crude model was 340^oC - 60 minutes - 5wt%. The predicted yield was 29.3wt%, while the measured one 27.0wt%. The relative error of the model was 8.8%, which is within literature findings. The highest yield was produced at 330^oC - 30 minutes - 7.5wt%, which is one of the 20 experimental points tested. It had 28.5wt% BO yield and an overall ER of 46.2%, which was also the highest from the CCD. CHNO analysis on 5 optimization campaign bio-oil samples showed a much improved deoxygenation, with the 330-30-2.5 sample having an oxygen content of 17.5wt% (54.2% reduction). GC-MS results showed a decrease in phenolic compounds, possibly due to repolymerization of decomposed compounds on the biochar. Water content in all bio-oils was below 0.5wt%.

The same 5 DOE BC samples were also characterized for proximate and ultimate analysis and XRD. The 330-30-2.5 point had the highest calorific value at 28.3 MJ/kg. Samples with

higher catalyst loading, had increased ash content and lower HHVs, due to catalyst deposition on the biochar. XRD showed that high temperature BC samples were slightly more crystalline than the lower temperature ones, but hydrotalcite was not clearly detected.

Overall, catalytic HTL with EB was successful since a significant volume of high calorific value bio-oil was produced, around 28.5 gr of bio-oil per 100 gr of dry EB. Its reduced oxygen content and increased HHV make it a suitable drop-in intermediate fuel for further upgrading via HDO, FCC and hydrotreating. Moreover, the biochar produced has a great potential as an alternative to conventional solid fuels such as lignite and coal. For Namibia however, its potential use may be as a soil amendment. In conclusion, the answer to the research question of the present MSc Thesis project is that Namibia's EB has significant potential as feedstock for catalytic HTL, by valorizing both the bio-oil and the biochar produced.

6| Recommendations

This chapter will include some recommendations and future work regarding the subject of HTL with EB. They will be separated for each product individually.

Bio-oil:

- More alkaline earth metal catalysts can be tested. In order to keep the whole process as much heavy metal free as possible, other minerals (colemanite) or alkaline earth metal oxides (MgO, CaO) can be tested to find the best performing one and increase total energy recovery.
- Aqueous phase could be recycled in order to increase bio-oil yield. The separated water phase (before the evaporation of water), can be used instead of Milli Q water. This can benefit the bio-oil yield, as a homogeneous catalyst is also inserted into the process (formic/acetic acid). AP recycle is important to be tested, as in a bigger and continuous scale (such as Steeper Energy's) [100] it is the only way to utilize all of this wastewater. Moreover, BO's oxygen content has been mentioned to be decreased after AP recycling [65] which makes this addition even more intriguing for our case.
- Scaling up the batch process or making a small continuous demonstration plant would be the better recommendation, as it is the only way to really assess the potential of HTL.

Biochar

- Further characterization of the BC samples can be performed to assess other applications such as soil amendment or metal adsorbent. SEM and surface area are some of the measurements that could give additional information on the produced biochar's properties.
- Catalyst recovery is an essential part when scaling up the process. As catalysts tend to accumulate in the biochar, some type of leaching could be performed to try and recover hydrotalcite from it. However, its activity could be reduced as some studies have showed that the catalyst activity is almost zero after 3 runs of recycling it [17].

Aqueous phase

- GC-MS, ICP-OES, TOC and COD measurements can be performed to further characterize AP and acquire a better understanding of the HTL and hydrotalcite effect. In addition, instead of using a rotary evaporator, Karl Fischer titration (not coulometric) could be used to measure the total water content and reduce the error for the mass balance.

Gas phase

- Gas phase should be captured and analyzed in a gas analyzer, instead of calculating by difference. This would increase the accuracy of the predicting model and an overall carbon balance could be made.

Bibliography

[1] Thomas Burdyny and Bernard Dam. "Fossil-fuel funding could speed energy transition". In: *Nature* 613.7945 (2023), p. 629. ISSN: 14764687. DOI: 10.1038/d41586-023-00141-x.

[2] IPCC. *Climate Change 2022, Mitigation of Climate Change Summary for Policymakers (SPM)*. 1. 2022, pp. 1–52. ISBN: 9781107415416. URL: https://www.ipcc.ch/report/ar6/wg2/.

[3] Rowland Brown, Dylan van Wyk, Christine V Gaskell, and Robert McGregor. "An assessment of the micro- and macroeconomic benefits of an Encroacher Bush Biomass Power Plant near Tsumeb in Namibia". In: 2018.

[4] Catherine Birch, Lawrie Harper-Simmonds, Pauline Lindeque, and Angus Middleton. "Benefits of bush control in Namibia. A national economic study for Namibia and a case for the Otjozondjupa Region. Report for the Economics of Land Degradation Initiative". In: (2016), pp. 1–52.

[5] JN de Klerk. "Bush Encroachment in Namibia: Report on Phase 1 of the Bush Encroachment Research, Monitoring, and Management Project". In: (2004), p. 273.

[6] R. Trede and R. Patt. "Value added end-use opportunities for Namibian encroacher bush". In: (2015), p. 157.

[7] IEA Bioenergy. *The Potential and Challenges of 'Drop-in' Biofuels - The key role that co-processing will play in production*. Vol. 1. January. 2019, p. 156. ISBN: 9781910154618.

[8] Xiaolei Zhang and Robert C. Brown. "Introduction to Thermochemical Processing of Biomass into Fuels, Chemicals, and Power". In: *Thermochemical Processing of Biomass: Conversion into Fuels, Chemicals and Power* (Jan. 2019), pp. 1–16. DOI: 10.1002/9781119417637.CH1. URL: https://onlinelibrary-wiley-com.tudelft.idm.oclc.org/doi/full/10.1002/9781119417637.ch1%20https://onlinelibrary-wiley-com.tudelft.idm.oclc.org/doi/abs/10.1002/9781119417637.ch1%20https://onlinelibrary-wiley-com.tudelft.idm.oclc.org/doi/10.1002/9781119417637.ch1.

[9] A. R.K. Gollakota, Nanda Kishore, and Sai Gu. "A review on hydrothermal liquefaction of biomass". In: *Renewable and Sustainable Energy Reviews* 81.August 2016 (2018), pp. 1378–1392. ISSN: 18790690. DOI: 10.1016/j.rser.2017.05.178. URL: http://dx.doi.org/10.1016/j.rser.2017.05.178.

[10] Manoj Kumar Jindal and Mithilesh K. Jha. "Hydrothermal liquefaction of wood: A critical review". In: *Reviews in Chemical Engineering* 32.4 (2016), pp. 459–488. ISSN: 01678299. DOI: 10.1515/revce-2015-0055.

[11] Douglas C. Elliott, Patrick Biller, Andrew B. Ross, Andrew J. Schmidt, and Susanne B. Jones. "Hydrothermal liquefaction of biomass: Developments from batch to continuous process". In: *Bioresource Technology* 178 (2015), pp. 147–156. ISSN: 18732976. DOI: 10.1016/j.biortech.2014.09.132. URL: http://dx.doi.org/10.1016/j.biortech.2014.09.132.

[12] Geert Haarlemmer, Chamseddine Guizani, Suzanne Anouti, Maxime Déniel, Anne Roubaud, and Sylvie Valin. "Analysis and comparison of bio-oils obtained by hydrothermal liquefaction and fast pyrolysis of beech wood". In: *Fuel* 174 (2016), pp. 180–188. ISSN: 00162361. DOI: 10.1016/j.fuel.2016.01.082.

[13] Samantha Eleanor Tanzer, John Posada, Sjors Geraedts, and Andrea Ramírez. "Lignocellulosic marine biofuel: Technoeconomic and environmental assessment for production in Brazil and Sweden". In: *Journal of Cleaner Production* 239 (2019), p. 117845. ISSN: 0959-6526. DOI: https://doi.org/10.1016/j.jclepro.2019.117845. URL: https://www.sciencedirect.com/science/article/pii/S0959652619327118.

[14] Rajaram Ghadge, Nitin Nagwani, Nikhlesh Saxena, Santanu Dasgupta, and Ajit Sapre. "Design and scale-up challenges in hydrothermal liquefaction process for biocrude production and its upgradation". In: *Energy Conversion and Management: X* 14.November 2021 (2022), p. 100223. ISSN: 25901745. DOI: 10.1016/j.ecmx.2022.100223. URL: https://doi.org/10.1016/j.ecmx.2022.100223.

[15] Daniele Castello, Thomas Helmer Pedersen, and Lasse Aistrup Rosendahl. "Continuous hydrothermal liquefaction of biomass: A critical review". In: *Energies* 11.11 (2018). ISSN: 19961073. DOI: 10.3390/en11113165.

[16] Ayaz Ali Shah, Kamaldeep Sharma, Muhammad Salman Haider, Saqib Sohail Toor, Lasse Aistrup Rosendahl, Thomas Helmer Pedersen, and Daniele Castello. "The Role of Catalysts in Biomass Hydrothermal Liquefaction and Biocrude Upgrading". In: *Processes* 10.2 (2022). ISSN: 22279717. DOI: 10.3390/pr10020207.

[17] Senthil Nagappan, Rahul R. Bhosale, Dinh Duc Nguyen, Nguyen Thuy Lan Chi, Vinoth Kumar Ponnusamy, Chang Soon Woong, and Gopalakrishnan Kumar. "Catalytic hydrothermal liquefaction of biomass into bio-oils and other value-added products – A review". In: *Fuel* 285 (Feb. 2021), p. 119053. ISSN: 0016-2361. DOI: 10.1016/J.FUEL.2020.119053.

[18] Marco Scarsella, Benedetta de Caprariis, Martina Damizia, and Paolo De Filippis. "Heterogeneous catalysts for hydrothermal liquefaction of lignocellulosic biomass: A review". In: *Biomass and Bioenergy* 140.May (2020), p. 105662. ISSN: 18732909. DOI: 10.1016/j.biombioe.2020.105662. URL: https://doi.org/10.1016/j.biombioe.2020.105662.

[19] Jianwen Lu, Jamison Watson, Jianli Zeng, Hugang Li, Zhangbing Zhu, Meng Wang, Yuanhui Zhang, and Zhidan Liu. "Biocrude production and heavy metal migration during hydrothermal liquefaction of swine manure". In: *Process Safety and Environmental Protection* 115 (Apr. 2018), pp. 108–115. ISSN: 0957-5820. DOI: 10.1016/J.PSEP.2017.11.001.

[20] Melodj Dosa, Marco Piumetti, Elahe Davarpanah, Giulia Moncaglieri, Samir Bensaid, and Debora Fino. "Natural Zeolites as Sustainable Materials for Environmental Processes". In: *Nanostructured Catalysts for Environmental Applications* (2021), pp. 367–381. DOI: 10.1007/978-3-030-58934-9{_}13. URL: https://link-springer-com.tudelft.idm.oclc.org/chapter/10.1007/978-3-030-58934-9_13.

[21] Xiuyi Yan, Wei Wang, Yanan Zhao, and Jinghui Zhou. "The Effect of Different Catalysts and Process Parameters on the Chemical Content of Bio-oils from Hydrothermal Liquefaction of Sugarcane Bagasse". In: 13.1 (2018), pp. 997–1018.

[22] Sarvesh Misar. "Drop-in biofuels from Olive Residues: Towards sustainable biofuels in the maritime sector Drop-in biofuels from Olive Residues". In: (2022).

[23] Hossein Mazaheri, Keat Teong Lee, and Abdul Rahman Mohamed. "Influence of temperature on liquid products yield of oil palm shell via subcritical water liquefaction in the presence of alkali catalyst". In: *Fuel Processing Technology* 110 (June 2013), pp. 197–205. ISSN: 0378-3820. DOI: 10.1016/J.FUPROC.2012.12.015.

[24] Benedetta de Caprariis, Paolo De Filippis, Antonietta Petrullo, and Marco Scarsella. "Hydrothermal liquefaction of biomass: Influence of temperature and biomass composition on the bio-oil production". In: *Fuel* 208 (2017), pp. 618–625. ISSN: 00162361. DOI: 10.1016/j.fuel.2017.07.054. URL: http://dx.doi.org/10.1016/j.fuel.2017.07.054.

[25] Yongsheng Zhang, Jamie Minaret, Zhongshun Yuan, Animesh Dutta, and Chunbao Charles Xu. "Mild hydrothermal liquefaction of highwater content agricultural residue for biocrude oil production: A parametric study". In: *Energies* 11.11 (2018). ISSN: 19961073. DOI: 10.3390/en11113129.

[26] Tahir Hussain Seehar, Saqib Sohail Toor, Kamaldeep Sharma, Asbjørn Haaning Nielsen, Thomas Helmer Pedersen, and Lasse Aistrup Rosendahl. "Influence of process conditions on hydrothermal liquefaction of eucalyptus biomass for biocrude production and investigation of the inorganics distribution". In: *Sustainable Energy and Fuels* 5.5 (2021), pp. 1477–1487. ISSN: 23984902. DOI: 10.1039/d0se01634a.

[27] Peter M. Mortensen, Jan Dierk Grunwaldt, Peter A. Jensen, and Anker D. Jensen. "Screening of catalysts for hydrodeoxygenation of phenol as a model compound for bio-oil". In: *ACS Catalysis* 3.8 (Aug. 2013), pp. 1774–1785. ISSN: 21555435. DOI: 10.1021/CS400266E/SUPPL{_}FILE/CS400266E{_}SI{_}001.PDF. URL: https://pubs-acs-org.tudelft.idm.oclc.org/doi/full/10.1021/cs400266e.

[28] Elpiniki Lappa, Per Sigaard Christensen, Maika Klemmer, Jacob Becker, and Bo Brummerstedt Iversen. "Hydrothermal liquefaction of Miscanthus × Giganteus: Preparation of the ideal feedstock". In: *Biomass and Bioenergy* 87 (2016), pp. 17–25. ISSN: 18732909. DOI: 10.1016/j.biombioe.2016.02.008.

[29] *Geography of Namibia - Wikipedia*. URL: https://en.wikipedia.org/wiki/Geography_of_Namibia.

[30] *Groundwater in Namibia*. URL: https://web.archive.org/web/20160729155617/http://www.iwrm-namibia.info.na/iwrm/fundaments-in-iwrm/groundwater-in-namibia/index.php.

[31] Namibia-Biomass Industry Group. "Availability, Quality and Suitability of Bush Biomass from Namibia for the Purpose of Substituting Fossil Fuels in Energy Generation in Hamburg". In: (2020), pp. 1–37. URL: https://www.dasnamibia.org/?wpfb_dl=119.

[32] Rosemary N. Shikangalah and Benjamin S. Mapani. "A review of bush encroachment in Namibia: From a problem to an opportunity?" In: *Journal of Rangeland Science* 10.3 (2020), pp. 251–266. ISSN: 2423642X.

[33] Adam P. Schreiner-McGraw, Enrique R. Vivoni, Hoori Ajami, Osvaldo E. Sala, Heather L. Throop, and Debra P.C. Peters. "Woody Plant Encroachment has a Larger Impact than Climate Change on Dryland Water Budgets". In: *Scientific Reports* 10.1 (Dec. 2020). ISSN: 20452322. DOI: 10.1038/S41598-020-65094-X.

[34] M. Verma, S. Godbout, S. K. Brar, O. Solomatnikova, S. P. Lemay, and J. P. Larouche. "Biofuels production from biomass by thermochemical conversion technologies". In: *International Journal of Chemical Engineering* January 2016 (2012). ISSN: 1687806X. DOI: 10.1155/2012/542426.

[35] Hanif A. Choudhury, Sankar Chakma, and Vijayanand S. Moholkar. "Biomass Gasification Integrated Fischer-Tropsch Synthesis: Perspectives, Opportunities and Challenges". In: *Recent Advances in Thermochemical Conversion of Biomass* (Jan. 2015), pp. 383–435. DOI: 10.1016/B978-0-444-63289-0.00014-4.

[36] Nicola J. Wagner, M. Coertzen, R. H. Matjie, and J. C. van Dyk. "Coal Gasification". In: *Applied Coal Petrology: The Role of Petrology in Coal Utilization* (Jan. 2008), pp. 119–144. DOI: 10.1016/B978-0-08-045051-3.00005-1.

[37] Dinesh Mohan, Charles U. Pittman, and Philip H. Steele. "Pyrolysis of wood/biomass for bio-oil: A critical review". In: *Energy and Fuels* 20.3 (May 2006), pp. 848–889. ISSN: 08870624. DOI: 10.1021/EF0502397/ASSET/IMAGES/LARGE/EF0502397H00010.JPEG. URL: https://pubs-acs-org.tudelft.idm.oclc.org/doi/full/10.1021/ef0502397.

[38] Chao Gai, Yuanhui Zhang, Wan Ting Chen, Peng Zhang, and Yuping Dong. "An investigation of reaction pathways of hydrothermal liquefaction using Chlorella pyrenoidosa and Spirulina platensis". In: *Energy Conversion and Management* 96 (2015), pp. 330–339. ISSN: 01968904. DOI: 10.1016/j.enconman.2015.02.056. URL: http://dx.doi.org/10.1016/j.enconman.2015.02.056.

[39] Diego López Barreiro, Sascha Riede, Ursel Hornung, Andrea Kruse, and Wolter Prins. "Hydrothermal liquefaction of microalgae: Effect on the product yields of the addition of an organic solvent to separate the aqueous phase and the biocrude oil". In: *Algal Research* 12 (Nov. 2015), pp. 206–212. ISSN: 2211-9264. DOI: 10.1016/J.ALGAL.2015.08.025.

[40] Xumeng Ge, Chun Chang, Lu Zhang, Shaoqing Cui, Xiaolan Luo, Shengjun Hu, Yusheng Qin, and Yebo Li. "Conversion of Lignocellulosic Biomass Into Platform Chemicals for Biobased Polyurethane Application". In: *Advances in Bioenergy* 3 (Jan. 2018), pp. 161–213. ISSN: 2468-0125. DOI: 10.1016/BS.AIBE.2018.03.002.

[41] Sushant Negi, Gaurav Jaswal, Kali Dass, Koushik Mazumder, Sasikumar Elumalai, and Joy K. Roy. "Torrefaction: a sustainable method for transforming of agri-wastes to high energy density solids (biocoal)". In: *Reviews in Environmental Science and Biotechnology* 19.2 (2020), pp. 463–488. ISSN: 15729826. DOI: 10.1007/s11157-020-09532-2. URL: https://doi.org/10.1007/s11157-020-09532-2.

[42] Dengyu Chen, Anjiang Gao, Kehui Cen, Jie Zhang, Xiaobing Cao, and Zhongqing Ma. *Investigation of biomass torrefaction based on three major components: Hemicellulose, cellulose, and lignin*. English. 2018.

[43] Abdul Sattar Jatoi et al. "Hydrothermal Liquefaction of Lignocellulosic and Protein-Containing Biomass: A Comprehensive Review". In: *Catalysts* 12.12 (2022). ISSN: 20734344. DOI: 10.3390/catal12121621.

[44] Ying Hong Xu and Ming Fei Li. "Hydrothermal liquefaction of lignocellulose for value-added products: Mechanism, parameter and production application". In: *Bioresource Technology* 342.September (2021), p. 126035. ISSN: 18732976. DOI: 10.1016/j.biortech.2021.126035. URL: https://doi.org/10.1016/j.biortech.2021.126035.

[45] Sanphawat Phromphithak, Thossaporn Onsree, Ruetai Saengsuriwong, and Nakorn Tippayawong. "Compositional analysis of bio-oils from hydrothermal liquefaction of tobacco residues using two-dimensional gas chromatography and time-of-flight mass spectrometry". In: *Science Progress* 104.4 (2021), pp. 1–12. ISSN: 20477163. DOI: 10.1177/00368504211064486.

[46] Douglas C. Elliott, Todd R. Hart, Gary G. Neuenschwander, Leslie J. Rotness, Guri Roesijadi, Alan H. Zacher, and Jon K. Magnuson. "Hydrothermal processing of macroalgal feedstocks in continuous-flow reactors". In: *ACS Sustainable Chemistry and Engineering* 2.2 (Feb. 2014), pp. 207–215. ISSN: 21680485. DOI: 10.1021/SC400251P/ASSET/IMAGES/LARGE/SC-2013-00251P{_}0004.JPEG. URL: https://pubs-acs-org.tudelft.idm.oclc.org/doi/full/10.1021/sc400251p.

[47] Umakanta Jena, K. C. Das, and J. R. Kastner. "Comparison of the effects of Na2CO3, Ca3(PO4)2, and NiO catalysts on the thermochemical liquefaction of microalga Spirulina platensis". In: *Applied Energy* 98 (Oct. 2012), pp. 368–375. ISSN: 0306-2619. DOI: 10.1016/J.APENERGY.2012.03.056.

[48] Melcureraj Lavanya, Arunachalam Meenakshisundaram, Sahadevan Renganathan, Senthil Chinnasamy, David Milton Lewis, Jaganathan Nallasivam, and Sailendra Bhaskar. "Hydrothermal liquefaction of freshwater and marine algal biomass: A novel approach to produce distillate fuel fractions through blending and co-processing of biocrude with petrocrude". In: *Bioresource Technology* 203 (Mar. 2016), pp. 228–235. ISSN: 0960-8524. DOI: 10.1016/J.BIORTECH.2015.12.013.

[49] Vinod Kumar et al. "Low-temperature catalyst based Hydrothermal liquefaction of harmful Macroalgal blooms , and aqueous phase nutrient recycling by microalgae". In: August 2018 (2019), pp. 1–9. DOI: 10.1038/s41598-019-47664-w.

[50] Laleh Nazari, Zhongshun Yuan, Sadra Souzanchi, Madhumita B. Ray, and Chunbao Xu. "Hydrothermal liquefaction of woody biomass in hot-compressed water: Catalyst screening and comprehensive characterization of bio-crude oils". In: *Fuel* 162 (Dec. 2015), pp. 74–83. ISSN: 0016-2361. DOI: 10.1016/J.FUEL.2015.08.055.

[51] Federica Conti, Saqib S. Toor, Thomas H. Pedersen, Tahir H. Seehar, Asbjørn H. Nielsen, and Lasse A. Rosendahl. "Valorization of animal and human wastes through hydrothermal liquefaction for biocrude production and simultaneous recovery of nutrients". In: *Energy Conversion and Management* 216 (July 2020), p. 112925. ISSN: 0196-8904. DOI: 10.1016/J.ENCONMAN.2020.112925.

[52] Derek R. Vardon, B. K. Sharma, John Scott, Guo Yu, Zhichao Wang, Lance Schideman, Yuanhui Zhang, and Timothy J. Strathmann. "Chemical properties of biocrude oil from the hydrothermal liquefaction of Spirulina algae, swine manure, and digested anaerobic sludge". In: *Bioresource Technology* 102.17 (Sept. 2011), pp. 8295–8303. ISSN: 0960-8524. DOI: 10.1016/J.BIORTECH.2011.06.041.

[53] P. Biller and A. B. Ross. "Potential yields and properties of oil from the hydrothermal liquefaction of microalgae with different biochemical content". In: *Bioresource Technology* 102.1 (2011), pp. 215–225. ISSN: 09608524. DOI: 10.1016/j.biortech.2010.06.028. URL: http://dx.doi.org/10.1016/j.biortech.2010.06.028.

[54] George W. Huber, Sara Iborra, and Avelino Corma. "Synthesis of transportation fuels from biomass: Chemistry, catalysts, and engineering". In: *Chemical Reviews* 106.9 (Sept. 2006), pp. 4044–4098. ISSN: 00092665. DOI: 10.1021/CR068360D/ASSET/IMAGES/MEDIUM/CR068360DF00035.GIF. URL: https://pubs-acs-org.tudelft.idm.oclc.org/doi/full/10.1021/cr068360d.

[55] P. M. Mortensen, J. D. Grunwaldt, P. A. Jensen, K. G. Knudsen, and A. D. Jensen. "A review of catalytic upgrading of bio-oil to engine fuels". In: *Applied Catalysis A: General* 407.1-2 (Nov. 2011), pp. 1–19. ISSN: 0926-860X. DOI: 10.1016/J.APCATA.2011.08.046.

[56] Daniele Castello, Muhammad Salman Haider, and Lasse Aistrup Rosendahl. "Catalytic upgrading of hydrothermal liquefaction biocrudes: Different challenges for different feedstocks". In: *Renewable Energy* 141 (2019), pp. 420–430. ISSN: 18790682. DOI: 10.1016/j.renene.2019.04.003. URL: https://doi.org/10.1016/j.renene.2019.04.003.

[57] Yusuf Celikbag, Shatori Meadows, Mehul Barde, Sushil Adhikari, Gisela Buschle-Diller, Maria L. Auad, and Brian K. Via. "Synthesis and Characterization of Bio-oil-Based Self-Curing Epoxy Resin". In: *Industrial and Engineering Chemistry Research* 56.33 (2017), pp. 9389–9400. ISSN: 15205045. DOI: 10.1021/acs.iecr.7b02123.

[58] Yusuf Celikbag, Md Nuruddin, Manik Biswas, Osei Asafu-Adjaye, and Brian K. Via. "Bio-oil-based phenol–formaldehyde resin: comparison of weight- and molar-based substitution of phenol with bio-oil". In: *Journal of Adhesion Science and Technology* 34.24 (2020), pp. 2743–2754. ISSN: 15685616. DOI: 10.1080/01694243.2020.1784540. URL: https://doi.org/10.1080/01694243.2020.1784540.

[59] Vinoth Kumar Ponnusamy, Senthil Nagappan, Rahul R. Bhosale, Chyi How Lay, Dinh Duc Nguyen, Arivalagan Pugazhendhi, Soon Woong Chang, and Gopalakrishnan Kumar. "Review on sustainable production of biochar through hydrothermal liquefaction: Physico-chemical properties and applications". In: *Bioresource Technology* 310.April (2020), p. 123414. ISSN: 18732976. DOI: 10.1016/j.biortech.2020.123414. URL: https://doi.org/10.1016/j.biortech.2020.123414.

[60] Zhengang Liu and Fu Shen Zhang. "Removal of lead from water using biochars prepared from hydrothermal liquefaction of biomass". In: *Journal of Hazardous Materials* 167.1-3 (Aug. 2009), pp. 933–939. ISSN: 0304-3894. DOI: 10.1016/J.JHAZMAT.2009.01.085.

[61] Li Jian Leng, Xing Zhong Yuan, Hua Jun Huang, Hou Wang, Zhi Bin Wu, Li Huan Fu, Xin Peng, Xiao Hong Chen, and Guang Ming Zeng. "Characterization and application of bio-chars from liquefaction of microalgae, lignocellulosic biomass and sewage sludge". In: *Fuel Processing Technology* 129 (Jan. 2015), pp. 8–14. ISSN: 0378-3820. DOI: 10.1016/J.FUPROC.2014.08.016.

[62] Saravanan R. Shanmugam, Sushil Adhikari, Hyungseok Nam, and Sourov Kar Sajib. "Effect of bio-char on methane generation from glucose and aqueous phase of algae liquefaction using mixed anaerobic cultures". In: *Biomass and Bioenergy* 108 (Jan. 2018), pp. 479–486. ISSN: 0961-9534. DOI: 10.1016/J.BIOMBIOE.2017.10.034.

[63] V. Karthik, P. Senthil Kumar, Dai Viet N. Vo, J. Sindhu, D. Sneka, B. Subhashini, K. Saravanan, and J. Jeyanthi. "Hydrothermal production of algal biochar for environmental and fertilizer applications: a review". In: *Environmental Chemistry Letters 2020 19:2* 19.2 (Nov. 2020), pp. 1025–1042. ISSN: 1610-3661. DOI: 10.1007/S10311-020-01139-X. URL: https://link-springer-com.tudelft.idm.oclc.org/article/10.1007/s10311-020-01139-x.

[64] Patrick Biller and Andrew B. Ross. "Hydrothermal processing of algal biomass for the production of biofuels and chemicals". In: *http://dx.doi.org.tudelft.idm.oclc.org/10.4155/bfs.12.42* 3.5 (2014), pp. 603–623. ISSN: 17597277. DOI: 10.4155/BFS.12.42. URL: https://www-tandfonline-com.tudelft.idm.oclc.org/doi/abs/10.4155/bfs.12.42.

[65] Jamison Watson, Tengfei Wang, Buchun Si, Wan Ting Chen, Aersi Aierzhati, and Yuanhui Zhang. "Valorization of hydrothermal liquefaction aqueous phase: pathways towards commercial viability". In: *Progress in Energy and Combustion Science* 77 (2020), p. 100819. ISSN: 03601285. DOI: 10.1016/j.pecs.2019.100819. URL: https://doi.org/10.1016/j.pecs.2019.100819.

[66] Mingxia Zheng, Lance C. Schideman, Giovana Tommaso, Wan Ting Chen, Yan Zhou, Ken Nair, Wanyi Qian, Yuanhui Zhang, and Kaijun Wang. "Anaerobic digestion of wastewater generated from the hydrothermal liquefaction of Spirulina: Toxicity assessment and minimization". In: *Energy Conversion and Management* 141 (June 2017), pp. 420–428. ISSN: 0196-8904. DOI: 10.1016/J.ENCONMAN.2016.10.034.

[67] Leichang Cao, Cheng Zhang, Huihui Chen, Daniel C.W. Tsang, Gang Luo, Shicheng Zhang, and Jianmin Chen. "Hydrothermal liquefaction of agricultural and forestry wastes: state-of-the-art review and future prospects". In: *Bioresource Technology* 245.June (2017), pp. 1184–1193. ISSN: 18732976. DOI: 10.1016/j.biortech.2017.08.196. URL: https://doi.org/10.1016/j.biortech.2017.08.196.

[68] Zheting Bi, Ji Zhang, Emily Peterson, Zeying Zhu, Chunjie Xia, Yanna Liang, and Tomasz Wiltowski. "Biocrude from pretreated sorghum bagasse through catalytic hydrothermal liquefaction". In: *Fuel* 188 (Jan. 2017), pp. 112–120. ISSN: 0016-2361. DOI: 10.1016/J.FUEL.2016.10.039.

[69] Joseph S.M. Samec, Jan E. Bäckvall, Pher G. Andersson, and Peter Brandt. "Mechanistic aspects of transition metal-catalyzed hydrogen transfer reactions". In: *Chemical Society Reviews* 35.3 (Feb. 2006), pp. 237–248. ISSN: 1460-4744. DOI: 10.1039/B515269K. URL: https://pubs-rsc-org.tudelft.idm.oclc.org/en/content/articlehtml/2006/cs/b515269k%20https://pubs-rsc-org.tudelft.idm.oclc.org/en/content/articlelanding/2006/cs/b515269k.

[70] Sungyup Jung, Eilhann E. Kwon, and Young Kwon Park. *Catalytic hydrodeoxygenation for upgrading of lignin-derived bio-oils*. BV, 2021, pp. 129–145. ISBN: 9780128202944. DOI: 10.1016/B978-0-12-820294-4.00010-7. URL: http://dx.doi.org/10.1016/B978-0-12-820294-4.00010-7.

[71] Zhe Zhu, Saqib Sohail Toor, Lasse Rosendahl, Donghong Yu, and Guanyi Chen. "Influence of alkali catalyst on product yield and properties via hydrothermal liquefaction of barley straw". In: *Energy* 80 (Feb. 2015), pp. 284–292. ISSN: 0360-5442. DOI: 10.1016/J.ENERGY.2014.11.071.

[72] Gizelle I. Almerindo, Luiz F.D. Probst, Carlos E.M. Campos, Rusiene M. De Almeida, Simoni M.P. Meneghetti, Mario R. Meneghetti, Jean Marc Clacens, and Humberto V. Fajardo. "Magnesium oxide prepared via metal–chitosan complexation method: Application as catalyst for transesterification of soybean oil and catalyst deactivation studies". In: *Journal of Power Sources* 196.19 (Oct. 2011), pp. 8057–8063. ISSN: 0378-7753. DOI: 10.1016/J.JPOWSOUR.2011.05.030.

[73] See Cheng Yim, Armando T. Quitain, Suzana Yusup, Mitsuru Sasaki, Yoshimitsu Uemura, and Tetsuya Kida. "Metal oxide-catalyzed hydrothermal liquefaction of Malaysian oil palm biomass to bio-oil under supercritical condition". In: *The Journal of Supercritical Fluids* 120 (Feb. 2017), pp. 384–394. ISSN: 0896-8446. DOI: 10.1016/J.SUPFLU.2016.05.044.

[74] John B. Claridge, Malcolm L.H. Green, Shik Chi Tsang, and Andrew P.E. York. "Conversion of propanal to pentan-3-one using lanthanide oxides". In: *Journal of the Chemical Society, Faraday Transactions* 89.7 (1993), pp. 1089–1094. ISSN: 09565000. DOI: 10.1039/FT9938901089.

[75] Shouyun Cheng, Lin Wei, Xianhui Zhao, and James Julson. "Application, deactivation, and regeneration of heterogeneous catalysts in bio-oil upgrading". In: *Catalysts* 6.12 (2016). ISSN: 20734344. DOI: 10.3390/catal6120195.

[76] Jacob R. Ludwig and Corinna S. Schindler. "Catalyst: Sustainable Catalysis". In: *Chem* 2.3 (Mar. 2017), pp. 313–316. ISSN: 2451-9294. DOI: 10.1016/J.CHEMPR.2017.02.014.

[77] Qiao Yi Chen, Thomas DesMarais, and Max Costa. "Metals and Mechanisms of Carcinogenesis." eng. In: *Annual review of pharmacology and toxicology* 59 (Jan. 2019), pp. 537–554. ISSN: 1545-4304 (Electronic). DOI: 10.1146/annurev-pharmtox-010818-021031.

[78] Brabu Balusamy, Burcu Ertit Taştan, Seyda Fikirdesici Ergen, Tamer Uyar, and Turgay Tekinay. "Toxicity of lanthanum oxide (La2O3) nanoparticles in aquatic environments." eng. In: *Environmental science. Processes & impacts* 17.7 (July 2015), pp. 1265–1270. ISSN: 2050-7895 (Electronic). DOI: 10.1039/c5em00035a.

[79] Tahir H. Seehar, Saqib S. Toor, Ayaz A. Shah, Thomas H. Pedersen, and Lasse A. Rosendahl. "Biocrude production from wheat straw at sub and supercritical hydrothermal liquefaction". In: *Energies* 13.12 (2020). ISSN: 19961073. DOI: 10.3390/en13123114.

[80] Zhe Zhu, Lasse Rosendahl, Saqib Sohail Toor, and Guanyi Chen. "Optimizing the conditions for hydrothermal liquefaction of barley straw for bio-crude oil production using response surface methodology". In: *Science of The Total Environment* 630 (July 2018), pp. 560–569. ISSN: 0048-9697. DOI: 10.1016/J.SCITOTENV.2018.02.194.

[81] *What Is Design of Experiments (DOE)? | ASQ*. URL: https://asq.org/quality-resources/design-of-experiments.

[82] NIST. *5.3.3.6.1. Central Composite Designs (CCD)*. URL: https://www.itl.nist.gov/div898/handbook/pri/section3/pri3361.htm.

[83] Francesco Brandi, Markus Antonietti, and Majd Al-Naji. "Controlled lignosulfonate depolymerization via solvothermal fragmentation coupled with catalytic hydrogenolysis/hydrogenation in a continuous flow reactor". In: *Green Chemistry* 23.24 (Dec. 2021), pp. 9894–9905. ISSN: 1463-9270. DOI: 10.1039/D1GC01714D. URL: https://pubs-rsc-org.tudelft.idm.oclc.org/en/content/articlehtml/2021/gc/d1gc01714d%20https://pubs-rsc-org.tudelft.idm.oclc.org/en/content/articlelanding/2021/gc/d1gc01714d.

[84] Pushpa Jha and Bhajan Dass. "Analysis of biomasses for their thermochemical transformations to biofuels". In: *International Journal of Energy Production and Management* 5.2 (2020), pp. 115–124. ISSN: 20563280. DOI: 10.2495/EQ-V5-N2-115-124.

[85] B Desisa and A Dilnesa. "Chemical composition and diluted acid hydrolysis pretreatment of Acacia mellifera sawdust as a raw material for bioethanol production". In: *World News of Natural Sciences* 14 (2017), pp. 36–46. URL: http://agro.icm.edu.pl/agro/element/bwmeta1.element.agro-6e5d4943-452d-4a58-90e5-447d49ee9f0e%0Ahttps://agro.icm.edu.pl/agro/element/bwmeta1.element.agro-6e5d4943-452d-4a58-90e5-447d49ee9f0e.

[86] Saikat Mitra et al. "Impact of heavy metals on the environment and human health: Novel therapeutic insights to counter the toxicity". In: *Journal of King Saud University - Science* 34.3 (Apr. 2022), p. 101865. ISSN: 1018-3647. DOI: 10.1016/J.JKSUS.2022.101865.

[87] Qingqing Guan, Taoxiu Mao, Qiulin Zhang, Rongrong Miao, Ping Ning, Junjie Gu, Senlin Tian, Qiuling Chen, and Xin Sheng Chai. "Catalytic gasification of lignin with Ni/Al2O3-SiO2 in sub/supercritical water". In: *Journal of Supercritical Fluids* 95 (2014), pp. 413–421. ISSN: 08968446. DOI: 10.1016/j.supflu.2014.10.015. URL: http://dx.doi.org/10.1016/j.supflu.2014.10.015.

[88] W. Shi, S. Li, H. Jin, Y. Zhao, and W. Yu. "The Hydrothermal Liquefaction of Rice Husk to Bio-crude Using Metallic Oxide Catalysts". In: *http://dx.doi.org.tudelft.idm.oclc.org/10.1080/15567703* 35.22 (Nov. 2013), pp. 2149–2155. ISSN: 15567036. DOI: 10.1080/15567036.2012.700996. URL: https://www-tandfonline-com.tudelft.idm.oclc.org/doi/abs/10.1080/15567036.2012.700996.

[89] Robert J. Evans, Thomas A. Milne, and Michael N. Soltys. "Direct mass-spectrometric studies of the pyrolysis of carbonaceous fuels. III. Primary pyrolysis of lignin". In: *Journal of Analytical and Applied Pyrolysis* 9.3 (1986), pp. 207–236. ISSN: 01652370. DOI: 10.1016/0165-2370(86)80012-2.

[90] Wei Hsin Chen, Yu Ying Lin, Hsuah Cheng Liu, Teng Chien Chen, Hung Chun Hung, and Chi Hui Chen. "Analysis of physicochemical properties of liquefaction bio-oil from food waste". In: *Energy Procedia* 158 (2019), pp. 61–66. ISSN: 18766102. DOI: 10.1016/j.egypro.2019.01.036. URL: https://doi.org/10.1016/j.egypro.2019.01.036.

[91] M. A. Deboer and K. Lammertsma. "Scarcity of rare earth elements". In: *ChemSusChem* 6.11 (2013), pp. 2045–2055. ISSN: 18645631. DOI: 10.1002/cssc.201200794.

[92] *Lanthanum - MMTA*. URL: https://mmta.co.uk/metals/la/.

[93] F. J.W.J. Labuschagné, A. Wiid, H. P. Venter, B. R. Gevers, and A. Leuteritz. "Green synthesis of hydrotalcite from untreated magnesium oxide and aluminum hydroxide". In: *http://mc.manuscriptcentral.com/tgcl* 11.1 (Jan. 2018), pp. 18–28. ISSN: 17517192. DOI: 10.1080/17518253.2018.1426791. URL: https://www-tandfonline-com.tudelft.idm.oclc.org/doi/abs/10.1080/17518253.2018.1426791.

[94] Grace N. Muriithi, Leslie F. Petrik, Wilson M. Gitari, and Frédéric J. Doucet. "Synthesis and characterization of hydrotalcite from South African Coal fly ash". In: *Powder Technology* 312 (May 2017), pp. 299–309. ISSN: 0032-5910. DOI: 10.1016/J.POWTEC.2017.02.018.

[95] T. Crommentuijn, M.D. Polder, and E.J. van de Plassche. *Maximum Permissible Concentrations and Negligible Concentrations for metals, taking background concentrations into account*. 1997.

[96] Albert Rivas-Ubach, Yina Liu, Thomas S. Bianchi, Nikola Tolić, Christer Jansson, and Ljiljana Paša-Tolić. "Moving beyond the van Krevelen Diagram: A New Stoichiometric Approach for Compound Classification in Organisms". In: *Analytical Chemistry* 90.10 (2018), pp. 6152–6160. ISSN: 15206882. DOI: 10.1021/acs.analchem.8b00529.

[97] Eurostat. *Production of lignite in the EU - statistics - Statistics Explained*. URL: https://ec.europa.eu/eurostat/statistics-explained/index.php?title=Production_of_lignite_in_the_EU_-_statistics#What_is_lignite_and_how_significant_is_this_fossil_fuel_in_the_EU.3F.

[98] C Krieger, C Calvaruso, C Morlot, S Uroz, L Salsi, and M-P Turpault. "Identification, distribution, and quantification of biominerals in a deciduous forest." eng. In: *Geobiology* 15.2 (Mar. 2017), pp. 296–310. ISSN: 1472-4669 (Electronic). DOI: 10.1111/gbi.12223.

[99] Javaid Akhtar and Nor Aishah Saidina Amin. "A review on process conditions for optimum bio-oil yield in hydrothermal liquefaction of biomass". In: *Renewable and Sustainable Energy Reviews* 15.3 (2011), pp. 1615–1624. ISSN: 13640321. DOI: 10.1016/j.rser.2010.11.054. URL: http://dx.doi.org/10.1016/j.rser.2010.11.054.

[100] Claus Uhrenholt Jensen, Julie Katerine Rodriguez Guerrero, Sergios Karatzos, Göran Olofsson, and Steen Brummerstedt Iversen. "Fundamentals of Hydrofaction™: Renewable crude oil from woody biomass". In: *Biomass Conversion and Biorefinery* 7.4 (2017), pp. 495–509. ISSN: 21906823. DOI: 10.1007/s13399-017-0248-8.

[101] Licella. "Production of Licella bio-crude oil as a platform for bio-chemicals , marine & aviation fuels". In: (2016).

[102] C U Jensen, S Karatzos, G Olofsson, and S B Iversen. "Hydrofaction™ of forestry residues to drop-in renewable transportation fuels 10". In: (2018).

[103] Vadim Yakovlev, M Alekseeva, and Sofia Khromova. "Stability of nickel-containing catalysts for hydrodeoxygenation of biomass pyrolysis products". In: *Catalysis in Industry* 4 (Oct. 2012). DOI: 10.1134/S2070050412040204.

[104] Dragos Tutunea, Ilie Dumitru, Laurentiu Racila, Oana Otat, Lucian Matei, and Ionut Geonea. "Characterization of Sunflower Oil Biodiesel as Alternative for Diesel Fuel". In: January (2019), pp. 172–180. DOI: 10.1007/978-3-319-94409-8{_}21.

[105] N. Rao Cheepurupalli and B. Anuradha. "Proximate and Ultimate Charaterization of Coal Samples from Southwestern Part of Ethiopia". In: *International Journal of Engineering and Advanced Technology* 9.2 (2019), pp. 1643–1648. DOI: 10.35940/ijeat.b3046.129219.

Appendix

A.1 Division of tasks

Table A.1: Division of MSc Thesis tasks.

Task	Organization	Name(s)
Conceptualization	TU Delft	Nikos Bias & Luis Cutz
Data analysis and interpretation		Nikos Bias & Luis Cutz
Final report writing		Nikos Bias
Final report editing		Nikos Bias & Luis Cutz
HTL experiments	TU Delft	Nikos Bias
Bomb calorimetry	TU Delft	Nikos Bias
Karl Fisher titration	TU Delft	Nikos Bias
TGA	TU Delft	Nikos Bias
ICP-OES sample preparation	TU Delft	Nikos Bias
ICP-OES	TU Delft	Michel van den Brink
GC-MS sample preparation	TU Delft	Nikos Bias
GC-MS	BasCat	Majd Al Naji
XRD	MSE, TU Delft	Rudd Hendrikx
CHNO analysis	Intertek B.V.	Joachim Dierckx

A.2 Product yields for screening and optimization campaign

This section provides all the available data regarding the yields from each campaign and for each product.

Table A.2: Product distribution for different catalysts at 300^{o}C and 15 min residence time

Sample 300 ^{o}C-15 min	Bio-oil yield (%)	Biochar yield (%)	Aqueous phase yield (%)	Gas yield (%)
Non-catalytic	19.69% (3.33)	33.00% (3.05)	23.02% (5.27)	24.29% (5.55)
Zeolite - 5%	25.04% (1.38)	37.56% (0.01)	22.30% (0.12)	15.10% (1.24)
La_2O_3 - 5%	24.46% (0.22)	36.84% (0.52)	26.78% (6.29)	11.92% (3.72)
Hydrotalcite - 5%	28.74% (0.28)	30.88% (0.06)	29.86% (1.71)	10.52% (1.37)
Ni/Si-Al - 5%	30.40% (0.05)	26.45% (0.33)	26.36% (3.53)	16.79% (3.80)

Table A.3: CCD randomized order for HTL experiments, provided by software Design Expert.

Run	Temperature (°C)	Residence time (min)	Catalyst loading (%)
1	270	30	2.5
2	270	10	7.5
3	330	30	7.5
4	330	30	2.5
5	270	30	7.5
6	270	10	2.5
7	330	10	7.5
8	300	15	5
9	330	10	2.5
10	300	15	5
11	300	15	5
12	300	15	5
13	300	15	5
14	340	15	5
15	300	60	5
16	300	5	5
17	300	15	0
18	250	15	5
19	300	15	5
20	300	15	10

Table A.4: Product distribution for each HTL run using the CCD approach.

Sample	Response 1 Bio-oil yield (%)	Response 2 Biochar yield (%)	Response 3 Aqueous Phase yield (%)	Response 4 Gaseous Phase (%)
270-30-2.5	19.43	34.12	27.43	19.02
270-10-7.5	22.71	36.44	33.71	7.16
330-30-7.5	28.48	26.23	25.43	19.86
330-30-2.5	25.60	26.54	26.80	21.06
270-30-7.5	18.96	36.56	32.29	12.19
270-10-2.5	18.27	38.66	27.91	15.16
330-10-7.5	25.03	27.44	27.35	20.18
300-15-5	24.38	30.63	25.71	19.29
330-10-2.5	20.86	28.35	28.17	22.62
300-15-5	24.04	30.62	29.42	15.89
300-15-5	24.67	30.85	26.09	18.40
300-15-5	19.97	32.96	29.36	17.70
300-15-5	22.06	31.60	28.37	17.97
340-15-5	23.87	27.43	29.39	19.31
300-60-5	20.49	31.39	25.28	22.85
300-5-5	19.66	31.67	34.09	14.58
300-15-0	14.59	38.43	18.32	28.65
250-15-5	13.18	52.02	26.56	8.25
300-15-5	22.46	29.74	26.10	21.70
300-15-10	23.33	32.16	36.04	8.47

A.3 Feedstock and product characterization additional data

Table A.5: Inorganic elemental composition of Acacia Mellifera obtained via ICP-OES.

Element	Concentration (mg/kg)
Ca	11783
K	2763
Mg	1618
P	1045
S	854
Fe	124
Sr	48
Zn	23
Ba	21
B	17
Cu	8
Co	3
Mo	3

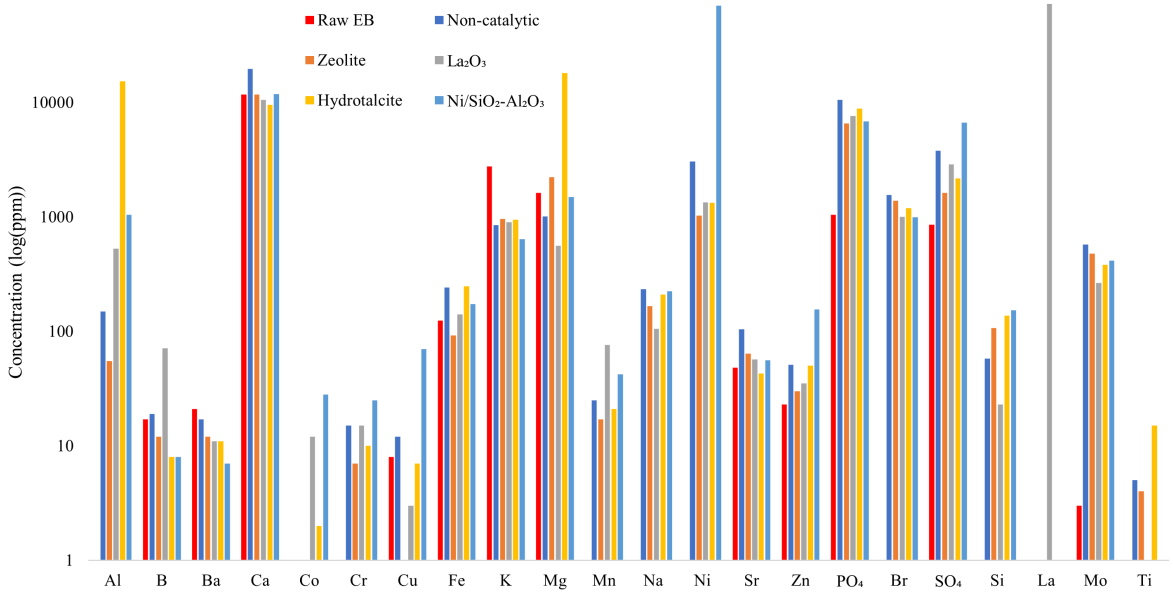

Figure A.1: ICP-OES for catalyst screening campaign

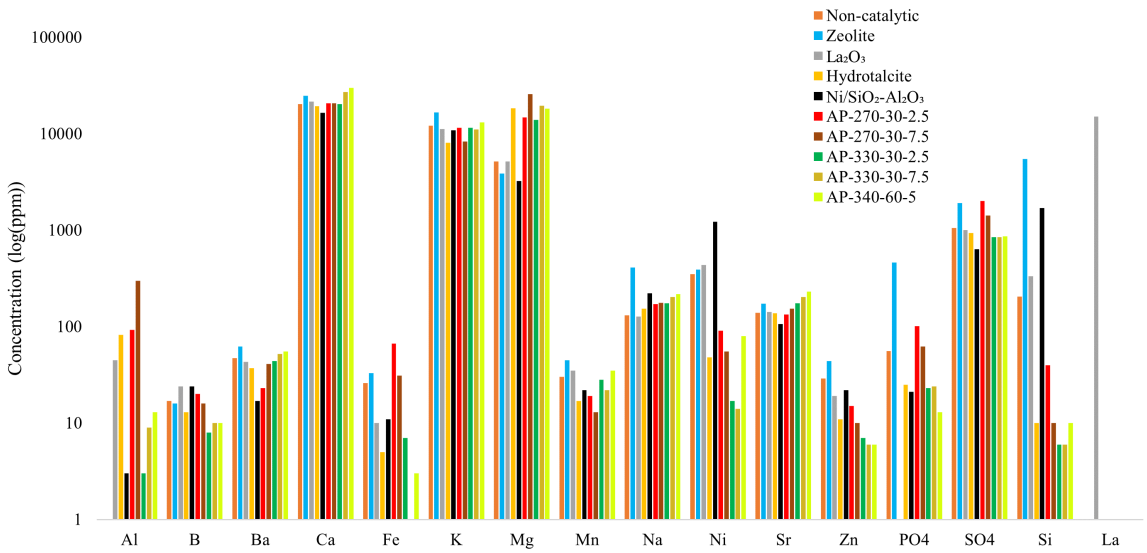

Figure A.2: ICP-OES for AP samples.

A.3.1 Proximate and Ultimate Analysis

Table A.6: CHNO analysis for all BO and BC samples from both campaigns.

Sample	C (%)	H(%)	N(%)	O(%)	H/C	O/C
Bio-oil						
Non-catalytic	52.7	6.1	1.3	39.9	1.39	0.57
Zeolite	64.5	9.6	0.9	25.0	1.79	0.29
La2O3	65.3	9.9	1.2	23.6	1.82	0.27
Hydrotalcite	54.3	6.2	1.4	38.1	1.37	0.53
Ni/Si-Al	50.0	5.7	1.1	43.2	1.37	0.65
BO-270-30-2.5	70.6	7.7	2.5	19.2	1.31	0.20
BO-270-30-7.5	63.8	7	1.6	27.6	1.32	0.32
BO-330-30-2.5	72.5	7.9	2.1	17.5	1.31	0.18
BO-330-30-7.5	71.6	7.8	1.9	18.7	1.31	0.20
BO-340-60-5	61.3	6.8	1.6	30.3	1.33	0.37
Biochar						
Non-catalytic	68.6	5.2	2.3	23.9	0.91	0.26
Zeolite	62.1	4.7	2.1	31.1	0.91	0.38
La2O3	64.2	5.3	2.5	28.0	0.99	0.33
Hydrotalcite	63.0	4.9	1.9	30.2	0.93	0.36
Ni/Si-Al	59.4	4.8	2.2	33.6	0.97	0.42
BC-270-30-2.5	64.9	5.7	3.1	26.3	1.05	0.30
BC-270-30-7.5	59.3	5.5	2.2	33	1.11	0.42
BC-330-30-2.5	69.3	5.3	2.6	22.8	0.92	0.25
BC-330-30-7.5	58.7	5.0	2.2	34.1	1.02	0.44
BC-340-60-5	63.2	4.9	2.2	29.7	0.93	0.35

Table A.7: GC-MS compounds from non-catalytic BO.

PK	RT	Area Pct	Library/ID
1	2.9007	0.9273	2-Cyclopenten-1-one
2	2.9804	0.3932	Cyclopentanone, 2-methyl-
3	3.06	0.2574	Cyclopentanone, 3-methyl-
4	3.8108	3.9424	2-Cyclopenten-1-one, 2-methyl-
5	3.8904	1.6759	Ethanone, 1-(2-furanyl)-
6	4.1179	0.55	2,5-Hexanedione
8	4.4933	0.6297	2(3H)-Furanone, dihydro-5-methyl-
9	4.6411	2.3379	2-Cyclopenten-1-one, 3-methyl-
11	5.1075	1.8257	2-Cyclopenten-1-one, 2,3-dimethyl-
12	5.4829	0.4778	2-Cyclopenten-1-one, 3,4-dimethyl-
14	5.7332	1.9858	2-Cyclopenten-1-one, 2,3-dimethyl-
16	6.0744	0.7798	Phenol, 2-methyl-
17	6.3019	0.6449	2-Cyclopenten-1-one, 3-ethyl-
18	6.3702	3.8085	Phenol, 3-methyl-
19	6.5181	13.428	Phenol, 2-methoxy-
20	6.6546	0.5015	Cyclopentanecarboxaldehyde, 2-methyl-3-methylene-
21	6.6887	0.4335	1-Isopropylcyclohex-1-ene
28	8.0082	2.5474	Creosol
30	9.214	2.62	Phenol, 4-ethyl-2-methoxy-
31	9.2709	0.9626	1H-Inden-1-one, 2,3-dihydro-
33	10.2378	12.7643	Phenol, 2,6-dimethoxy-
34	10.4084	1.9314	Phenol, 2-methoxy-4-propyl-
38	11.9896	1.1749	1,4-Dimethoxy-2,3-dimethylbenzene
46	14.822	0.8556	Ethanone, 1-(4-hydroxy-3,5-dimethoxyphenyl)-
50	17.0743	3.8238	n-Hexadecanoic acid
51	18.7238	4.4571	Oleic Acid
52	18.7693	1.9764	Oleic Acid
53	18.9058	0.7632	Octadecanoic acid
57	23.763	0.743	9-Octadecenamide, (Z)-

Table A.8: GC-MS compounds from zeolite BO

PK	RT	Area Pct	Library/ID
1	2.9234	0.842	2-Cyclopenten-1-one
2	2.9917	0.341	Cyclopentanone, 2-methyl-
3	3.0599	0.223	Cyclopentanone, 3-methyl-
4	3.2306	0.273	Butanoic acid, 3-methyl-
7	3.8107	3.112	2-Cyclopenten-1-one, 2-methyl-
8	3.8903	0.699	Ethanone, 1-(2-furanyl)-
9	3.9472	0.707	Butyrolactone
10	4.1178	0.436	2,5-Hexanedione
16	4.6525	1.692	2-Cyclopenten-1-one, 3-methyl-
19	5.1075	1.603	2-Cyclopenten-1-one, 2,3-dimethyl-
20	5.4715	0.389	2-Cyclopenten-1-one, 3,4-dimethyl-
23	5.7331	1.514	2-Cyclopenten-1-one, 2,3-dimethyl-
26	6.0744	0.627	Phenol, 2-methyl-
27	6.3019	0.546	2-Cyclopenten-1-one, 3-ethyl-
28	6.3929	2.741	p-Cresol
29	6.5066	10.318	Phenol, 2-methoxy-
36	7.4394	0.356	Phenol, 2,3-dimethyl-
37	7.7238	0.705	Phenol, 4-ethyl-
38	7.7807	0.458	Creosol
40	7.9513	0.314	3-Heptyne
41	7.9968	2.058	Creosol
50	9.0888	1.465	1,2-Benzenediol, 3-methoxy-
51	9.2026	2.611	Phenol, 4-ethyl-2-methoxy-
55	9.9534	0.446	1H-Inden-1-one, 2,3,4,5,6,7-hexahydro-
57	10.2264	8.102	Phenol, 2,6-dimethoxy-
58	10.2719	0.588	Eugenol
60	10.397	1.916	Phenol, 2-methoxy-4-propyl-
65	11.1819	0.737	Digermane, ethyl-
73	13.1157	0.356	2-Ethoxy-4-anisaldehyde
82	14.822	0.665	Ethanone, 1-(4-hydroxy-3,5-dimethoxyphenyl)-
88	16.6306	0.155	Hexadecanoic acid, methyl ester
91	17.0629	2.418	n-Hexadecanoic acid
92	17.1312	0.159	Pyrene, hexadecahydro-
95	18.7123	1.686	9-Octadecenoic acid, (E)-
96	18.7578	1.897	Oleic Acid
97	18.8943	0.418	Octadecanoic acid
101	21.3287	0.160	Benzylidene-l-ornithine
103	22.4889	0.201	2',4'-Dihydroxyacetophenone oxime
104	22.9667	0.264	4H-Naphtho[2,3-b]pyran-4-one, 5,6-dihydroxy-8-methoxy-2-methyl-

Table A.9: GC-MS results for La_2O_3 BO.

PK	RT	Area Pct	Library/ID
1	2.9122	0.8082	2-Cyclopenten-1-one
2	2.9804	0.502	Cyclopentanone, 2-methyl-
3	3.0487	0.3965	(R)-(+)-3-Methylcyclopentanone
5	3.2762	0.1214	Pyridine, 3-methyl-
8	3.8108	3.1418	2-Cyclopenten-1-one, 2-methyl-
9	3.8904	0.7375	Ethanone, 1-(2-furanyl)-
10	3.9359	0.8586	Butyrolactone
18	4.6412	1.8621	2-Cyclopenten-1-one, 3-methyl-
19	4.937	0.416	2(3H)-Furanone, dihydro-5,5-dimethyl-
21	5.1076	2.2873	2-Cyclopenten-1-one, 2,3-dimethyl-
25	5.7332	2.2084	2-Cyclopenten-1-one, 2,3-dimethyl-
28	6.0745	0.7692	Phenol, 2-methyl-
30	6.302	0.6828	2-Cyclopenten-1-one, 3-ethyl-
31	6.393	3.2111	p-Cresol
32	6.5068	11.2649	Phenol, 2-methoxy-
33	6.6433	1.5208	Cyclopentanecarboxaldehyde, 2-methyl-3-methylene-
39	7.4623	0.2851	Phenol, 2,3-dimethyl-
40	7.7239	0.7443	Phenol, 4-ethyl-
41	7.7808	0.5905	2-Methoxy-6-methylphenol
43	7.9969	2.4637	Creosol
44	8.122	0.2374	Phenol, 3,4-dimethyl-
54	9.2027	2.4886	Phenol, 4-ethyl-2-methoxy-
62	10.2151	4.7445	Phenol, 2,6-dimethoxy-
63	10.272	0.3815	Eugenol
64	10.3971	1.9617	Phenol, 2-methoxy-4-propyl-
67	10.9204	0.4239	Vanillin
68	11.1138	0.6917	Benzenemethanol, .alpha.,4-dimethyl-
79	12.5129	1.4952	Homovanillyl alcohol
80	12.5698	0.6259	Phenol, 2-methoxy-4-(methoxymethyl)-
86	13.5594	0.4478	Benzene, 1,4-bis(methoxymethyl)-2,3,5,6-tetramethyl-
96	16.6308	0.2538	Hexadecanoic acid, methyl ester
97	16.7331	0.2882	4,4'-Bis(tetrahydrothiopyran)
99	17.063	3.3122	n-Hexadecanoic acid
103	18.7238	4.5449	Oleic Acid
104	18.8945	0.5721	Octadecanoic acid
105	19.6338	0.2076	Bicyclo[3.1.0]hexane, 4-methylene-1,6-diphenyl-

Table A.10: GC-MS compounds for Hydrotalcite BO.

PK	RT	Area Pct	Library/ID
1	2.9235	0.95	2-Cyclopenten-1-one
2	2.9917	0.5081	Cyclopentanone, 2-methyl-
3	3.0713	0.3661	Cyclopentanone, 3-methyl-
5	3.2875	0.1523	Pyridine, 3-methyl-
8	3.8221	3.4621	2-Cyclopenten-1-one, 2-methyl-
9	3.9017	0.6837	Ethanone, 1-(2-furanyl)-
10	3.9472	0.8602	Butyrolactone
15	4.5046	0.653	3-Ethylcyclopentanone
16	4.6525	2.0908	2-Cyclopenten-1-one, 3-methyl-
19	5.1075	2.2675	2-Cyclopenten-1-one, 2,3-dimethyl-
20	5.4715	0.7559	2-Cyclopenten-1-one, 3,4-dimethyl-
22	5.7332	1.7994	2-Cyclopenten-1-one, 2,3-dimethyl-
24	6.0744	1.1032	Phenol, 2-methyl-
26	6.3019	0.6847	2-Cyclopenten-1-one, 3-ethyl-
27	6.3815	3.2286	p-Cresol
28	6.518	11.4677	Phenol, 2-methoxy-
29	6.6432	1.2389	Cyclopentanecarboxaldehyde, 2-methyl-3-methylene-
35	7.4394	0.2874	Phenol, 2,5-dimethyl-
36	7.7238	0.8059	Phenol, 4-ethyl-
37	7.7807	0.4313	2-Methoxy-6-methylphenol
39	7.9969	2.3279	Creosol
40	8.1106	0.2284	Phenol, 3,4-dimethyl-
42	8.2243	0.2049	4,5,6,6a-Tetrahydro-2(1H)-pentalenone
49	9.0661	1.7637	1,2-Benzenediol, 3-methoxy-
50	9.2026	2.5483	Phenol, 4-ethyl-2-methoxy-
54	9.9534	0.2752	Spiro[4.4]nonane, 1-methylene-
56	10.2264	7.9973	Phenol, 2,6-dimethoxy-
57	10.3857	1.8065	Phenol, 2-methoxy-4-propyl-
76	14.0599	0.6199	3-Hydroxy-4-methoxycinnamic acid
79	14.822	0.2841	Ethanone, 1-(4-hydroxy-3,5-dimethoxyphenyl)-
85	16.6307	0.21	Hexadecanoic acid, methyl ester
87	17.0857	4.7136	n-Hexadecanoic acid
88	18.2915	0.2725	11-Octadecenoic acid, methyl ester
89	18.7237	3.7801	Oleic Acid
90	18.7693	1.4419	Oleic Acid
91	18.9058	1.3142	Octadecanoic acid
93	20.6007	0.5813	(+)-s-2-Phenethanamine, 1-methyl-N-vanillyl-

Table A.11: GC-MS compounds from nickel BO.

PK	RT	Area Pct	Library/ID
1	2.9349	0.1846	2-Cyclopenten-1-one
2	2.9804	0.9112	Cyclopentanone, 2-methyl-
3	3.06	0.3115	(R)-(+)-3-Methylcyclopentanone
4	3.2534	0.4111	Butanoic acid, 3-methyl-
6	3.6401	0.4478	Cyclohexanone
7	3.8108	3.3541	2-Cyclopenten-1-one, 2-methyl-
8	3.8904	0.6872	Ethanone, 1-(2-furanyl)-
9	3.9473	0.7206	Butyrolactone
11	4.243	0.5568	Cyclopentanone, 2-ethyl-
13	4.5047	0.5852	3-Ethylcyclopentanone
14	4.6525	1.7734	2-Cyclopenten-1-one, 3-methyl-
17	5.1075	1.8699	2-Cyclopenten-1-one, 2,3-dimethyl-
18	5.4716	0.7476	2-Cyclopenten-1-one, 3,4-dimethyl-
21	5.7332	1.4479	2-Cyclopenten-1-one, 2,3-dimethyl-
23	6.0176	0.2972	2-Hexenal, (E)-
24	6.0744	0.6545	Phenol, 2-methyl-
25	6.1541	0.2376	Ethanone, 1-(1H-pyrrol-2-yl)-
26	6.3019	0.5707	2-Cyclopenten-1-one, 3-ethyl-
27	6.3816	4.0647	p-Cresol
28	6.5181	9.9285	Phenol, 2-methoxy-
30	6.6432	1.0027	Cyclopentanecarboxaldehyde, 2-methyl-3-methylene-
36	7.7239	0.9304	Phenol, 4-ethyl-
37	7.7808	0.4762	2-Methoxy-6-methylphenol
39	7.9969	3.0003	Creosol
40	8.1106	0.2495	Phenol, 3,4-dimethyl-
44	8.5998	0.7599	Phenol, 3-ethyl-5-methyl-
47	9.0775	1.5466	1,2-Benzenediol, 3-methoxy-
48	9.214	2.9224	Phenol, 4-ethyl-2-methoxy-
52	9.9534	0.2489	1H-Inden-1-one, 2,3,4,5,6,7-hexahydro-
53	10.2378	8.6656	Phenol, 2,6-dimethoxy-
54	10.3971	2.5384	Phenol, 2-methoxy-4-propyl-
56	10.9203	0.3118	Vanillin
64	12.5015	1.1711	Homovanillyl alcohol
75	14.8221	0.4818	Ethanone, 1-(4-hydroxy-3,5-dimethoxyphenyl)-
81	16.6307	0.192	Hexadecanoic acid, methyl ester
83	17.0858	4.3089	n-Hexadecanoic acid
85	18.7807	5.3374	Oleic Acid
86	18.9172	1.3179	Octadecanoic acid
89	21.3287	0.1685	Benzylidene-l-ornithine
91	22.489	0.1996	2',4'-Dihydroxyacetophenone oxime

Table A.12: GC-MS results for BO-270-30-2.5

PK	RT	Area Pct	Library/ID
1	2.8895	1.1404	2-Cyclopenten-1-one
2	2.9577	0.2463	Cyclopentanone, 2-methyl-
3	3.0373	0.1359	(R)-(+)-3-Methylcyclopentanone
7	3.7881	2.0224	2-Cyclopenten-1-one, 2-methyl-
8	3.8563	1.0107	Ethanone, 1-(2-furanyl)-
9	3.9132	0.7872	Butyrolactone
10	4.0839	0.4698	2,5-Hexanedione
16	4.6185	1.1226	2-Cyclopenten-1-one, 3-methyl-
19	5.0735	1.2635	2-Cyclopenten-1-one, 2,3-dimethyl-
23	5.6081	1.7726	2-Cyclopenten-1-one, 2-hydroxy-3-methyl-
24	5.6992	0.8528	2-Cyclopenten-1-one, 2,3-dimethyl-
25	6.0063	0.5488	2-Cyclopenten-1-one, 2-hydroxy-3,4-dimethyl-
26	6.0518	0.3191	Phenol, 2-methyl-
28	6.2793	0.5076	2-Cyclopenten-1-one, 3-ethyl-
29	6.3589	2.5472	p-Cresol
30	6.484	7.0593	Phenol, 2-methoxy-
32	6.7229	0.3768	Benzofuran, 2-methyl-
35	6.9504	1.2687	2-Cyclopenten-1-one, 3-ethyl-2-hydroxy-
42	7.724	0.2825	Phenol, 4-ethyl-
45	7.9742	0.8177	Creosol
47	8.2245	0.6695	2-Hydroxy-3-propyl-2-cyclopenten-1-one
48	8.3837	0.1734	2-Naphthalenol
56	9.18	1.6921	Phenol, 4-ethyl-2-methoxy-
57	9.2369	0.7326	1H-Inden-1-one, 2,3-dihydro-
62	10.2151	7.4164	Phenol, 2,6-dimethoxy-
63	10.363	0.977	Phenol, 2-methoxy-4-propyl-
66	10.8977	0.8083	Vanillin
69	11.4437	1.411	Phenol, 2-methoxy-4-(1-propenyl)-
71	11.9669	1.1883	Apocynin
75	12.4788	2.2453	Homovanillyl alcohol
79	13.1045	0.3612	1-(3,4-methylenedioxyphenyl)propane-1-ol
80	13.15	0.3568	2,3,7-Trimethylindole
81	13.2751	0.4114	Phenol, 2,6-dimethoxy-4-(2-propenyl)-
88	14.3899	0.6434	Phenol, 2,6-dimethoxy-4-(2-propenyl)-
90	14.7994	0.7881	Ethanone, 1-(4-hydroxy-3,5-dimethoxyphenyl)-
98	16.0962	0.7249	2-(Heptyloxycarbonyl)benzoic acid
100	16.4716	0.2957	Tricyclo[9.2.2.2(4,7)]heptadeca-1(14),2,4(17),5,7(16),11(15),12-heptaene
101	16.6081	0.2765	Hexadecanoic acid, methyl ester
104	17.0744	4.3376	n-Hexadecanoic acid
105	18.2689	0.472	9-Octadecenoic acid (Z)-, methyl ester
106	18.7239	5.9944	9-Octadecenoic acid, (E)-
107	18.8945	1.2824	Octadecanoic acid
108	19.6225	0.4125	2,5-Piperazinedione, 3-benzyl-6-isopropyl-
109	19.9296	0.2679	2,5-Piperazinedione, 3-benzyl-6-isopropyl-
112	21.2947	0.398	Pregna-5,17(20)-dien-3-ol, (3.beta.,17E)-
124	26.4477	0.5427	2,4-Diamino-5-benzyl-6-phenylthieno[2,3-d]pyrimidine
128	30.6224	0.2716	3-Oxoallobetulane

Table A.13: GC-MS results for BO-270-30-7.5

PK	RT	Area Pct	Library/ID
1	2.8893	0.8418	2-Cyclopenten-1-one
2	2.9575	0.3218	Cyclopentanone, 2-methyl-
3	3.0372	0.1947	Cyclopentanone, 3-methyl-
7	3.7879	2.2354	2-Cyclopenten-1-one, 2-methyl-
8	3.8676	0.6639	Ethanone, 1-(2-furanyl)-
9	3.9131	0.7153	Butyrolactone
10	4.0951	0.1937	2,5-Hexanedione
12	4.3339	0.2881	1,4-Hexadiene
13	4.4818	0.4146	3-Ethylcyclopentanone
14	4.6183	1.3114	2-Cyclopenten-1-one, 3-methyl-
17	5.0847	1.8973	2-Cyclopenten-1-one, 2,3-dimethyl-
20	5.5852	0.7056	1,2-Cyclopentanedione, 3-methyl-
21	5.699	0.9736	2-Cyclopenten-1-one, 2,3-dimethyl-
24	6.0516	0.3806	Phenol, 2-methyl-
25	6.1312	0.2039	Ethanone, 1-(1H-pyrrol-2-yl)-
27	6.3587	2.6153	p-Cresol
28	6.4839	8.33	Phenol, 2-methoxy-
34	7.0982	0.4272	Cyclohexane, (1-methylethylidene)-
38	7.7124	0.3132	Phenol, 4-ethyl-
41	7.9741	1.1551	Creosol
43	8.2243	0.4446	2-Hydroxy-3-propyl-2-cyclopenten-1-one
51	9.1798	1.899	Phenol, 4-ethyl-2-methoxy-
52	9.2367	0.6439	1H-Inden-1-one, 2,3-dihydro-
56	9.9192	0.2811	Adamantane
57	10.215	8.4015	Phenol, 2,6-dimethoxy-
58	10.3629	1.2776	Phenol, 2-methoxy-4-propyl-
60	10.8975	0.5025	Vanillin
65	11.6824	0.6292	9-Borabicyclo[3.3.1]nonane, 9-ethyl-
66	11.9554	0.9055	Apocynin
72	13.0929	0.2686	1-(3,4-methylenedioxyphenyl)propane-1-ol
74	13.2749	0.3573	2-Propenoic acid, 3-(4-hydroxy-3-methoxyphenyl)-
84	14.7992	1.0017	Ethanone, 1-(4-hydroxy-3,5-dimethoxyphenyl)-
92	16.6079	0.3924	Hexadecanoic acid, methyl ester
95	17.097	6.0388	n-Hexadecanoic acid
98	18.2687	0.564	11-Octadecenoic acid, methyl ester
100	18.4962	0.2859	Methyl stearate
101	18.7351	6.8441	Oleic Acid
102	18.9057	1.8523	Octadecanoic acid
103	19.0536	0.1047	2-Methyl-Z,Z-3,13-octadecadienol
108	21.2945	0.5323	Pregna-5,17(20)-dien-3-ol, (3.beta.,17E)-
110	22.4548	0.1676	N'-(2,4,6(1H,3H,5H)-Trioxopyrimidin-5-ylidenemethyl)-2-nitrobenzhydrazide
117	24.7754	0.3876	2H-1,4-Benzodiazepin-2-one, 7-bromo-1,3-dihydro-1,3-dimethyl-5-[2-pyridyl]-

Table A.14: GC-MS results for BO-330-30-7.5

PK	RT	Area Pct	Library/ID
1	2.9576	0.6325	Cyclopentanone, 2-methyl-
2	3.0372	0.4535	(R)-(+)-3-Methylcyclopentanone
3	3.2306	0.5775	Pyridine, 3-methyl-
5	3.5719	0.1279	Cyclopentanone, 2,4-dimethyl-
7	3.788	2.8458	2-Cyclopenten-1-one, 2-methyl-
8	3.9245	0.6063	Butyrolactone
9	4.1292	0.1418	Pyridine, 3,5-dimethyl-
12	4.4819	0.8435	3-Ethylcyclopentanone
14	4.6184	2.0512	2-Cyclopenten-1-one, 3-methyl-
17	5.0848	2.5298	2-Cyclopenten-1-one, 2,3-dimethyl-
18	5.4374	0.7181	2-Cyclopenten-1-one, 3,4-dimethyl-
21	5.7104	2.7977	2-Cyclopenten-1-one, 2,3-dimethyl-
25	6.2678	0.9277	2-Cyclopenten-1-one, 3-ethyl-
26	6.3816	2.1924	p-Cresol
27	6.4157	1.3153	p-Cresol
28	6.4726	5.5162	Phenol, 2-methoxy-
30	6.6432	0.7514	1-Isopropylcyclohex-1-ene
41	7.4281	0.4284	Phenol, 2,4-dimethyl-
44	7.7011	0.9846	Phenol, 4-ethyl-
48	7.9741	1.979	Creosol
59	9.0548	1.026	1,2-Benzenediol, 3-methoxy-
60	9.1799	1.9877	Phenol, 4-ethyl-2-methoxy-
61	9.2481	1.0242	1H-Inden-1-one, 2,3-dihydro-
63	9.578	0.2795	1H-Inden-1-one, 2,3-dihydro-2-methyl-
65	9.7259	0.4842	1-Methylindan-2-one
70	10.1809	1.7024	Phenol, 2,6-dimethoxy-
89	11.9896	1.1378	1H-Indole, 2,5-dimethyl-
96	13.1499	0.7875	2,3,7-Trimethylindole
108	16.608	0.4396	Hexadecanoic acid, methyl ester
109	17.063	5.2433	n-Hexadecanoic acid
110	18.2688	0.2087	11-Octadecenoic acid, methyl ester
112	18.4963	0.1313	Methyl stearate
113	18.6783	2.1188	9-Octadecenoic acid, (E)-
114	18.7352	1.8566	9-Octadecenoic acid, (E)-
115	18.883	1.4198	Octadecanoic acid
117	21.2946	0.2648	Androsta-1,4-diene-3,11-dione

A.4 CCD additional data

Table A.15: Analysis of variance (ANOVA) for the BO yield model from Design-Expert.

Source	Sum of Squares	df	Mean Square	F-value	p-value	
Model	227.13	9	25.24	7.67	0.0028	significant
A-Temperature	104.60	1	104.60	31.80	0.0003	
B-Residence Time	17.51	1	17.51	5.32	0.0465	
C-Catalyst	35.23	1	35.23	10.71	0.0096	
AB	11.23	1	11.23	3.41	0.0978	
AC	1.19	1	1.19	0.3604	0.5631	
BC	6.79	1	6.79	2.06	0.1848	
A^2	19.89	1	19.89	6.05	0.0362	
B^2	24.89	1	24.89	7.56	0.0225	
C^2	22.20	1	22.20	6.75	0.0289	
Residual	29.61	9	3.29			
Lack of Fit	24.02	5	4.80	3.44	0.1275	not significant
Pure Error	5.59	4	1.40			
Cor Total	256.74	18				

Table A.16: ANOVA for the BC yield model from Design-Expert

Source	Sum of Squares	df	Mean Square	F-value	p-value	
Model	577.54	9	64.17	8.64	0.0012	significant
A-Temperature	360.56	1	360.56	48.53	<0.0001	
B-Residence Time	17.24	1	17.24	2.32	0.1587	
C-Catalyst	5.54	1	5.54	0.7451	0.4083	
AB	3.42	1	3.42	0.4607	0.5127	
AC	0.2592	1	0.2592	0.0349	0.8556	
BC	7.37	1	7.37	0.9922	0.3427	
A^2	69.56	1	69.56	9.36	0.0120	
B^2	12.32	1	12.32	1.66	0.2267	
C^2	18.56	1	18.56	2.50	0.1451	
Residual	74.29	10	7.43			
Lack of Fit	68.22	5	13.64	11.25	0.0095	significant
Pure Error	6.07	5	1.21			
Cor Total	651.83	19				

Table A.17: ANOVA for the AP yield model from Design-Expert

Source	Sum of Squares	df	Mean Square	F-value	p-value	
Model	180.68	9	20.08	1.97	0.1523	not significant
A-Temperature	8.04	1	8.04	0.7904	0.3949	
B-Residence Time	16.03	1	16.03	1.58	0.2380	
C-Catalyst	91.13	1	91.13	8.95	0.0135	
AB	3.21	1	3.21	0.3154	0.5867	
AC	20.64	1	20.64	2.03	0.1849	
BC	7.53	1	7.53	0.7400	0.4098	
A^2	0.0334	1	0.0334	0.0033	0.9555	
B^2	3.07	1	3.07	0.3020	0.5947	
C^2	0.6007	1	0.6007	0.0590	0.8130	
Residual	101.77	10	10.18			
Lack of Fit	86.71	5	17.34	5.76	0.0387	significant
Pure Error	15.05	5	3.01			
Cor Total	282.45	19				

Table A.18: ANOVA for the gas phase yield model from Design-Expert

Source	Sum of Squares	df	Mean Square	F-value	p-value	
Model	497.51	9	55.28	10.36	0.0005	significant
A-Temperature	131.46	1	131.46	24.63	0.0006	
B-Residence Time	17.05	1	17.05	3.19	0.1042	
C-Catalyst	172.18	1	172.18	32.26	0.0002	
AB	11.23	1	11.23	2.10	0.1775	
AC	15.65	1	15.65	2.93	0.1176	
BC	6.90	1	6.90	1.29	0.2820	
A^2	23.09	1	23.09	4.33	0.0642	
B^2	0.4838	1	0.4838	0.0906	0.7695	
C^2	0.2710	1	0.2710	0.0508	0.8263	
Residual	53.38	10	5.34			
Lack of Fit	34.77	5	6.95	1.87	0.2545	not significant
Pure Error	18.61	5	3.72			
Cor Total	550.89	19				

Table A.19: CCD quadratic model coefficients for each HTL product.

	BO yield	BC yield	AP yield	Gas yield
Intercept	-138.24125	374.18390	-8.34905	-155.86479
Temperature	0.984861	-2.00010	0.080843	1.12280
Residence Time	-0.609946	-1.09315	0.589778	1.12008
Catalyst	1.31087	-1.61776	8.40877	-7.84387
Temperature * Residence Time	0.003791	0.002093	-0.002027	-0.003792
Temperature * Catalyst	0.005133	-0.002400	-0.021417	0.018650
Residence Time * Catalyst	-0.034733	0.036200	-0.036589	0.035033
Temperature²	-0.001644	0.002975	0.000065	-0.001714
Residence Time²	-0.005626	0.003922	0.001958	-0.000777
Catalyst²	-0.153053	0.136576	-0.024572	0.016503

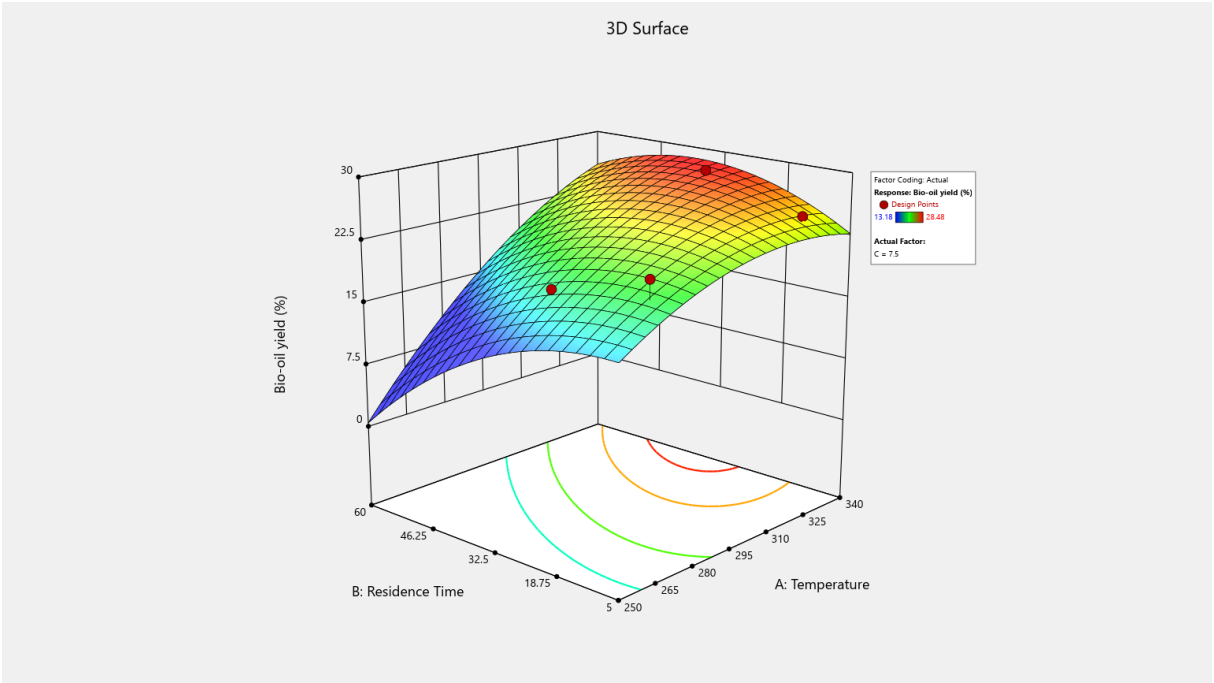
3D Surface
Bio-oil yield (%)
30
22.5
15
7.5
0
60
46.25
32.5
18.75
5
B: Residence Time
250
265
280
295
310
325
340
A: Temperature
Factor Coding: Actual
Response: Bio-oil yield (%)
Design Points
13.18
28.48
Actual Factor:
C = 7.5

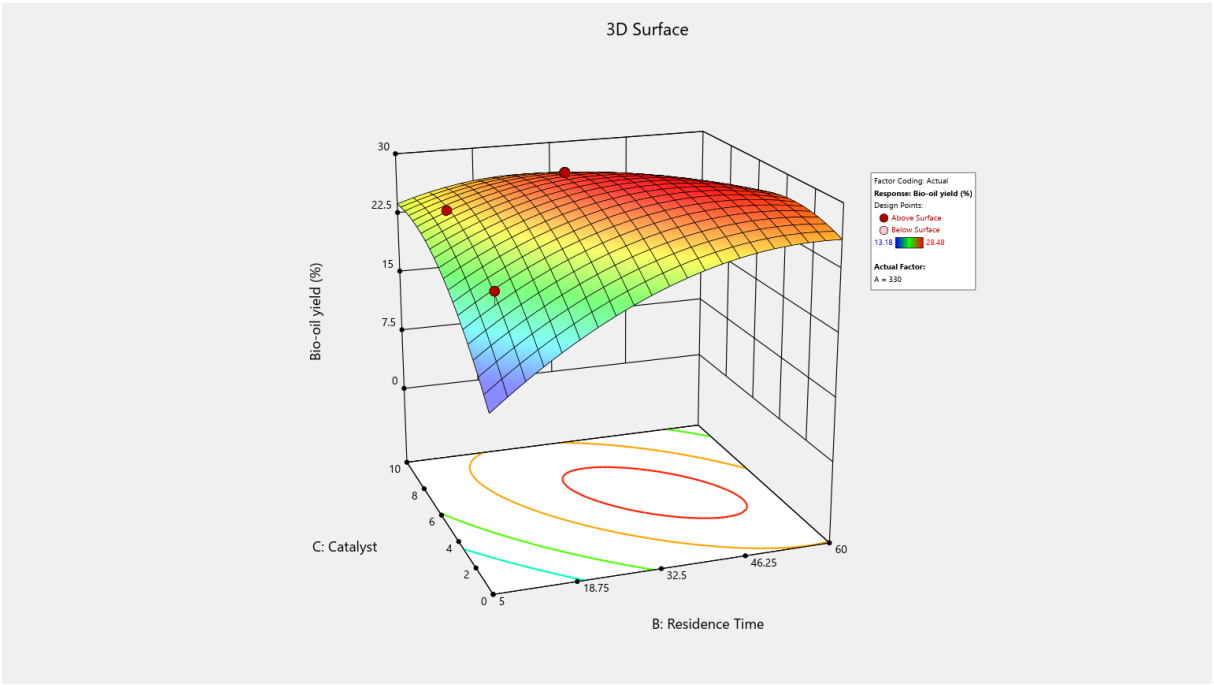
3D Surface
Bio-oil yield (%)
30
22.5
15
7.5
0
10
8
6
4
2
0
C: Catalyst
5
18.75
32.5
46.25
60
B: Residence Time
Factor Coding: Actual
Response: Bio-oil yield (%)
Design Points:
Above Surface
Below Surface
13.18
28.48
Actual Factor:
A = 330

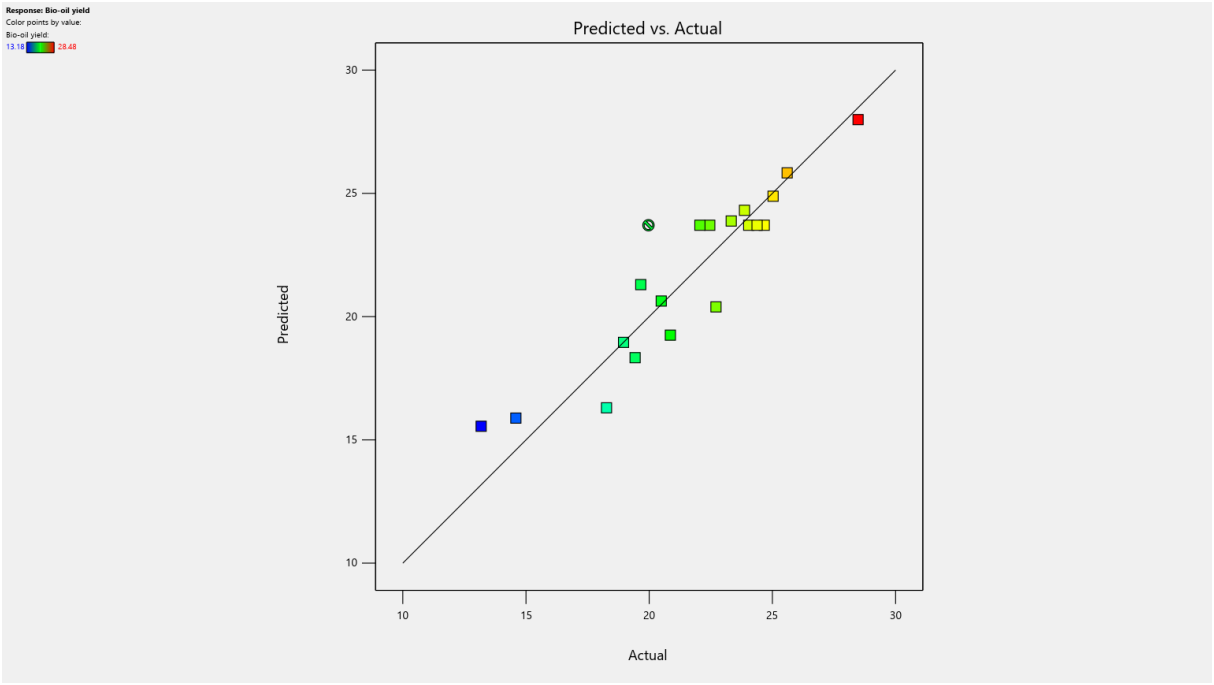
Response: Bio-oil yield
Color points by value:
Bio-oil yield:
13.18
28.48
Predicted vs. Actual
Predicted
Actual
10
15
20
25
30

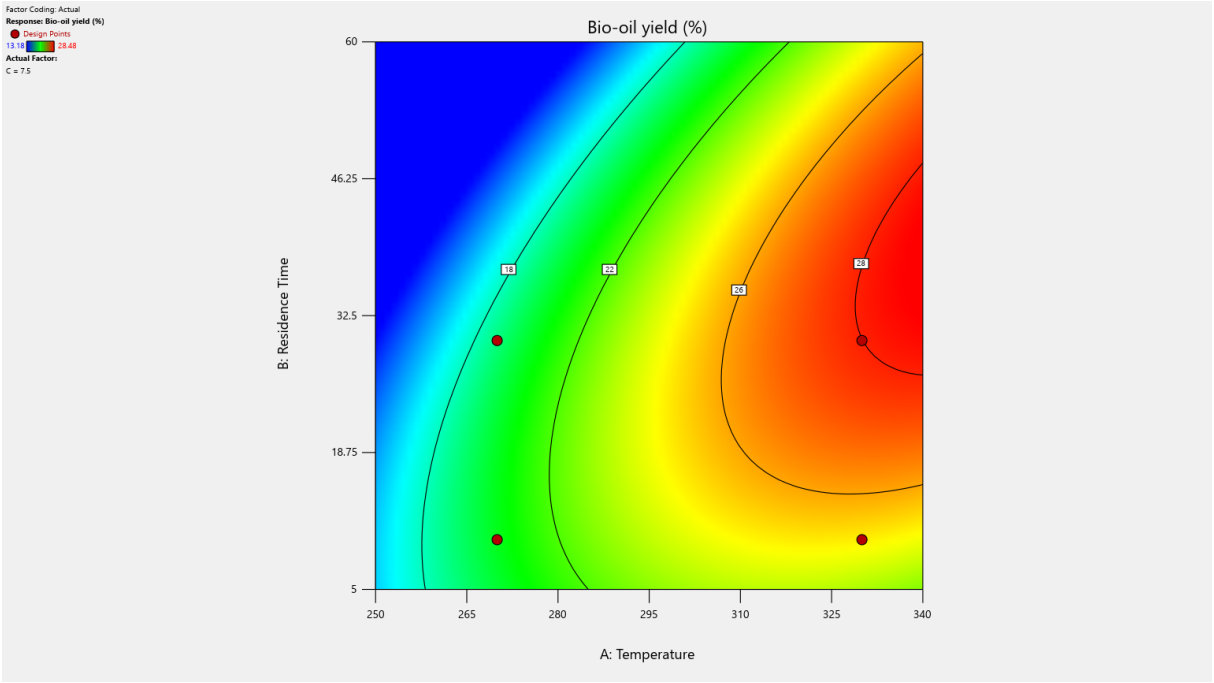
Factor Coding: Actual
Response: Bio-oil yield (%)
Design Points
13.18
28.48
Actual Factor:
C = 7.5
Bio-oil yield (%)
B: Residence Time
A: Temperature
60
46.25
32.5
18.75
5
250
265
280
295
310
325
340
18
22
26
28

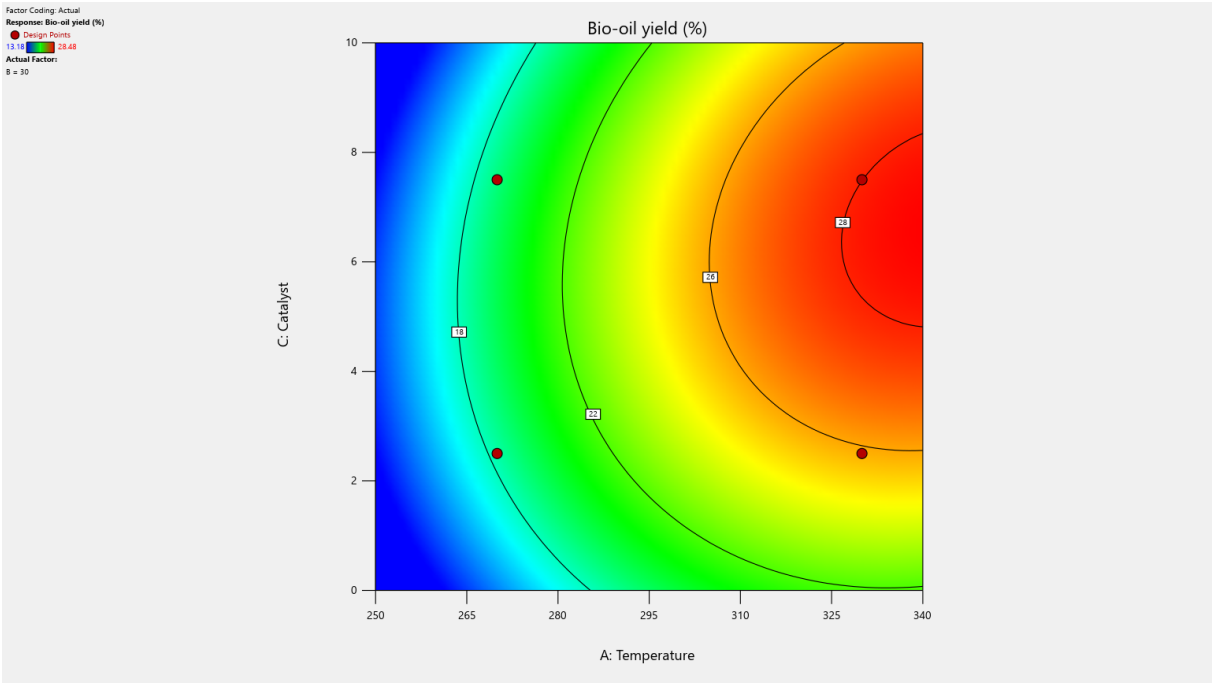
Factor Coding: Actual
Response: Bio-oil yield (%)
Design Points
13.18
28.48
Actual Factor:
B = 30
Bio-oil yield (%)
C: Catalyst
A: Temperature
10
8
6
4
2
0
250
265
280
295
310
325
340
18
22
26
28

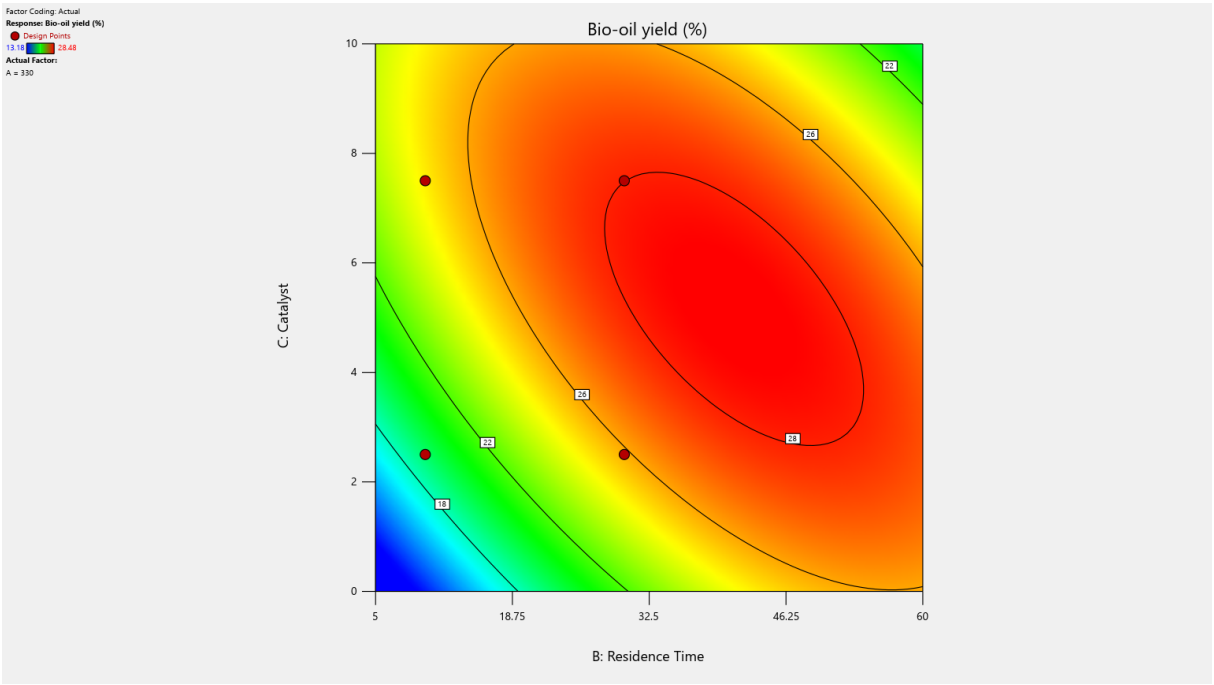
Factor Coding: Actual
Response: Bio-oil yield (%)
Design Points
13.18
28.48
Actual Factor:
A = 330
Bio-oil yield (%)
C: Catalyst
B: Residence Time
10
8
6
4
2
0
5
18.75
32.5
46.25
60
18
22
26
28

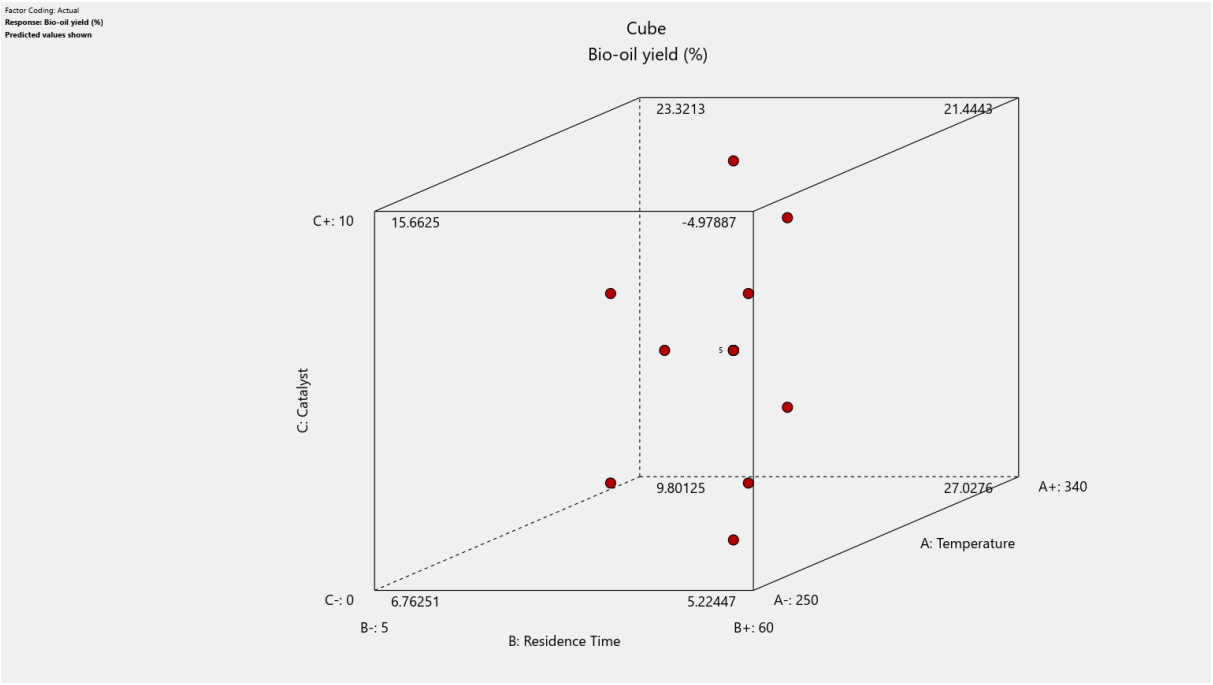
Factor Coding: Actual
Response: Bio-oil yield (%)
Predicted values shown
Cube
Bio-oil yield (%)
23.3213
21.4443
C+: 10
15.6625
-4.97887
5
C: Catalyst
9.80125
27.0276
A+: 340
A: Temperature
C-: 0
6.76251
5.22447
A-: 250
B-: 5
B+: 60
B: Residence Time